Alma Mater Studiorum · Università di Bologna

Scuola di Scienze

Corso di Laurea Magistrale in Fisica del Sistema Terra

Sea level trends in the Mediterranean from tide gauges and satellite altimetry

Relatore:

Prof. Susanna Zerbini

Presentata da:

François Vincent Rocco

Sessione III

Anno Accademico 2014/2015

Abstract

Sea level variation is one of the parameters directly related to climate change. Monitoring sea level rise is an important scientific issue since many populated areas of the world and megacities are located in low-lying regions.

At present, sea level is measured by means of two main techniques: the tide gauges and the satellite radar altimetry. The sea level trends estimated from tide gauge data are not directly comparable with those computed from satellite records. Tide gauges measure sea-level relatively to a ground benchmark, hence, their measurements are directly affected by local vertical ground motions. On the other hand, satellite radar altimetry measures sea-level relative to a geocentric reference and are not affected by vertical land motions.

In this study, the linear relative sea level trends of 35 tide gauge stations distributed across the Mediterranean Sea area have been computed over the period 1993-2014. In order to extract the real sea-level variation, the vertical land motion has been estimated using the observations of available GPS stations and removed from the tide gauges records. These GPS-corrected trends have then been compared with satellite altimetry measurements over the same time interval (AVISO data set). A further comparison has been performed, over the period 1993-2013, using the CCI satellite altimetry data set which has been generated using an updated modelling and a wider gridding compared to that of AVISO.

The first chapter of this dissertation gives an overview of the palaeo data and current sea level observations, a basic description of the tide gauges and satellite altimetry, and an analysis of the main causes of global mean sea level rise. The second chapter introduces the region analyzed and the data sets from which the tide gauge, GPS and satellite altimetry data have been selected and acquired. The third chapter illustrates the strategies used to compute reliable trends from each kind of data. The results are described in the fourth chapter.

The absolute sea level trends obtained from satellite altimetry and GPS-corrected tide gauge data are mostly consistent, meaning that GPS data have provided reliable corrections for most of the sites. The trend values range between +2.5 and +4 mm/yr almost everywhere in the Mediterranean area, the largest trends were found in the Northern Adriatic Sea and in the Aegean. These results are in agreement with estimates of the global mean sea level rise over the last two decades and previous investigations concerning sea level in the Mediterranean Sea. In those cases when GPS data were not available, information on the vertical land motion deduced from the differences between absolute and relative trends are in agreement with the results of other studies.

Sommario

La variazione del livello del mare rappresenta uno dei parametri direttamente legati al cambiamento climatico. Monitorare l'innalzamento del livello marino è importante poiché molte regioni densamente popolate e megalopoli del mondo sono localizzate in aree costiere a bassa quota.

Attualmente, il livello del mare viene misurato per mezzo di due tecniche principali: i mareografi e la radar altimetria da satellite. I trend di livello del mare stimati dai dati mareografici non sono direttamente confrontabili con quelli calcolati dai dati satellitari. I mareografi, infatti, misurano il livello del mare relativamente ad un caposaldo geodetico posto al suolo, quindi, questi dati possono essere contaminati dai movimenti verticali del terreno. D'altra parte, la radar altimetria misura il livello del mare rispetto a un riferimento geocentrico e non è influenzata dai movimenti verticali del suolo.

In questo studio, sono stati calcolati i trend lineari di livello del mare di 35 stazioni mareografiche distribuite nel Bacino Mediterraneo, nel periodo 1993-2014. Per ottenere la reale variazione del livello marino, il movimento verticale del suolo è stato determinato, usando le osservazioni delle stazioni GPS disponibili, e rimosso dai trend stimati con i mareografi. I trend così corretti sono stati confrontati con quelli calcolati dai dati satellitari durante lo stesso intervallo di tempo (AVISO data set). Un ulteriore confronto è stato effettuato per il periodo 1993-2013, usando i dati di radar altimetria del set CCI, recentemente divenuto disponibile e che utilizza una modellistica più recente ed una risoluzione spaziale maggiore di quella di AVISO.

Il primo capitolo di questa dissertazione presenta una panoramica dei paleo dati e delle osservazioni recenti e attuali del livello del mare, una descrizione basilare dei mareografi e dell'altimetria da satellite, e un'analisi delle principali cause dell'innalzamento globale osservato del livello del mare. Il secondo capitolo descrive la regione analizzata e i dati mareografici, GPS e satellitari selezionati. Il terzo capitolo illustra le strategie utilizzate per ottenere trend affidabili da ciascun tipo di dati. I risultati ottenuti vengono forniti nel quarto capitolo.

I trend di livello del mare assoluti ottenuti dalla radar altimetria e dai dati mareografici corretti per la variazione verticale del suolo sono nella grande maggioranza dei casi consistenti, indicando che i dati GPS hanno fornito correzioni valide nelle varie stazioni oggetto dello studio. I valori stimati dei trend sono compresi tra +2,5 e + 4 mm/a nell'area del Mediterraneo, i trend maggiori sono stati rilevati nell'Adriatico settentrionale e nel Mar Egeo. Questi risultati sono in accordo con le stime di innalzamento globale del livello del mare, dell'ordine di +3,3 mm/a durante gli ultimi 20 anni, e con altre indagini relative al livello del mare nel Mediterraneo. Nei casi in cui non erano disponibili dati GPS, le informazioni sul movimento verticale del suolo ricavate dalle differenze tra trend assoluto e relativo del mare sono in accordo con i risultati ottenuti da altri studi.

Contents

List of Figures

List of Tables

Chapter 1

Sea level rise observations and causes

The Fifth Assessment Report (AR5) of the Intergovernmental Panel on Climate Change (IPCC) [2013] has established that the warming of the climate system is unequivocal, and, furthermore, that anthropogenic activities are contributing to the climate change. The impacts of global warming have become a question of growing interest in the scientific community, and ongoing discussions on which policies might be effective in response to the climate variations are taking place. Global warming has already given rise to several visible consequences, in particular the increase of the ocean temperature and heat content [Antonov et al., 2005; Levitus et al., 2012], and of melting of glaciers [Gardner et al., 2013], and ice mass from the Greenland and Antarctica ice sheets [Shepherd et al., 2012].

One of the key indicators of climate change is the sea level. Ocean warming causes thermal expansion of sea waters, hence sea level rise. Similarly, water from land ice melt ultimately reaches the oceans, thus also causing sea level rise. Direct sea level observations available since the mid-to-late nineteenth century from *in situ* tide gauges and, since the early 1990s, from high-precision altimeter satellites, indeed, show that sea level is rising [Nerem et al., 2010; Church and White, 2011], with potentially negative impacts in many low-lying regions of the world.

Coastal zones have changed profoundly during the 20th century with growing populations and economies. Today, many of the world's megacities are situated on the coast; however, coastal developments have generally occurred with little regard to the consequences of rising sea levels. It is estimated that almost 10% of the world population is living in low-lying coastal zones, thus, sea level rise is generally considered as a major threat of climate change [McGranahan et al.,

2007]. During the twentieth century, shoreline erosion has been observed in many area of the world [Bird, 1987], however, it remains unclear whether this is due to climate-related sea level rise [Vellinga and Leatherman, 1989] or to more local non-climatic factors such as ground subsidence, coastal management, waves and currents, deficit in sediment supply, etc., [Bird, 1996]. Nevertheless, it is virtually certain that in the coming decades, the expected acceleration of sea level rise, in response to continuing global warming, will intensify the vulnerability of many low-lying, densely populated coastal regions of the world [Wong et al., 2013]. An improved understanding of sea level rise and variability is required in order to reduce the uncertainties associated with future projections, and hence contribute to a more effective coastal planning and management.

1.1 Past sea level estimations

The Earth's climate has changed throughout history, thereby sea level has changed and continues to change on all time scales. Palaeoclimate information facilitates understanding of Earth system feedbacks on time scales longer than a few centuries, which cannot be evaluated from short instrumental records. Past climate changes also document transitions between different climate states, against which the recent changes can be compared to assess whether or not they are unusual. On time scales between a few thousand to several hundred thousand years, sea level variability responds to an orbital forcing, which denote variations in the Earth's orbital parameters as well as changes in its axial tilt. Orbital forcing is considered responsible of the transitions between glacial and interglacial periods [Lisiecki, 2010; Huybers, 2011].

Over the glacial cycles sea level can oscillate by more than 100 m as the great ice sheets waxed and waned. These changes in sea level, and the related global average temperature changes, are a direct response to changes in the solar radiation reaching the Earth's surface; in turn, these solar radiation variations are due to alteration of the Earth's orbit around the sun. Also, feedbacks processes associated with the related changes in the Earth's albedo and greenhouse gas concentrations amplify the initial solar radiation changes [Masson-Delmotte et al., 2013]. The relations between sea level, $C0_2$ concentration, sea surface temperature and orbital parameters are illustrated in Figure 1.1.

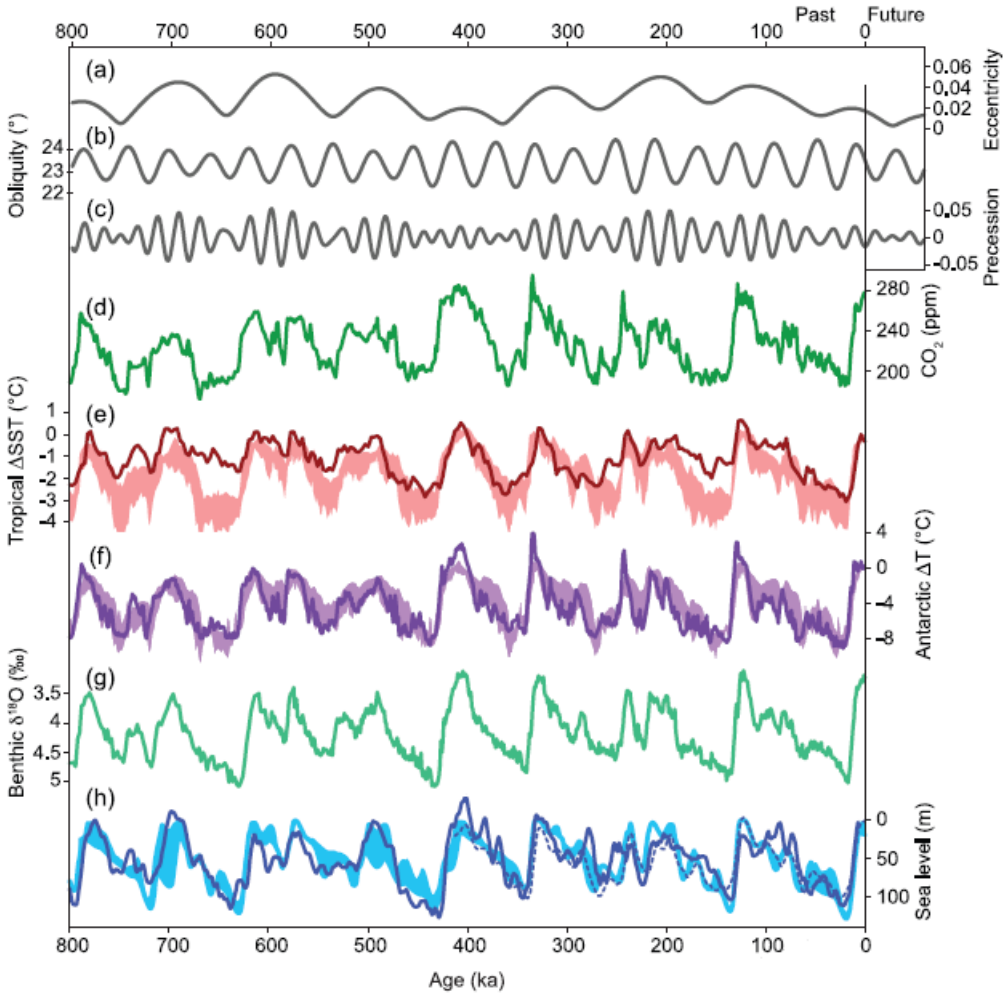

Figure 1.1: *Orbital parameters and proxy records over the past 800,000 yr. (a) Eccentricity. (b) Obliquity. (c) Precessional parameter [Berger and Loutre, 1991]. (d) Atmospheric concentration of CO_2 from Antarctic ice cores [Petit et al., 1999; Siegenthaler et al., 2005; Ahn and Brook, 2008; Lüthi et al., 2008]. (e) Tropical sea surface temperature stack [Herbert et al., 2010]. (f) Antarctic temperature stack based on up to seven different ice cores [Petit et al., 1999; Blunier and Brook, 2001; Watanabe et al., 2003; European Project for Ice Coring in Antarctica (EPICA) Community Members, 2006; Jouzel et al., 2007; Stenni et al., 2011]. (g) Stack of benthic $\delta^{18}O$, a proxy for global ice volume and deep-ocean temperature [Lisiecki and Raymo, 2005]. (h) Reconstructed sea level [dashed line: Rohling et al., 2010; solid line: Elderfield et al., 2012]. Lines represent orbital forcing and proxy records, shaded areas represent the range of simulations with climate models [Grid Enabled Integrated Earth System Model-1, GENIE-1, Holden et al., 2010a; Bern3D, Ritz et al., 2011], climate–ice sheet models of intermediate complexity [CLIMate and BiosphERe model, CLIMBER-2, Ganopolski and Calov, 2011] and an ice sheet model [Ice sheet model for Integrated Earth system studies, IcIES, Abe-Ouchi et al., 2007] forced by variations of the orbital parameters and the atmospheric concentrations of the major greenhouse gases [From Masson-Delmotte et al., 2013].*

Ice ages are characterized by a low average level of the oceans, up to 130 m below the current level during the last glacial maximum happened around 21,000 years ago [Lambeck et al., 2014]. On the contrary, interglacial periods are marked by high sea level. During the last interglacial (between 116,000 and 129,000 years ago) some palaeodata suggest rates of sea level rise perhaps as high as 1.6 ± 0.8 m/century [Rohling et al., 2008] and sea level about 4–6m above present-day values [Masson-Delmotte et al., 2013] (Fig 1.2).

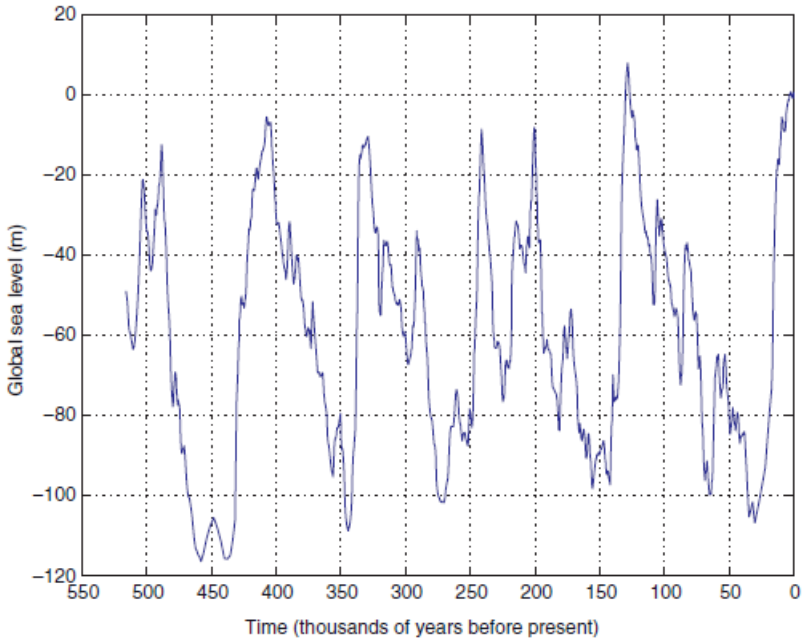

Figure 1.2: *Sea level over the last 500,000 years. This sea level estimate is based on carbonate $\delta^{18}O$ measurements in the central Red Sea [From Rohling et al., 2008].*

From its level at the last glacial maximum until the beginning of the Holocene, the current interglacial period that began 11,700 years ago, the sea level has risen at an average rate of about 12 mm/yr [Alley et al., 2005; Lambeck et al., 2014]. From about 6,000 to 2,000 years ago, sea level rose more slowly, and during the last 2,000 years the mean sea level has remained quasi stable with a rate of sea level change that did not exceed 0.5 mm/yr [Lambeck et al., 2014], until a recent acceleration since the end of the Nineteenth century, clearly detected in the oldest instrumental observations from tide gauges [Wöppelmann et al., 2008]. All these past evolutions have been reconstructed from palaeoclimate and geological data. The isotopic composition (ratio $0^{18}/0^{16}$ in foraminifera and corals) allows estimating the volumes of ice sheets and ocean temperatures to deduce the sea level [Erez, 1978].

1.2 Tide Gauges

For the twentieth century and the last decade, two main techniques of sea level observation exist: tide gauges and satellite radar altimetry. Tide gauges measure sea level relatively to the ground, hence data are directly affected by corresponding ground motions. If one is interested in the climate-related components of sea level rise, vertical land motions need to be removed. On the other hand, for studying coastal impacts of sea level rise, it is the relative (including vertical land motion as measured by tide gauges) sea level rise that is of interest. Satellite radar altimetry, unlike tide gauges, measures sea level relative to a geodetic reference frame and thus are not affected by vertical land motion. Data derived from tide gauges are geographically limited while altimeter-measured sea level is characterized by global coverage.

The earliest extended sea level measurements were made in Europe during the eighteenth century. These data were visual observations of the heights and times of high and low waters. Many entrances to docks were equipped with what were then called "tide gauges", graduated markings on their stone walls to indicate water depth over the dock sill. Visual measurements could have had centimeter-level accuracy in calm weather conditions, but would have been much less accurate in the presence of waves [Woodworth et al., 2011].

A more accurate measurement of sea level is possible since the 1830s thanks to automatic tide gauges, capable of recording the full tidal curve, not just the high and low waters. These instruments employed a tube, known as a stilling well, with a float connected to a wire, running over pulleys to a pen moving up and down as the tide rose and fell, thereby drawing a tidal curve on a rotating drum of paper.

New technologies have since replaced float gauges at many locations such as radar gauges, which emit a radar signal towards the sea surface and measure the travel time of the reflected signal in order to deduce water level. However, it is important to note that float gauges have provided the bulk of the historical sea level data set, and they still constitute a large fraction of the global network. In order to measure long-term sea-level changes accurately, tide gauge observations must be compared to a well-defined fixed level or datum. Benchmarks are commonly used for this purpose as they are located on a stable surface to provide a local height reference level. The stability of a particular benchmark cannot be guaranteed, thus, it is good practice to measure the elevation of the tide gauge benchmark relative to a group of other local benchmarks, and to check them periodically to ensure that they maintain, or not, these elevations relative to one another (Fig

1.3).

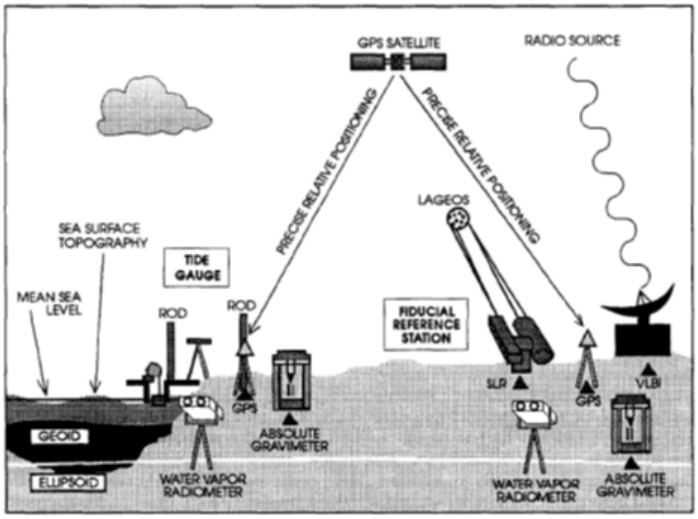

Figure 1.3: *Schematic diagram showing the tide gauge connections to SLR/VLBI reference system [From Zerbini et al., 1996].*

Tide gauge data have some limitations. First of all, they have a heterogeneous spatial distribution. The Permanent Service for Mean Sea Level [PSMSL; Woodworth and Player, 2003] is the largest global data bank, about 2000 stations, for long term tide gauge sea level observations concerning the twentieth century. Figure 1.4 presents an overview of the data holdings. There are much greater contributions from the Northern Hemisphere and from the second half of the twentieth century. This bias should always be kept in mind when calculating global mean sea level rise.

Another major difficulty is that tide gauge records are relative to the local land, thus they measure the combined effect of ocean volume change and vertical land motion (VLM). In active tectonic and volcanic regions, or in areas subject to strong ground subsidence due to natural causes (for examples, sediment loading in river deltas) or human activities (groundwater and hydrocarbons extraction), tide gauge data are directly affected by relevant ground motions. One component of the VLM is the post-glacial rebound, the viscoelastic response of the Earth crust and mantle to last deglaciation (nowadays called glacial isostatic adjustment, GIA). The problem of correcting the tide gauge records for the VLM has only been partially solved. Most studies of twentieth century time series are only accounting for the GIA [Douglas, 1991, 1997; Church and White, 2011], since this is the only vertical motion that can be described globally by a physical model. Land motions due to GIA are described by global geodynamic models of the Earth continued

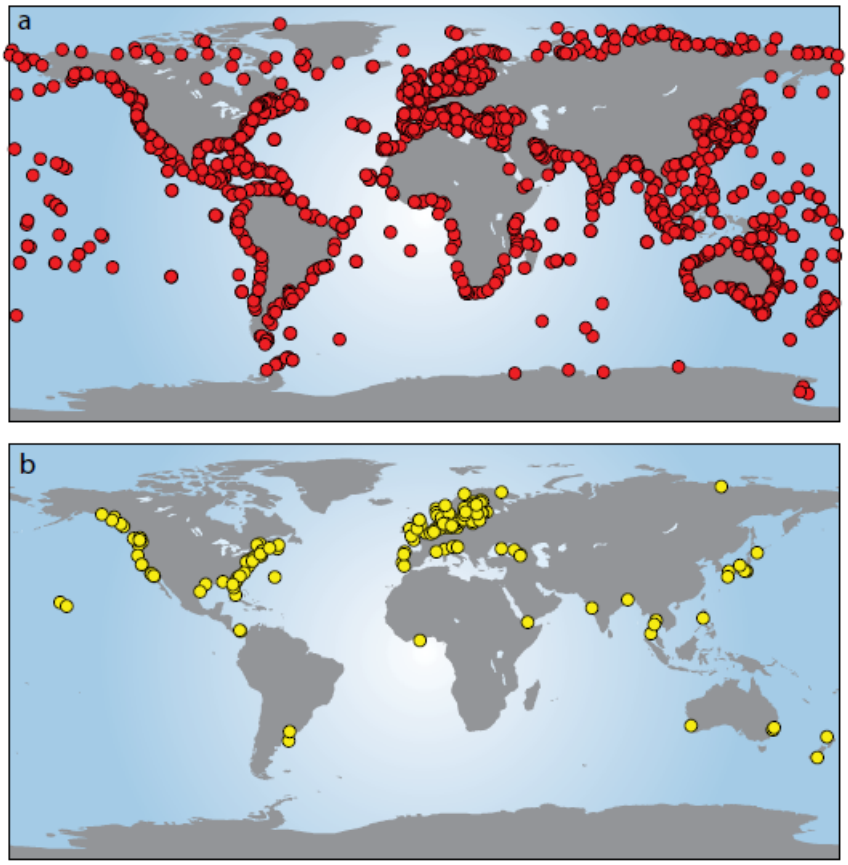

Figure 1.4: *Overview of PSMSL tide gauge database. (a)Stations represented in the data set of the Permanent Service for Mean Sea Level (PSMSL). (b)Stations with long records containing more than 60 years of data [From Woodworth et al., 2011].*

response to deglaciation [Peltier, 2001, 2004]. However, in some areas, VLM due to tectonic activity, groundwater mining, or ground fluids exploitation is larger than GIA and can affect the estimate of reliable sea-level rates [King et al., 2012; Wöppelmann et al., 2013]. An alternative approach is the use of space geodetic techniques to measure directly VLM and to correct the tide gauge data [Zerbini et al., 1996; Bouin and Wöppelmann, 2010]. More recently, Global Positioning System (GPS) receivers have been installed at tide gauge sites to measure VLM. However, these VLM measurements are only available since mid-late 1990s at the earliest, and could only be extrapolated into the past, if the assumption of a constant trend can be made. Additionally, at present the GPS installations do not cover all tide gauge sites [Santamarìa-Gòmez et al., 2012]. The information on VLM provided by GPS at tide gauges is the approach used in this study, and will be discussed in more detail in the following chapter.

1.3 Satellite Radar Altimetry

Since the early 1990s, sea level is routinely measured with quasi-global coverage and a few days/weeks revisit time (called "orbital cycle") by altimeter satellites. Compared to tide gauges, which provide sea level relative to the Earth crust, satellite altimetry measures sea level variations relative to the center of mass of the Earth. As a result, satellite altimetry measurements of sea level are made in an absolute reference system and do not need to be corrected for VLM.

1.3.1 Basic principle

The concept of the satellite altimetry measurement is simple [Chelton et al., 2001]: the onboard radar altimeter transmits microwave radiation toward the sea surface and is partly reflected back to the satellite. The signal two-way travel time is measured and the satellite distance from the sea surface can then be estimated. Figure 1.5 presents a schematic diagram of how satellite radar altimetry works.

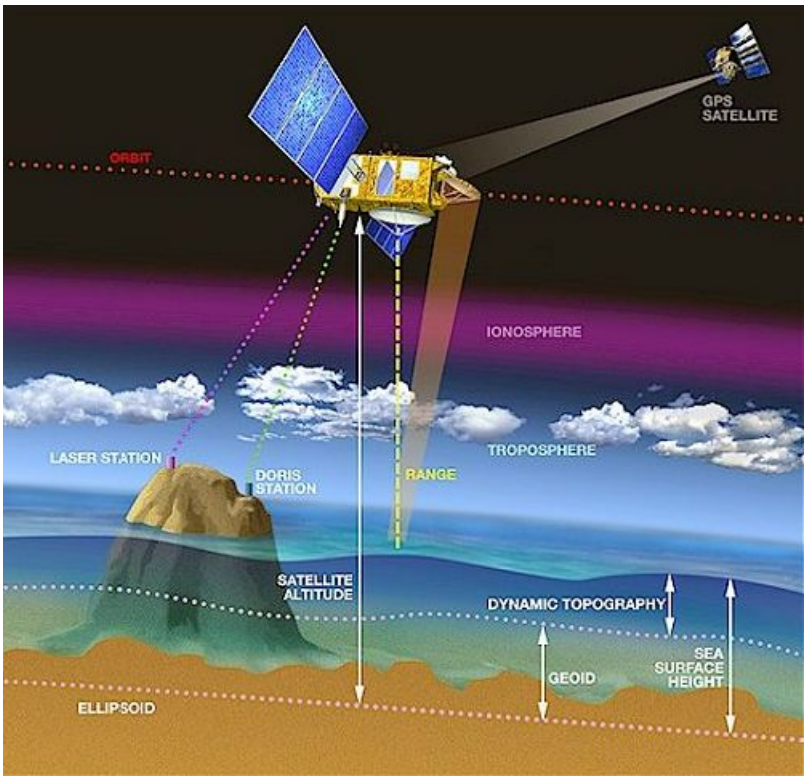

Figure 1.5: *Altimetry principle: Altimeters emit signals toward the Earth, and receive the echo from the sea surface, after the reflection. The sea surface height is obtained by the difference between the satellite's position relative to the reference ellipsoid and the satellite distance from the sea surface (range) (From AVISO).*

Radar altimeters permanently transmit signals at high frequency (over 1700 pulses per second) toward the Earth, and receive the echoes from the sea surface. The signal round-trip time between the satellite and the sea surface is deduced by analyzing the echo waveform. This is the curve describing the power of the signal reflected back to the altimeter. The electromagnetic radiation transmitted by the satellite is attenuated while going through the atmosphere and finally the pulse leading edge hits the water surface. As the incident pulse strikes the surface, it illuminates a circular region increasing linearly with time. After the pulse trailing edge has intersected the surface, it remains constant. At this moment, the return waveform has reached its peak. Travelling back to the satellite, the signal power is further attenuated by both the atmosphere and because the reflected signal no longer comes from directly below (Fig 1.6, left panel).

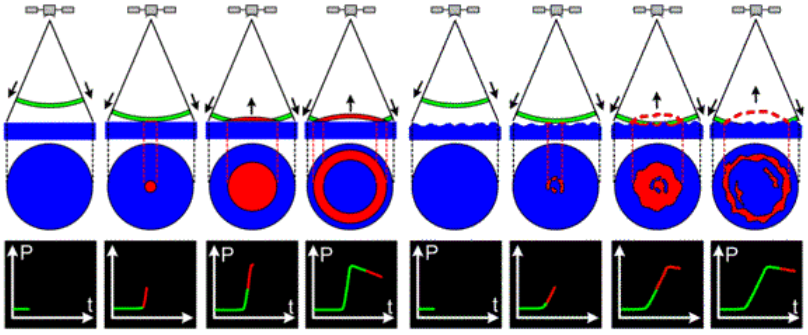

Figure 1.6: *Pulses reflection over a flat (left) and rough sea (right) (adapted from AVISO).*

This description is what happens over an ideal flat ocean, such standard waveform is also named "Brown Model" [Brown, 1977]. Surfaces characterized by significant slopes, such as those present in rough seas, make accurate interpretation more difficult. In this case, the pulse strikes the crest of one wave and of a series of other crests, causing the reflected wave amplitude to increase more gradually compared to the case of the flat ocean (Fig 1.6, right panel). From the change in slope of the waveform leading edge, the Significant Wave Height (SWH) can be estimated. The SWH is defined to be the average crest-to-trough height of the 1/3 highest waves and is usually denoted as $H_{1/3}$. The power of the return signal is also related to the sea surface roughness which is highly correlated with near-surface winds, thus, wind speed can be estimated from empirical formulae relating it to the signal backscattered power [Chelton and McCabe, 1985]. The return time is defined as the moment in which the mid-point of the waveform leading edge is detected (Fig 1.7).

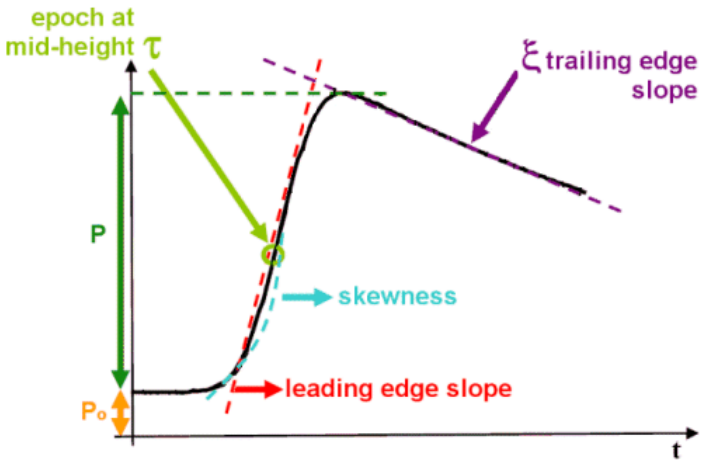

Figure 1.7: *Basic waveform shape. Several parameters can be deduced: epoch at mid-height gives the time the radar pulse took to travel the satellite-surface distance and back again; P is the energy of the pulse which can be used to calculate the backscatter coefficient; Po is the instrumental noise; the leading edge slope can be related to the significant wave height (SWH); the skewness is the leading edge curvature; the trailing edge slope is linked to any mispointing of the radar antenna (i.e. any deviation from nadir of the radar pointing) (from AVISO).*

The time measurement, scaled by the speed of light in the vacuum, yields a range measurement:

$$R = \frac{ct}{2} \tag{1.1}$$

The travel time needs to be known very accurately (a precision of 30 ps is required to achieve an accuracy of 1 cm on the height), so the actual measurements are formed by averaging a large number of individual radar echoes. These final observations, called the Geophysical Data Records (GDRs), are the data which will be further processed. Once the range has been calculated, the quantity of scientific interest can be computed, namely the sea surface height (SSH), that is the sea surface above a reference ellipsoid:

$$SSH = S–R \tag{1.2}$$

where S is the satellite altitude above the reference ellipsoid and R is the range. Thus, the ability to determine with high accuracy the satellite orbit is a key factor in satellite altimetry, since any error in the satellite orbit radial component will directly affect the SSH measurement. Precise orbits are provided by the space agencies.

1.3.2 Corrections of altimeter measurements

Several sources of error affect the altimeter measurements. They can be grouped in four different categories:

- instrumental errors;
- satellite position errors;
- signal propagation errors;
- geophysical errors.

1.3.2.1 Instrumental errors

To obtain accurate range measurements, the measured two-way travel time must be corrected for a number of instrumental errors (for detailed information, see Chelton et al., 1989, 2001). Under instrumental errors we can identify: the Doppler shift effect, caused by a change in the frequency of the returned signal due to the relative velocity between the satellite and the sea surface; the effect of accelerations of the spacecraft relative to the sea surface; the oscillator drift; altimeter calibration and pointing angle errors. The last one is the largest, resulting in a 2 cm range error for a 0.2° off-nadir pointing. Some of these errors can be evaluated on the ground before launch, and some during the initial mission calibration phase.

1.3.2.2 Satellite position errors

Many efforts have been made since the beginning of the satellite altimetry era to develop techniques capable of minimizing the orbit errors, since high precision is required for oceanographic applications [Tapley et al., 1994; Le Traon and Ogor, 1998; Rudenko et al., 2012; Couhert et al., 2015]. Precise Orbit determination (POD) is the procedure allowing estimating the three-dimensional position of the satellite center-of-mass, at regularly spaced time intervals, in a well-defined reference frame. POD combines accurate and complex mathematical models, describing the dynamics of the satellite motion with high precision observations of the satellite position [Tapley et al., 2000]. The motion of a close Earth satellite is perturbed by a number of forces which are, in relative order of importance:

- Earth gravity field including solid Earth and ocean tides;
- gravity perturbations due to the Moon, Sun and major planets;

- direct solar and Earth albedo radiation pressure;
- atmospheric drag;

Uncertainties in modeling the Earth gravity field have long been the main source of orbit error in POD. Gravity force models have greatly improved since the beginning of the altimetry era, thanks to dedicated gravity missions like GRACE (Gravity Recovery and Climate Experiment) and the more recent GOCE (Gravity Field and Steady-State Ocean Circulation Explorer), launched in March 2002 and March 2009, respectively [Pavlis et al., 2008; Mayer-Gürr et al., 2012]. The current models for the various gravitational effects are well documented in the International Earth Rotation Service (IERS) Conventions [IERS, 2010]. Non-gravitational forces such as solar radiation pressure and atmospheric drag, depend on the size and shape of the spacecraft, thus their modeling is easier for satellites with a simple geometry.

Radar altimetry measurements cannot provide an accurate determination of the satellite orbit, thus, independent observations of the satellite motion are required. Three main types of tracking techniques are employed to acquire these observations, each with different measurement characteristics, temporal and geographic coverage. Most recent altimetry satellites can be tracked by means of, at least, two techniques. Usually, a laser retroreflector array onboard the spacecraft, or just a few corner cube retroreflectors, support tracking by the satellite laser ranging (SLR) technique. Other systems include Doppler Orbitography and Radiopositioning Integrated by Satellite (DORIS) and the Global Positioning System (GPS).

1.3.2.3 Signal propagation errors

We can distinguish two main sources of error: the atmospheric refraction delay and the sea-state bias.

Atmospheric refraction

The effects of atmospheric refraction are generally expressed in terms of path delay. The presence of the atmosphere delayed the propagation of the altimeter signal, increasing the measured two-way travel time, which differs from the estimate assuming the free-space value for the speed of light. Failure to correct for atmospheric refraction results in a range estimate that is longer than the true range. Ionospheric and tropospheric refraction errors are considered separately; in

turn, tropospheric error can be broken down into dry and wet tropospheric delay.

Ionospheric refraction

Ionospheric refraction of altimetric radar signals is due to the dielectric properties of the upper atmosphere associated with the presence of free electrons. These are produced by the ionization, in the high atmosphere, of the incident solar radiation. The effective light speed is reduced by an amount depending on the Total Electron Content (TEC) and on the wavelength of the radar signal [Callahan, 1984]. The range delay is estimated from models of the vertically integrated electron density. However, the TEC is mainly correlated with the geomagnetic field, therefore is characterized by significant spatial variations. The TEC is also correlated with the solar activity and thus present strong diurnal and seasonal variability. Therefore, given that the delay depends on the signal wavelength, it can be estimated using a dual frequency altimeter. The information obtained from different frequencies allows estimating a reliable delay correction [Imel, 1994].

Dry tropospheric refraction

The dry component of atmospheric refraction is, by far, the largest correction that need to be applied to altimeter measurements. The mass of dry air molecules in the atmosphere causes an overestimation of the measured range of about 2.3 m. The correction is directly proportional to the atmospheric pressure measured at sea level and, in units of centimeters, can be approximated by [Chelton et al., 2001]:

$$\Delta SSH_{dry} \approx 0.2277 P_0 (1 + 0.0026 \cos 2\varphi) \tag{1.3}$$

where P_0 is the sea level pressure expressed in mbar and φ is the latitude of the measured sea surface point.

Wet tropospheric refraction

The wet tropospheric correction includes both the water vapor and the cloud liquid water droplet contributions to atmospheric refraction. The water content in the troposphere is highly variable in space and time, causing path delays ranging from 5 cm to 30 cm, according to the elevation angle of the observation. The wet tropospheric correction is computed using both on-board microwave radiometer measurements [Keihm et al., 1995], and atmospheric models of water vapor content [Fernandes et al., 2010, 2014].

Sea-state bias

The effect of the actual sea state on the reflected signal is referred as the sea-state bias (SSB). The size of the reflecting area depends on the roughness of the sea surface. At wave troughs the reflection is higher than at wave crests. Systematic corrections are required because the sea surface height measured by the altimeter is biased toward wave troughs. The SSB correction ε can be expressed as a percentage of the SWH [Tran et al., 2010]:

$$\varepsilon \approx \beta \cdot SWH \tag{1.4}$$

where β is between 1 and 5%. More accurate SSB corrections are obtained using empirical models derived from SWH and wind speed observations and from numerical ocean wave models [Tran et al., 2010].

1.3.2.4 Geophysical errors

A satellite radar altimeter measures the instantaneous sea surface height that is affected by time-dependent geophysical effects, including solid earth and ocean tides, polar tide, ocean loading and high and low frequency sea surface response to atmospheric pressure and wind stress. By removing these effects time independent SSHs are obtained.

Ocean tides and ocean loading corrections

Ocean tides are periodic deformations of sea surface resulting from gravitational attraction of celestial bodies, in particular, the Moon and the Sun. The relative movements of the Moon and the Sun with respect to the Earth, combined with the Earth own rotation, result in periodic displacements of water masses with different order of magnitude. In open ocean, tide amplitudes are typically 1-2 m, while they can reach several meters in coastal regions [Le Provost, 2001]. The most recent models use assimilated altimeter data as constraints and estimate tides globally with high spatial resolution [Ray et al., 2013]. Ocean tides also cause oceanic mass redistribution with associated load change on the crust, therefore, producing time-varying deformations of the Earth. The ocean tidal loading effect is computed from ocean tide models [Ray, 1998].

Solid Earth tide correction

The solid Earth tide is the elastic periodic deformation of the Earth's crust,

including the ocean bottom, due to luni-solar forcing. Solid Earth tides occur at the same frequencies as the ocean tides with amplitudes of about 50 cm. The solid Earth tide correction can be derived from tide-generating potential models depending upon Love numbers assuming an elastic Earth with uniform mass [Cartwright and Tayler, 1971; Cartwright and Edden, 1973].

Polar tide correction

The pole tide is a tide-like motion of the ocean surface, resulting from small effects due to the variation of the Earth rotation axis. These perturbations primarily occur at annual period, and at a 433-day period called the Chandler wobble, with amplitudes of about 2 cm. The pole tide correction is provided by models which require knowledge of the pole position [Wahr, 1985; Desai, 2002].

Atmospheric pressure and wind forcing correction

The Inverse Barometer (IB) is a correction accounting for variations in sea surface height due to atmospheric pressure variations (atmospheric loading). The ocean responds directly to atmospheric pressure changes: sea level rises (falls) in connection with low (high) pressure systems. The inverse barometer correction assumes an instantaneous static local response of the sea level to pressure variations, so that the total pressure at the ocean bottom is constant. The correction is expressed by the following equation [Dorandeu and Le Traon, 1999]:

$$IB = -0.9948(P - P_{Ref}) \tag{1.5}$$

where P is the instantaneous local sea level pressure in millibar and P_{Ref} is the time varying mean global surface atmospheric pressure over the oceans in millibar. In many applications, P_{Ref} is assumed to be constant, equal to 1013.3 mbar. The scale factor of -0.9948 implies that a local increase of 1 mbar in atmospheric pressure locally depresses the sea surface by about 1 cm. More precise corrections can be calculated using meteorological models. The ocean response to meteorological forcing is not completely accounted for by simply applying the inverse barometer correction [Wunsch and Stammer, 1997]. The classic IB formulation identifies the static response of the ocean to atmospheric pressure forcing, while wind effects are totally ignored [Carrere and Lyard, 2003]. Several studies have pointed out that the ocean has a clear dynamic response to pressure forcing at high frequencies (periods below 3 days) and at high latitudes, and that wind effects prevail around the 10 days period [Fukumori et al., 1998; Ponte and Gaspar, 1999]. Therefore,

this high frequency variability is corrected by using independent ocean models. At present, the effect due to atmospheric pressure and wind forcing are combined in the so called Dynamic Atmospheric Correction (DAC) [Carrere and Lyard, 2003; Carrere et al., 2015].

1.3.3 Sea Level Anomalies

With the introduction of the models described above, the expression for the measured sea surface height can be rewritten in a more complete form as follows:

$$SSH = S_{cor} - (R + h_i + h_{iono} + h_{dry} + h_{wet} + h_{ssb} + h_{otide} + h_{ol} + h_{stide} + h_{ptide} + h_{dac}) \tag{1.6}$$

where S_{cor} is the satellite altitude corrected for orbit errors, R is the instantaneous distance between the altimeter antenna and ocean surface. The following corrections represent h_i the sum of the instrumental errors, h_{iono} the ionospheric delay, h_{dry} the dry tropospheric component, h_{wet} the wet tropospheric component, h_{ssb} the sea-state bias, h_{otide} the ocean tide, h_{ol} the ocean loading, h_{stide} the solid Earth tide, h_{ptide} the pole tide and h_{dac} the dynamic atmospheric effect, respectively. The SSH obtained in this way is time-independent and is the sum of three remaining components. They are the height of the geoid above the reference ellipsoid, and both a permanent and a variable part of the ocean dynamic topography. The geoid is an equipotential surface of the Earth gravity field and can be defined as the static part of the sea surface. In absence of other forcings, the sea surface would be a surface of constant gravity potential corresponding to the marine geoid. Because the gravity field varies geographically, the geoid is an undulated surface and is, generally, described in terms of geoid undulations N, that is the heights of the geoid with respect to the reference ellipsoid. Geoid undulations are in the order of ± 100 m. The highest negative values, -106 m, are found in the Indian Ocean, whereas the highest positive values are encountered over Indonesia (+85 m) and in the Northern Atlantic Ocean (+61 m) [Limpach, 2010]. A schematic diagram of the effect of a bump and a depression at the ocean floor on the sea surface is shown in Figure 1.8.

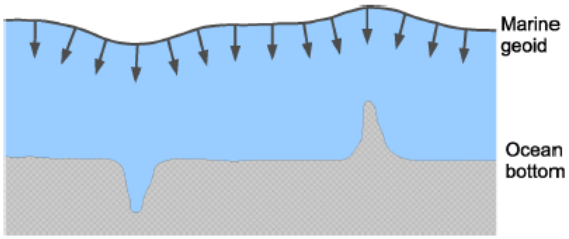

Figure 1.8: *Schematic diagram of a bump and a depression at the ocean bottom and the corresponding marine geoid. Vectors indicate the gravitational acceleration along the geoid [From Limpach, 2010].*

The ocean topography can be divided into a quasi-stationary part called the mean dynamic topography (MDT), with amplitude of magnitude of about 1 m, and a time-variable component due to change in the ocean circulation, the amplitude of which is in order of a few decimeters (Fig 1.9). The sum of the permanent and the variable part is known as the absolute dynamic topography (ADT) which is the sea surface height relative to the geoid, and is represented by the following equation:

$$SSH = N + ADT \tag{1.7}$$

The time variable part of the SSH is used in oceanographic studies. The Sea

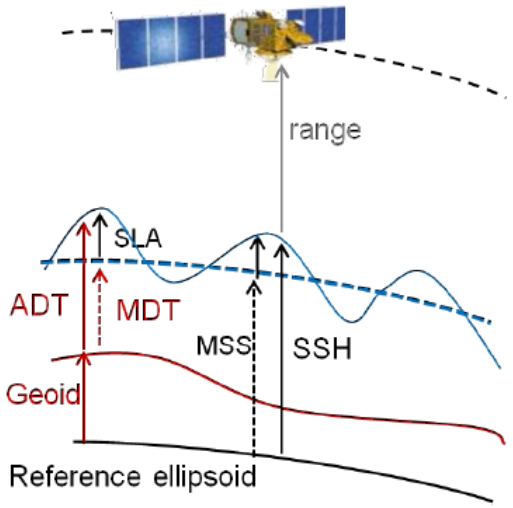

Figure 1.9: *Altimetry heights naming convention. (from AVISO).*

Level Anomaly SLA, computed by subtracting from the SSH a temporal reference $\langle SSH \rangle$ is defined as follows:

$$SLA(\varphi, \lambda, t) = SSH(\varphi, \lambda, t) - \langle SSH(\varphi, \lambda) \rangle \tag{1.8}$$

This temporal reference can be both a Mean Profile (MP) and a gridded Mean Sea Surface (MSS). The MSS represents the ocean surface averaged over an appropriate time period in order to remove annual, semi-annual, seasonal and spurious sea surface height signals [Picot et al., 2003]. The MSS corresponds to the sum of the geoid undulation N and of the mean dynamic topography MDT, over a selected time period, and it is referred to a given ellipsoid [Hernandez and Schaeffer, 2001].

1.3.4 Satellite altimetry missions

The development of accurate satellite altimeter systems started in the early 1970s and made possible the first nearly global observations of sea level. These early altimeters were intended to demonstrate proof of the concept of radar altimetry. However, till the launch of TOPEX/Poseidon (T/P), on August 10 1992, these measurements were severely affected by the inadequate knowledge of the Earth gravity field, contributing to a poor determination of the orbits of the altimetry satellites. This joint NASA/CNES (the USA and the French space agencies, respectively) was launched with the main objective of observing and understanding ocean circulation. Numerous improvements were made to Topex/Poseidon compared to previous altimetry systems. This included a specially-designed satellite, a suite of sensors, satellite tracking systems and orbit configuration, as well as the development of an optimal gravity field model for precision orbit determination, and a dedicated ground system for mission operations. Follow-on missions are those of the Jason series, which have inherited the T/P main features, although technological improvements constantly contribute to upgrading these satellites. Satellite altimetry has become an operational technique, therefore the availability of these observations is guaranteed for the future. Table 1.1 presents, starting from 1990s, the history, perspective and characteristics of satellite altimetry missions.

Table 1.1: *Summary of Satellite radar altimetry missions.*

Past Missions	Agency	Launch	End	Orbit inclination	Altitude (km)	Orbital cycle (days)	Tracking Systems
ERS-1	ESA	17/07/1991	10/03/2000	98,52°	785	35	PRARE, SLR
Topex/Poseidon	NASA/CNES	10/08/1992	18/01/2006	66°	1336	9,9156	DORIS,GPS,SLR
ERS-2	ESA	21/04/1995	05/09/2011	98,52°	785	35	PRARE, SLR
GFO	US Navy/NOAA	10/02/1998	22/10/2008	108°	880	17	DORIS, GPS, SLR
Jason-1	NASA/CNES	07/12/2001	01/07/2013	66°	1336	9,9156	DORIS, GPS, SLR
Envisat	ESA	01/03/2002	09/05/2012	98,55°	800	35	DORIS, SLR
Current Missions							
Jason-2	NASA/CNES/ Eumetsat/NOAA	20/06/2008	-	66°	1336	9,9156	DORIS, GPS, SLR
Cryosat	ESA	08/04/2010	-	92°	717	369	DORIS, SLR
HY-2A	China academy of space technology	15/08/2011	-	99,3°	971	14	DORIS, SLR
Saral	ISRO/CNES	25/02/2013		98,54°	800	35	DORIS, SLR
Future missions							
Jason-3	NASA/CNES/ Eumetsat/NOAA	17/01/2016	-	66°	1336	9,9156	-
Sentinel-3	ESA	04/02/2016	-	98,64°	814,5	27	-
Jason-CS	ESA/Eumetsat/EU/ CNES/NOAA/NASA	2017	-	66°	1336	10	-
SWOT	CNES/NASA/ CSA/UKSA	2020	-	77,6°	890	21	-

1.4 Causes and Observations of current GMSL

1.4.1 Main factors of current global mean sea level rise

The main factors causing current GMSL rise are the thermal expansion of sea waters, land ice loss, and fresh water mass exchange between oceans and land water reservoirs (Fig 1.10); these different components have been the subject of many studies [Antonov et al., 2005; Rignot et al., 2011; Shepherd et al., 2012; Wada 2012]. These contributions vary in response to natural climate variability and global climate change [Rhein et al., 2013].

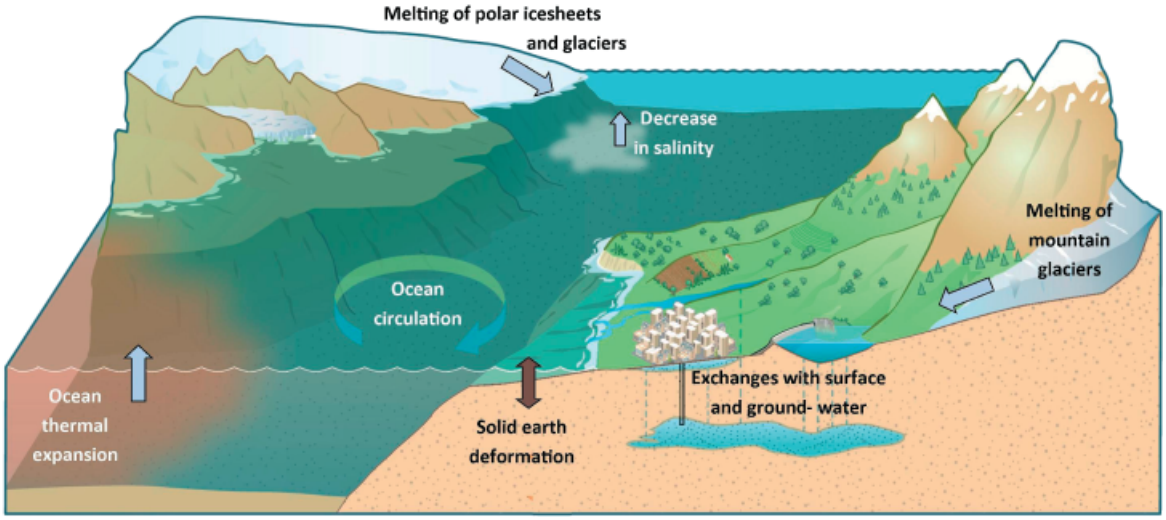

Figure 1.10: *Schematic of climate-sensitive processes and components that can influence global and regional sea level. Changes in any one of the components or processes shown will result in a sea level change [From Cazenave and Le Cozannet, 2014].*

The oceans are a central component of the climate system, by storing and transporting large amounts of heat. Indeed, more than 90% of the heat absorbed by the Earth over the last 50 years due to global warming is stored in the ocean [Levitus et al.,2012]. As the oceans warm, they expand and sea level rises, resulting in changes of the ocean water density (steric effect). It is estimated that for a 1000 m column of sea water the expansion is about 1 or 2 cm for every 0.1°C of temperature increase [Church et al., 2010]. Density changes induced by temperature changes are called thermosteric, while density changes induced by salinity changes are called halosteric. Both are important for regional sea-level changes [Durack and Wijffels, 2010]; however only the thermosteric contribution is significant for the global average ocean volume change. Thermosteric sea level

rise was a major contributor to 20th century sea level rise, and is projected to continue during the 21st century and for centuries into the future [Rhein et al., 2013]. Ocean thermal expansion has been estimated from analyses of Expandable Bathy Thermographers (XBT) data collected over the past 50 years by ships [Ishii and Kimoto, 2009; Levitus et al., 2012], and during the last 10 years by automatic profiling floats of the Argo system, mostly in the upper layers (up to depths of 700-2000 m). These data indicate that the ocean heat content has increased during the past few decades, in particular, since 1970 [Ishii and Kimoto, 2009; Levitus et al., 2012], resulting in a significant thermosteric sea level rise (Fig 1.11). Although very sparse, the few available deep ocean temperature measurements (below 2000 m) indicate that the deep ocean has also warmed [Purkey and Johnson, 2010] in the recent decades, but its exact contribution to sea level rise remains uncertain. In addition, to the much improved observational database, data assimilation techniques combining observations and models are now being applied to the ocean. This approach helps overcoming the inadequate data distribution and allows synthesizing all available data in one consistent estimate of the evolving ocean [Gregory et al., 2001]. Since the 1960s and 1970s, global ocean and coupled atmosphere-ocean general circulation models (AOGCMs) have been developed, and they improved rapidly as numerical techniques and ocean data sets increased. These models are the basis for the projections of global averaged steric sea level rise and the regional distribution of sea level rise during the 21st century and beyond [Gregory et al., 2006, 2013].

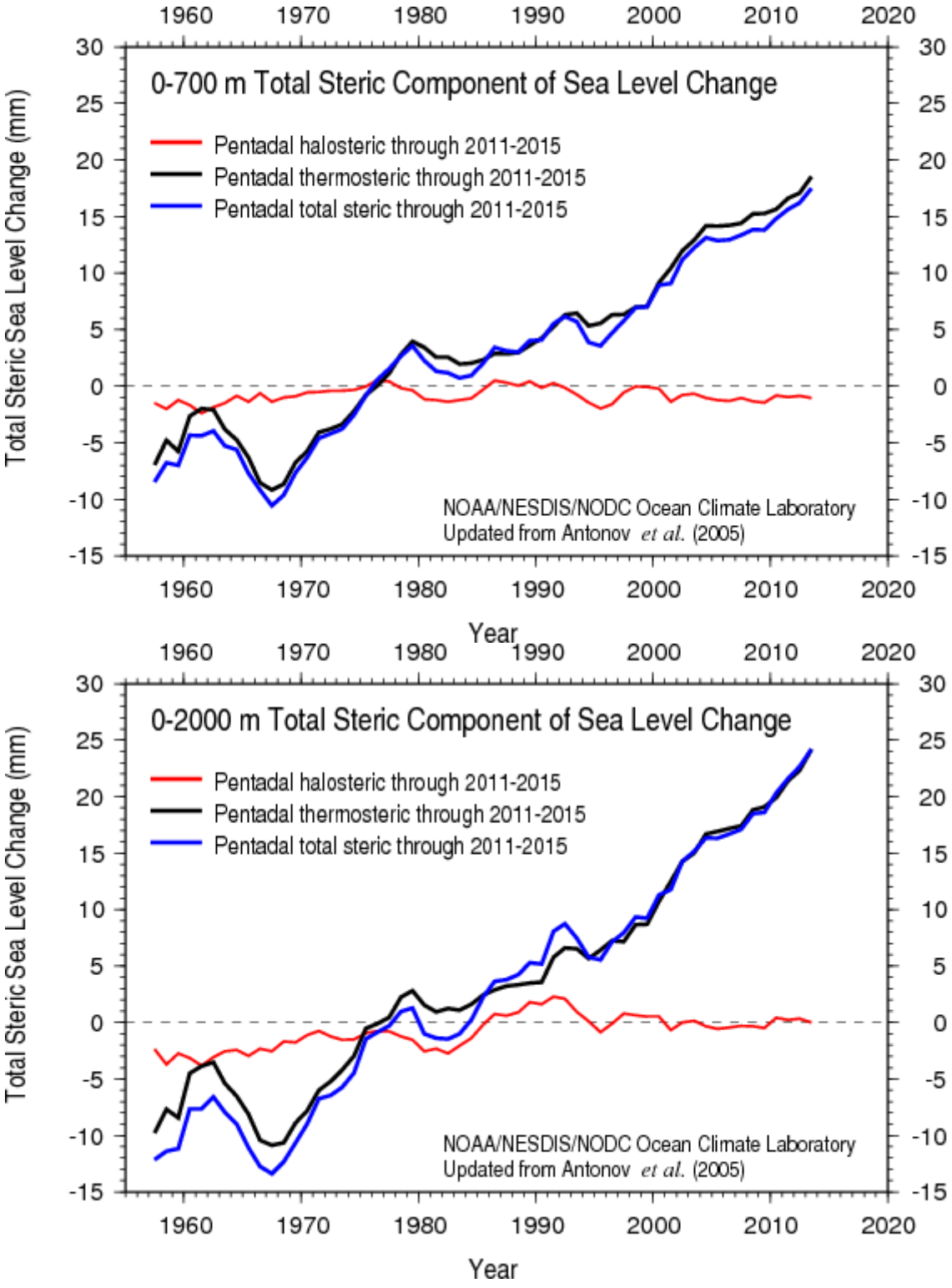

Figure 1.11: *Time series of halosteric (red curve), thermosteric (black curve) and total steric sea level component (mm) for the 0-700 m (top) and 0-2000 m (bottom) layers based on running pentadal (five-year) analyses. Reference period is 1955-2015. Each pentadal estimate is plotted at the midpoint of the 5-year period [updated from Antonov et al., 2005, NOAA 2015].*

The other main contribution to sea level rise is provided by the increase of water mass due to melting of mountain glaciers and ice sheets from Greenland and Antarctica. GMSL change resulting from ocean mass variation is called barystatic. A signal of added mass to the ocean propagates around the globe such that all regions experience a sea level change [Lorbacher et al., 2012]. In addition, an influx of freshwater changes ocean temperature and salinity, and thus, changes ocean currents and local sea level [Stammer, 2008]; these signals need decades to propagate around the global ocean. The amount of barystatic sea level change due to the addition or removal of water mass is called sea level equivalent (SLE). This is the conversion of a water mass (ice, liquid or vapor) into a volume, by using a density value equal to 1000 kg m^{-3} divided by the present day ocean surface equal to $3.625 \cdot 10^{14} m^2$. Thus, a water mass of $362.5 \cdot 10^{12}$ kg need to be added to the ocean to cause 1 mm of global mean sea level rise.

Being very sensitive to global warming, mountain glaciers and small ice caps have retreated worldwide during the twentieth century, with significant acceleration since the early 1990s [Meier et al., 2007]. Changes in glaciers are measured through the survey of glacier extension, mass and volume by means of a wide range of observational techniques [Vaughan et al., 2013]. Most glaciers are now monitored using remote sensing methods such as aerial photography and satellite imaging [Leclercq and Oerlemans, 2012], and by GPS observations [King, 2004]. Since 2003, accurate measurement of the Earth gravity field variations from the GRACE satellites provide a most significant contribution in estimating ice mass variation/changes [Gardner et al., 2013]. For the mass balance of ice sheets, little is known before the 1990s because of inadequate and incomplete observations. It is estimated that if totally melted, Greenland and West Antarctica (the instable part of the continent) would raise sea level by about 7 m and 3-5 m, respectively [Lemke et al., 2007]. Even a small amount of ice mass loss from the ice sheets would be able to produce substantial sea level rise; thus, the contribution of the ice sheets to GMSL need to be controlled with higher precision. Since the early 1990s, different remote sensing observations (airborne and satellite radar and laser altimetry, interferometric synthetic aperture radar –InSAR–, and space gravimetry from the GRACE mission) have provided important observations of the mass balance of the ice sheets, indicating that Greenland and West Antarctica are losing mass with an accelerated rate [Velicogna, 2009; Rignot et al., 2011]. For the period 1993-2003, less than 15% of the rate of global sea level rise was due to the ice sheets [Lemke et al., 2007], but this contribution has nearly doubled since 2003-2004 [Shepherd et al., 2012; Vaughan et al., 2013]. In addition to these observations, Regional

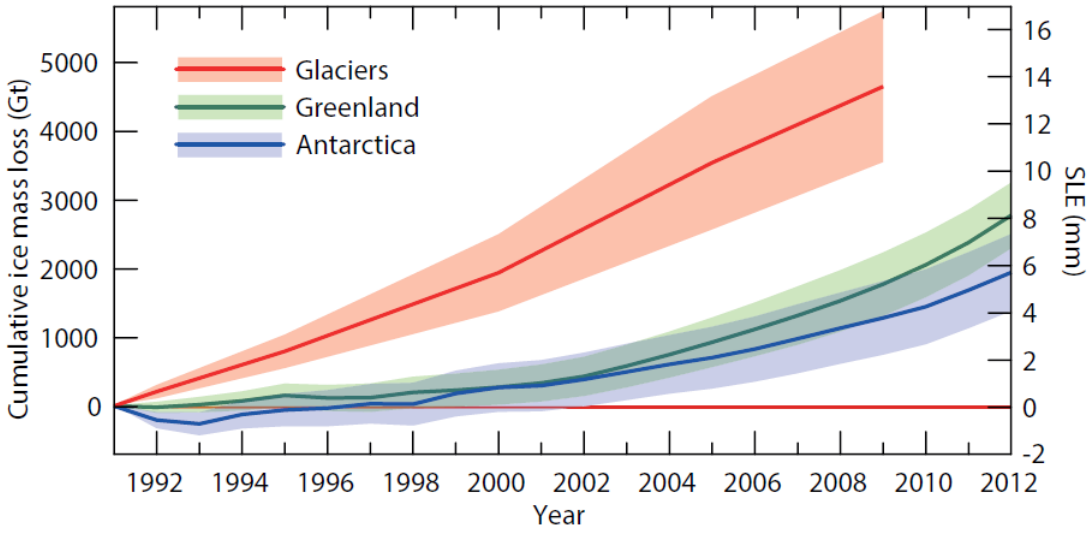

Figure 1.12: *Contribution of Glaciers and Ice Sheets to sea level change. Cumulative ice mass loss from glacier and ice sheets (in sea level equivalent) is 1.0 to 1.4 mm/yr for 1993-2009 and 1.2 to 2.2 mm/yr for 2005-2009 [From Vaughan et al., 2013].*

Climate Models (RCMs) are now the primary source of ice sheet surface mass balance (SMB) projections. They incorporate, or are coupled to, sophisticated representations of the snow and ice surfaces mass and energy budget [Lenaerts et al., 2012]. SMB is primarily the difference between snow accumulation and ablation (the total melted snow and ice). These models require information on the state of the atmosphere and of the ocean at its boundary. These information are derived from reanalysis data sets or AOGCMs. The main challenge, faced by models attempting to assess sea level change from glaciers, is the small number of glaciers for which mass budget observations are available (about 380) [Cogley, 2009a], as compared to the total number (more than 170,000) [Arendt et al., 2012]. Statistical techniques are used to derive relations between observed SMB and climate variables for the small sample of surveyed glaciers, these relations are then used for unsurveyed regions of the world. These techniques often include area-volume scaling to estimate glacier volume from their more readily observable areas [Marzeion et al., 2012; Hirabayashi et al., 2013].

An additional contribution to changing sea level comes from the storage of water on land: in lakes, dams, rivers, wetlands, soil moisture, snow cover, permafrost, and aquifers. These respond to both climate variations and to anthropogenic activities (dam building, underground water mining, irrigation, urbanization, deforestation, etc.). No global data sets exist to estimate the historical land water components; estimates of climate related changes in land water storage over the

past few decades rely on global hydrological models [Milly et al., 2010] and, since 2002, on space gravimetry observations from the GRACE mission that allows direct determination of the total land water storage variations due to the combination of climate variability and human activities [Llovel et al., 2011]. Model-based estimates of land water storage change, caused by natural climate variability, do not suggest any long-term climatic trend during the second half of the twentieth century [Milly et al., 2003; Ngo-Duc et al., 2005]; however, they documented interannual to decadal fluctuations, equivalent to several millimeters of sea level. Recent studies have shown that the observed GMSL interannual variability correlates with ENSO (El Niño Southern Oscillation) indices [Nerem et al., 2010] and is inversely related to ENSO-driven changes of terrestrial water storage, especially in the tropics [Llovel et al., 2011]. During El Niño events, sea level (and ocean mass) tends to increase [Chambers, 2011; Cazenave et al., 2012]. The reverse happens during La Niña events, as seen during 2010-2011, when there was a decrease in GMSL due to a temporary increase in water storage on the land, especially in Australia, northern South America, and southeast Asia [Boening et al., 2012]. Human interventions on land water storage also induce sea level changes. Chao et al. [2008] showed that dam building along rivers and associated reservoir impoundments has lowered sea level by about -0.5 mm/yr during the second half of the twentieth century. Inversely, groundwater extraction for crop irrigation in regions of intensive agriculture has led to a few tenths of mm/yr sea level rise [Wada et al., 2013]. Although subject to considerable uncertainty, estimates for the past few decades suggest near cancelation between net groundwater depletion and dam/reservoir contribution [Konikow, 2011; Wada et al., 2012]. However, the situation might change in the future because of expected increasing groundwater depletion and decreasing dam building, leading to a net positive contribution to sea level [Konikow, 2011; Wada et al., 2012, 2013].

1.4.2 Observed sea level rise and budget estimations

Many studies have been published in recent years on the comparison between observed sea level rise and the sum of the estimated single contributions [Church et al., 2011; 2013; Hanna et al. 2013; Dieng et al., 2015]. The observed sea level change from instrumental records is mainly composed of tide gauge measurements over the past two centuries, and, since the early 1990s, of satellite-based radar altimeter measurements.

The estimate of the long-period (centennial period) GMSL rise, using the tide

gauge records data base [Holgate et al., 2013; PSMSL 2015] is challenging. In fact, tide gauges sample the ocean sparsely and non-uniformly, with a bias towards coastal sites and the Northern Hemisphere, there are a few sites at latitude greater than 60°, and significant interannual and decadal-scale fluctuations are present in all time series [Church and White, 2011; Hay et al., 2013]. Many authors have compute the mean rate of twentieth century GMSL rise from the available tide gauges data, all with different approaches [Jevrejeva et al., 2006; Holgate, 2007; Jevrejeva et al., 2008; Church and White, 2011]. The estimates of GMSL rise obtained from these studies ranges from 1.6 to 1.9 mm/yr. Also, IPCC AR5 [2013] suggests that there is a 95% probability that GMSL rise from 1901 to 1990 was greater than 1.3 mm/yr. However, independent model and data-based estimates of the individual sources of GMSL, including mass flux from glaciers and ice sheets, thermal expansion of oceans, and changes in land water storage, are insufficient to account for the GMSL rise estimated from tide gauge records [Gregory et al., 2013]. Church et al. [2013] presents a list of contributing effects to GMSL rise from 1901 to 1990 (see Table 1.2), the total budget turns out to be $+0.5 \pm 0.4$ mm/yr (90% Confidence Interval - CI) lower than the tide gauge derived rate of $+1.5 \pm 0.2$ mm/yr (90% CI) estimated by Church and White [2011] for the same period. This discrepancy has been attributed to underestimation of almost all possible sources: thermal expansion, glacier mass balance, and Greenland or Antarctic ice sheet mass balance [Church et al., 2013].

Table 1.2: *Global mean sea level budget (mm/yr) over different time intervals from observations and from model-based contributions. The modeled thermal expansion and glacier contributions are computed from the CMIP5 (Coupled Model Intercomparison Project Phase 5 [IPCC AR5, 2013]) results, using the model of Marzeion et al. [2012a] for glaciers. The land water contribution is due to anthropogenic intervention only, not including climate-related fluctuations. Notes: a) data for all glaciers extend to 2009, not 2010; b) This contribution is not included in the total because glaciers in Greenland are included in the observational assessment of the Greenland ice sheet; c) Difference between observed GMSL rise and the sum of the individual components [From Church et al., 2013].*

Source	1901–1990	1971–2010	1993–2010
Observed contributions to global mean sea level (GMSL) rise			
Thermal expansion	–	0.8 [0.5 to 1.1]	1.1 [0.8 to 1.4]
Glaciers except in Greenland and Antarctica[a]	0.54 [0.47 to 0.61]	0.62 [0.25 to 0.99]	0.76 [0.39 to 1.13]
Glaciers in Greenland[a]	0.15 [0.10 to 0.19]	0.06 [0.03 to 0.09]	0.10 [0.07 to 0.13][b]
Greenland ice sheet	–	–	0.33 [0.25 to 0.41]
Antarctic ice sheet	–	–	0.27 [0.16 to 0.38]
Land water storage	–0.11 [–0.16 to –0.06]	0.12 [0.03 to 0.22]	0.38 [0.26 to 0.49]
Total of contributions	–	–	**2.8 [2.3 to 3.4]**
Observed GMSL rise	**1.5 [1.3 to 1.7]**	**2.0 [1.7 to 2.3]**	**3.2 [2.8 to 3.6]**
Modelled contributions to GMSL rise			
Thermal expansion	0.37 [0.06 to 0.67]	0.96 [0.51 to 1.41]	1.49 [0.97 to 2.02]
Glaciers except in Greenland and Antarctica	0.63 [0.37 to 0.89]	0.62 [0.41 to 0.84]	0.78 [0.43 to 1.13]
Glaciers in Greenland	0.07 [–0.02 to 0.16]	0.10 [0.05 to 0.15]	0.14 [0.06 to 0.23]
Total including land water storage	**1.0 [0.5 to 1.4]**	**1.8 [1.3 to 2.3]**	**2.8 [2.1 to 3.5]**
Residual[c]	**0.5 [0.1 to 1.0]**	**0.2 [–0.4 to 0.8]**	**0.4 [–0.4 to 1.2]**

A more recent study performed by Hay et al. [2015] revisits the analysis of GMSL since the start of the twentieth century using two statistical methods: Kalman smoothing (KS) and Gaussian process regression (GPR). Both approaches naturally accommodate spatially sparse and temporally incomplete sampling of a global sea level field, thus providing a rigorous, probabilistic framework for uncertainty propagation, correcting also for a distribution of GIA and ocean models (see Hay et al., 2015, for complete description of these methods). The mean GMSL rate for 1901-1990 estimated from the KS and GPR analysis are, respectively, 1.2 $\pm$ 0.2 mm/yr and 1.1 $\pm$ 0.4 mm/yr, significantly lower than the estimates of other studies for the same period (Fig 1.13). This estimate closes the sea-level budget for 1901-1990 estimated in AR5 [Church et al., 2013] without appealing to an underestimation of individual contributions from ocean thermal expansion, glacier melting, or ice sheet mass balance [Hay et al., 2015].

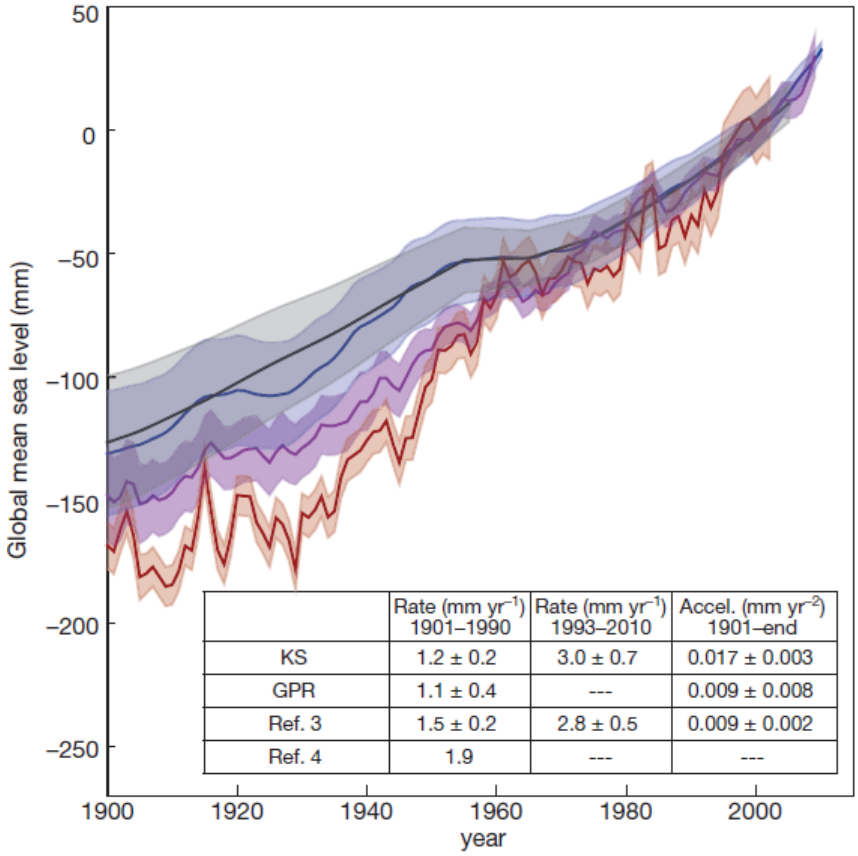

	Rate (mm yr^{-1}) 1901–1990	Rate (mm yr^{-1}) 1993–2010	Accel. (mm yr^{-2}) 1901–end
KS	1.2 ± 0.2	3.0 ± 0.7	0.017 ± 0.003
GPR	1.1 ± 0.4	---	0.009 ± 0.008
Ref. 3	1.5 ± 0.2	2.8 ± 0.5	0.009 ± 0.002
Ref. 4	1.9	---	---

Figure 1.13: *Time series of GMSL for the period 1900-2010. Shown are estimates of GMSL based on KS (blue curve), GPR (black curve), Ref.3 refers to Church and White [2011] (magenta curve) and Ref.4 to Jevrejeva et al., [2008] (red curve). Shaded regions show ±1σ uncertainty. Inset, trends for 1901-1990 and 1993-2010, and accelerations, all with 90% CI (not available for Jevrejeva et al., [2008]). Since the GPR methodology outputs decadal sea level, no trend is estimated for 1993-2010 [From Hay et al., 2015].*

Budget studies are more reliable for the satellite altimetry era due to the introduction of several global observation systems. In addition to satellite radar altimetry, the GRACE mission, the network of Argo buoys, the InSAR and GPS techniques, made it possible to accurately quantify each budget component (Fig 1.14).

In Church et al., 2013, the observed rate of global mean sea level rise over the 1993-2010 time span is compared to estimates of the sum of individual components. The rate of GMSL rise for this period is +3.2 ± 0.4 mm/yr, based on the average of altimeter time series published by multiple groups [Ablain et al., 2009; Beckley et al., 2010; Nerem et al., 2010; Church and White, 2011; Masters et al., 2012]. The tide gauges analysis from Church and White [2011] for the 1993-2010 period gives a rate of +2.8 ± 0.5 mm/yr. The result of the KS method from Hay et al.

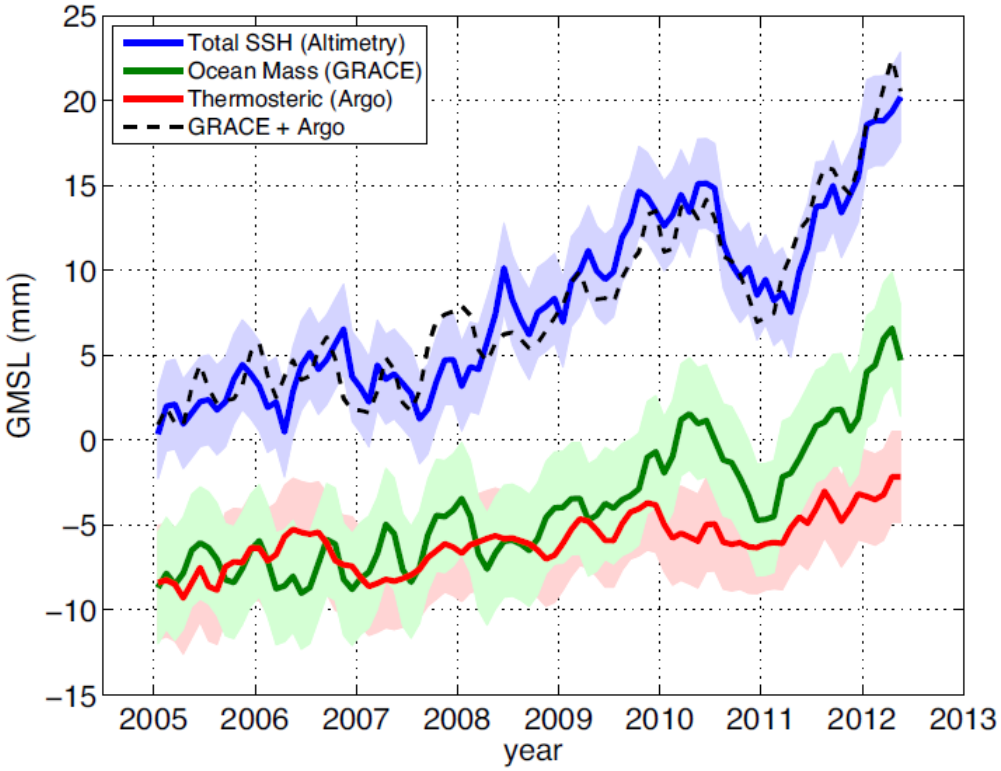

Figure 1.14: *Global mean sea level from altimetry from 2005 to 2012 (blue line). Ocean mass changes are shown in green (as measured by Gravity Recovery and Climate Experiment (GRACE)) and thermosteric sea level changes (as measured by the Argo Project) are shown in red. The black line shows the sum of the ocean mass and thermosteric contributions [From Church et al., 2013].*

[2015] is in agreement with the previous results, providing a rate of +3.0 ± 0.7 mm/yr. The different analysis show that the rate of sea level rise during the last two decades is about twice as much the mean rise of the twentieth century. Hay et al. [2015] calculate an acceleration of 0.009 ± 0.002 mm/yr^2 based on the Church and White [2011] time series, but, using the GMSL rate calculated with the KS method (1.2 ± 0.2 mm/yr for the period 1900-1990) the estimated acceleration is significantly higher and equal to 0.017 ± 0.003 mm/yr^2. It has been suggested that this higher rate cannot be attributed to decadal variations, it rather reflects a recent acceleration of the global mean rise (since the early 1990s) [Merrifield et al., 2009]. However, this was questioned by other studies stating that, because of low-frequency, multidecadal sea level fluctuations, any recent acceleration is hard to detect [Chambers et al., 2012]. While, on the one hand, this is certainly a matter of concern because of the relatively short length of the altimetry record, on the other, it is worth mentioning that the altimetry-based rate of sea level rise is remarkably stable. Since more than a decade, continuous sea level time series

give a nearly constant rate value in the range of 3.1 - 3.3 mm/yr [Cazenave and Llovel, 2010; Cazenave and Le Cozannet, 2014].

For the satellite altimetry era, the contributions from thermal expansion, including a small, poorly known contribution from the deep ocean, glaciers, Greenland, and Antarctica, in percentage of the observed 3.2 mm/yr rate of GMSL rise, are 34% [Cazenave and Llovel, 2010], 27% [Gardner et al., 2013], 10%, and 8.5%, respectively [Shepherd et al., 2012]. This means that ocean warming and total land ice melt explain 34% and 45.5% respectively of the global mean rise for the altimetry period, leaving a residual term of about 20%. Church et al. [2013] consider an additional contribution equaling 12% for the anthropogenic land water storage change (net effect of groundwater depletion and dam/reservoir retention). These values lead to quasi closure of the sea level budget over the altimetry era, but the combination of systematic errors and/or lack of information on some components, like ocean heat content below 2000 m, hinders perfect closing of the sea level budget [Church et al., 2013; Dieng et al., 2015].

Chapter 2

Data selection and acquisition

2.1 Regional sea level and vertical land motion

Sea level is not rising uniformly (Fig. 2.1). Satellite altimetry observations, over the last two decades, have revealed that rates of sea level rise at regional scale may differ substantially from the global mean rise. This spatial variability is mostly due to the redistribution of heat, salt and water mass, associated with ocean dynamical processes [Stammer et al., 2013].

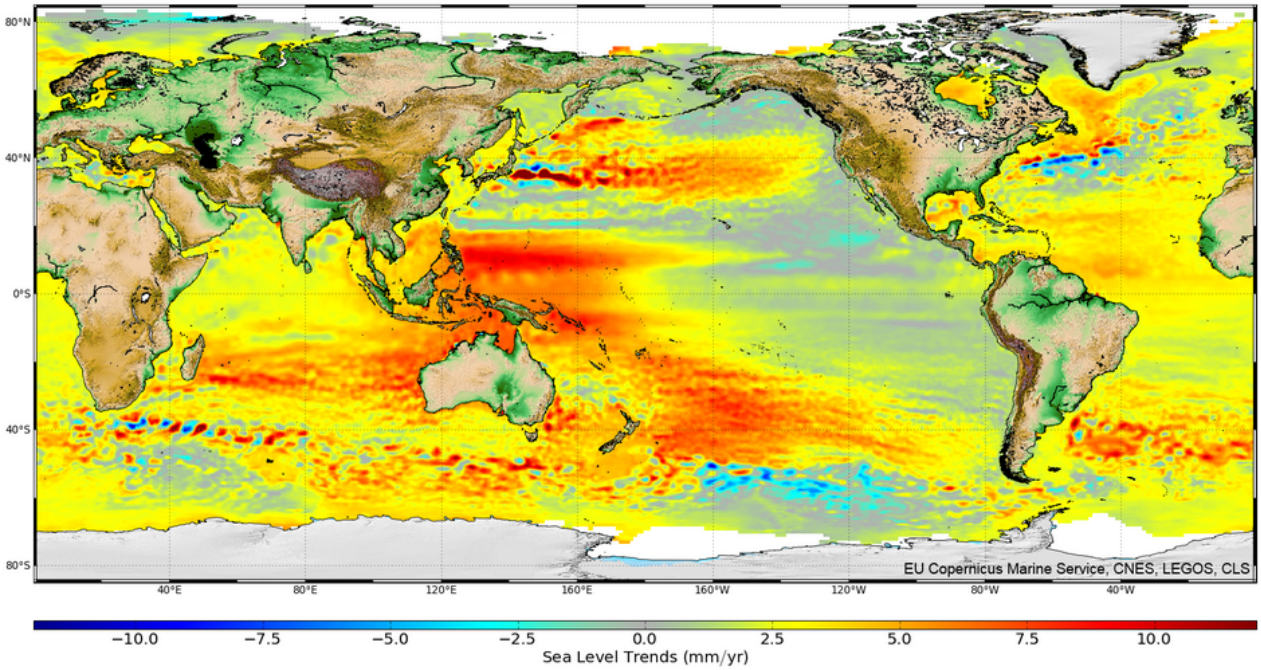

Figure 2.1: *Spatial trend patterns of altimetry-based global sea level over 1993–2014. Gridded multi-mission SSALTO/DUACS data (from AVISO).*

Tide gauges measurements also suggest substantial spatial variations in sea

level. However, tide gauge records are the sum of two components:

- the absolute sea level, the same measured by satellite altimetry, which is the climate-related component of the sea level variability;
- the vertical land motion (VLM) of the tide gauge benchmark, to which the sea level observations are referred.

Any vertical motion at a tide gauge site affects the measured sea level. The VLM can be equal or larger than the local absolute sea level signal, thus masking the climatic-related information of the tide gauge record [Douglas, 2001]. Therefore, the principal difference between the data acquired by satellite altimetry and tide gauges is due to the VLM [Nerem and Mitchum, 2002]. In order to correct the tide gauge records, the vertical land motion need to be estimated; one possible approach is the use of space geodetic techniques [Zerbini et al., 1996; Wöppelmann et al., 2007]. Among them, the most used is the GPS. While models account only for the GIA, permanent GPS stations, co-located at tide gauge sites, measure accurately and continuously vertical motions.

Figure 2.2 illustrates a tide gauge station co-located with a GPS antenna/receiver and satellite altimetry sea level measurements. The tide gauge measures the relative sea level (S). This record is referred to a ground benchmark which can be subjected to VLM (U); these are estimated by means of GPS data. The satellite altimeter measures the absolute sea level (N), referred to the Earth's center of mass. The absolute sea level at the tide gauge site can be estimated by

$$N = S + U \tag{2.1}$$

In the ideal case study presented in the figure, it is assumed that the tide gauge and the satellite are observing the same sea level at the coast and offshore, respectively, and that the GPS is measuring the VLM affecting the tide gauge station [Wöppelmann et al., 2009].

Despite the many efforts done to combine the information from tide gauges and GPS measurements, the availability of co-located GPS stations is still limited [Santamarìa-Gòmez et al., 2012]. Because of this, the correction of relative sea level trends, using GPS-derived estimates of VLM, requires careful consideration. High-accuracy GPS observations are only available since early-mid 1990s (the earliest GPS data in this study begin in 1996). Therefore, to correct tide gauge data collected prior to early 1990s, one should extrapolate to the past a constant GPS-derived VLM rate. It is obvious that this assumption might not be correct,

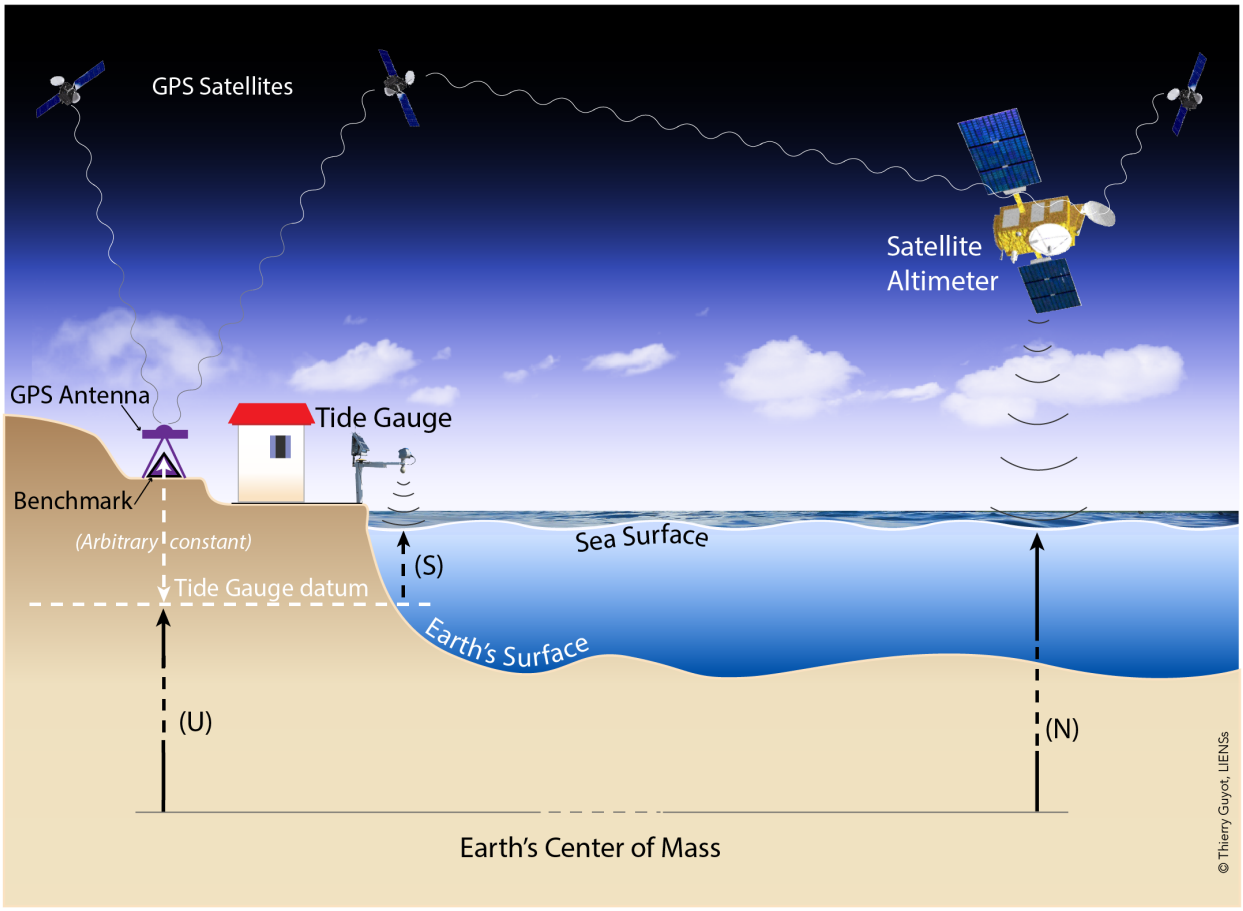

Figure 2.2: *Scheme of a GPS-equipped tide gauge station and satellite altimetry measurements [From Wöppelmann et al., 2009].*

especially in active tectonic areas and in regions subject to strong subsidence or uplift [Ballu et al., 2011; Raucoles et al., 2013]. However, many authors support this assumption [Woodworth, 1990; Douglas 2001; Wöppelmann et al., 2007; Santamarìa-Gòmez et al., 2012]. A further problem might arise if the GPS receiver and the tide gauge site are not co-located. In fact, the VLM measured at the GPS station might not be representative of that affecting the tide gauge benchmark. The vertical motion can differ significantly even over short distances of few meters in unstable regions. However, GPS and tide gauge stations can be separated by several kilometers, as long as the ground upon which the instruments are settled undergoes the same vertical motion [Bevis et al., 2002]. Thus, it is recommended that the tide gauge and the GPS should be as close as possible, in order to avoid a bias applying the VLM correction. The best case is, of course, when a GPS is directly installed on top of the tide gauge station. Therefore, a distance threshold, in which a GPS station is considered suitable to correct the VLM at a tide gauge, should be identified according to the stability of the area. Typical maximum distances can be in the order of 15-20 km [Mazzotti et al., 2007; Wöppelmann et al. 2007; Santamarìa-Gòmez et al., 2012].

In this study, by following the preceding considerations, tide gauges time series are analyzed over the period 1993-2014. The records are corrected for the VLM, using the observations of the nearest GPS station, when available. The results are then compared with satellite altimetry measurements during the same time interval. The area investigated is the Mediterranean Sea, with particular focus on the Adriatic area.

2.1.1 Mediterranean Sea

The Mediterranean Sea is located between Africa and Europe and has a surface of $2.5 \cdot 10^6 \text{km}^2$. It is connected to the Atlantic Ocean through the Gibraltar Straits, which is roughly 13 km wide at its narrowest point. The basin is surrounded by populated areas, and many of them are low-lying regions, vulnerable to sea level rise [Tanhua et al., 2013]. Due to its semi-enclosed nature, the Mediterranean Sea is strongly influenced by the seasonal atmospheric variations over Europe and North Africa [Gomis et al., 2012]. The net evaporation over the basin exceeds the precipitations and the river inflow [Tanhua et al., 2013]. The loss of water at the surface is compensated by the water mass received from the Atlantic Ocean, through the Gibraltar Straits. However, this balance is not perfectly attained and this gives rise to a mean sea level tendency (Fig. 2.3). The Gibraltar Straits

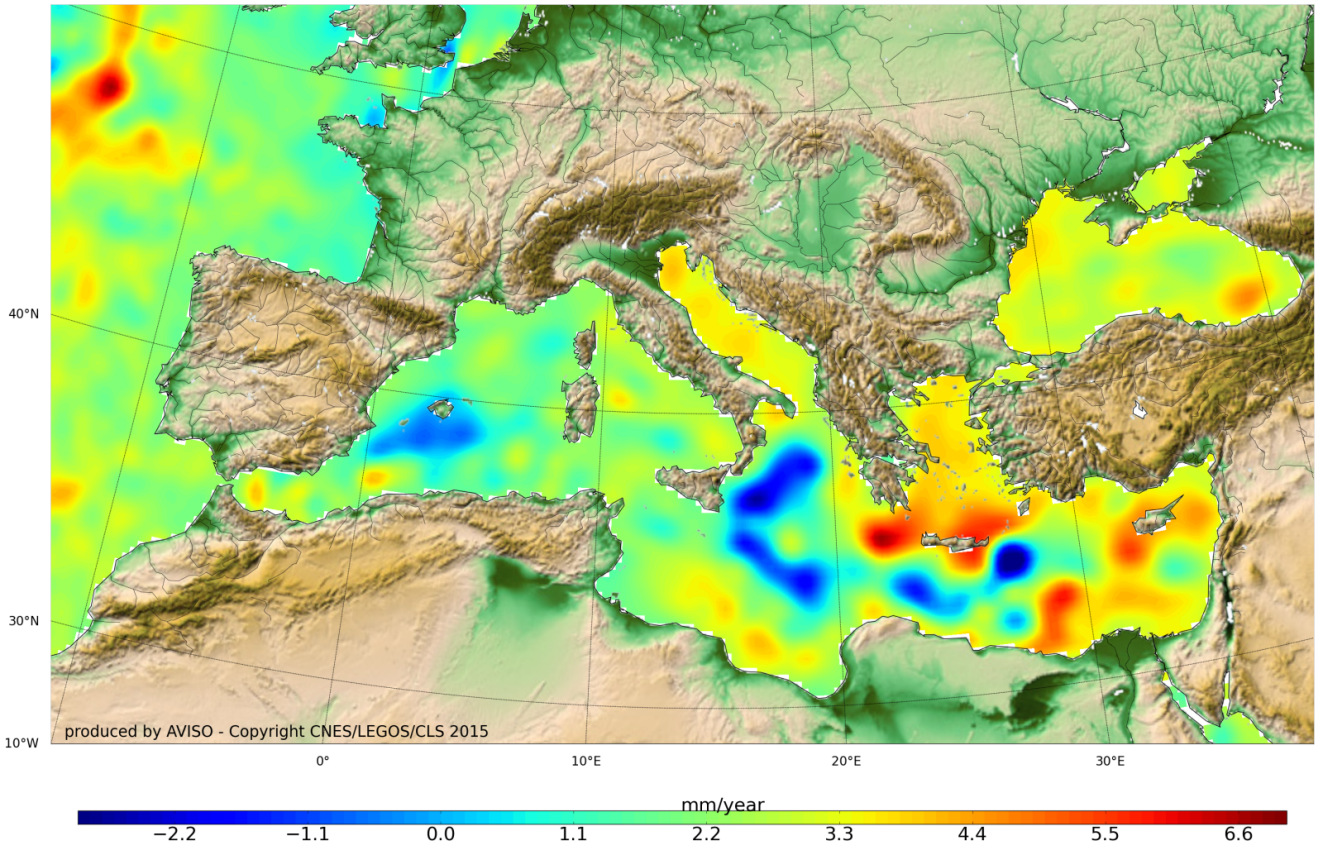

Figure 2.3: *Regional trends of sea level anomalies in the Mediterranean Sea over 1993-2014 from altimetry-based data (from AVISO).*

mass transport and the surface water flux are called the incompressible terms. They are the mass component of the mean sea level in the Mediterranean Sea, which is the main contributor to its variability [Pinardi et al., 2014]. The second contribution to the mean sea level tendency of the basin comes from the steric component, which is due to the buoyancy fluxes that account for the thermosteric and halosteric components.

Active tectonics is widespread in the Mediterranean region [Zerbini et al., 1996; Becker et al., 2002]. The collisions between the African, Eurasian and Arabic plates have produced a very complex tectonic regime of micro-plates, and volcanic activity and earthquakes may cause sudden or gradual land movements [Jimenez-Munt et al., 2003]. In coastal areas, land subsidence is frequent, especially in river deltas such as those of the Nile and the Po, which are subject to the balance between deposition and compaction of sediments. The Adriatic Sea is the northern part of the Mediterranean Sea. It extends over an area in the order of 10^5km^2 and it is connected to the Mediterranean through the Otranto Straits in the south. There

are many tide gauges along the Adriatic coasts, and three of them are among the longest records in the world (Marina di Ravenna (former Porto Corsini), Trieste and Venice). The Northern Adriatic is an area particularly vulnerable to sea level rise, subjected to both natural and anthropogenic subsidence [Zerbini et al., 2007]. It is thus important to correctly estimate the VLM affecting the tide gauges in this region, in order to accurately identify climate-related sea level variations.

2.2 Tide gauge data

A total of 35 tide gauge stations have been selected because their time series, over the period of this analysis 1993-2014, are complete to, at least, 85% [Douglas, 2001; Wöppelmann et al., 2007]. The records were taken from two different networks: the Permanent Service for Mean Sea Level (PSMSL) [http://www.psmsl.org/] and the Rete Mareografica Nazionale (RMN) [http://www.mareografico.it/] of the Italian Istituto Superiore per la Protezione e Ricerca Ambientale (ISPRA).

2.2.1 Permanent Service for Mean Sea Level

The PSMSL was established in 1933. Since then, it has collected and analyzed sea level data from the global network of tide gauges. The sea level data used in this analysis are monthly means from the Revised Local Reference (RLR) dataset. RLR data are the most appropriate for scientific purposes. In fact, these records are checked and corrected for local datum change, thus reducing them to a common reference level using the tide gauge datum history [Woodworth and Player, 2003]. The common datum is arbitrarily set at approximately 7000 mm below mean sea level, in order to avoid negative numbers in the resulting RLR monthly mean values. In the Mediterranean Sea, more than 100 tide gauges are available. However, the spatial distribution is not uniform and a limited number of stations are present in the southern part of the basin. Among the available stations, 22 have the required 85% of complete data for the period 1993-2014. The metadata of these stations and the percentage of completeness of their time series are presented in Table 2.1.

Table 2.1: *Tide gauge stations belonging to the PSMSL used in this work. The first column lists the tide gauge location (nearest city), the second indicates the country, third and fourth the geographical coordinates (as provided by PSMSL) and the last shows the percentage of completeness of the time series.*

Tide Gauge	Country	Longitude Deg.	Latitude Deg.	Data percentage (1993-2014)
Barcelona	Spain	2.17	41.34	91
Ceuta		-5.32	35.89	94
L'Estartit		3.20	42.05	100
Malaga		-4.42	36.71	94
Tarifa		-5.60	36.01	94
Valencia		-0.31	39.44	93
Marseille	France	5.35	43.28	87
Toulon		5.91	43.11	92
Trieste	Italy	13.76	45.65	100
Bakar	Croatia	14.53	45.3	95
Dubrovnik		18.06	42.66	95
Rovinj		13.63	45.08	95
Split-Gradska Luka		16.44	43.51	95
Zadar		15.23	44.12	88
Alexandroupolis	Greece	25.88	40.84	95
Katakolon		21.32	37.64	93
Khalkis North		23.59	38.47	92
Khios		26.14	38.37	88
Leros		26.85	37.13	92
Levkas		20.71	38.83	89
Siros		24.95	37.44	90
Thessaloniki		22.93	40.63	93

2.2.2 Rete Mareografica Nazionale

The RMN was created in 1998. The present network is composed of 36 stations evenly distributed across the Italian national territory. The sea level data are available as quality checked hourly values. Each record is referred to a local benchmark, which is controlled by means of high precision leveling measurements. Data collected before 1998 by the pre-existing stations can be found in the RMN

archive. The stations selected from the RMN are 13. Among them, 10 present 85% of the complete time series for the chosen analysis period. The Cagliari and Otranto stations were included because they both are very close to the required percentage of data (82% for both records). The Ortona station was included, although not reaching 85%, with the aim to have 12 stations evenly distributed on the east and west coast of the Adriatic basin. Table 2.2 lists the selected stations; seven of these time series, identified with an asterisk, present a discontinuity in summer 1998 due to change of the tide gauge instrument. A datum shift was therefore estimated for these stations. This will be described in detail in the following chapter.

Table 2.2: *Tide gauge stations from the RMN. The first column lists the tide gauge location (nearest city), the second and the third the geographical coordinates, and the last shows the percentage of completeness of the time series. The asterisk indicates that the stations were corrected for a datum shift occurring in mid-1998.*

Tide Gauge	Longitude Deg.	Latitude Deg.	Data percentage (1993-2014)
Ancona	13.51	43.62	93
Bari*	16.87	41.14	85
Cagliari	9.11	39.21	82
Catania*	15.09	37.50	88
Genova	8.90	44.40	91
Livorno*	10.30	43.55	89
Napoli*	14.27	40.84	88
Ortona	14.41	42.36	78
Otranto*	18.50	40.15	82
Ravenna	12.28	44.49	99
Salerno*	14.75	40.68	86
Taranto*	17.22	40.48	94
Venezia Punta della Salute	12.33	45.43	100

2.3 Global Positioning System Data

GPS data were used to correct the tide gauge time series for VLM. The minimum data span recommended to estimate reliable vertical velocities is three years [Blewitt and Lavallée, 2002]. Thus, only GPS records longer than 3 years were

considered. Where available, GPS stations within 20 km from a tide gauge site were selected to provide estimates of VLM. Among all the available sites, only 21 GPS stations satisfy these requirements. The GPS data were obtained from two main databases and from the archive of Department of Physics and Astronomy (DIFA) of the University of Bologna. The databases are those of the Système d'Observation du Niveau des Eaux Littorales (SONEL) [http://www.sonel.org/], and the Nevada Geodetic Laboratory (NGL) [http://geodesy.unr.edu/]. The time series of the TRIM (Trieste) and PORT (Ravenna) stations were taken from the DIFA archive (personal communication) while the CAGZ (Cagliari), CEUT (Ceuta), DUBR (Dubrovnik) and GENO (Genova) records were downloaded from the SONEL databank, those of the remaining 15 stations were collected from the NGL. The products available at SONEL are weekly time series of the vertical component of the station position, while NGL and DIFA provide daily time series of the height of the stations. Table 2.3 lists the metadata of the stations used, as well as their distances from the nearest tide gauge. In Figure 2.4 the locations of both tide gauge and GPS stations are shown.

Table 2.3: *GPS stations used in the analysis. Column 1 lists the station acronym, columns 2 and 3 the geographic coordinates latitude and longitude, column 4 the location of the nearest tide gauge, column 5 the distance between GPS and tide gauge, columns 6 and 7 show the starting and ending date of the time series, respectively, column 8 the total data span.*

GPS Station ID	Longitude (Deg.)	Latitude (Deg.)	Nearest tide gauge	Distance GPS-TG (km)	First epoch, (year)	Last epoch, (year)	Time series duration (years)
MARS	5.35	43.28	Marseille	0.00	1998.6250	2014.9584	16.33
TARI	-5.60	36.01	Tarifa	0.01	2010.3750	2014.9584	4.58
TRIM	13.76	45.65	Trieste	0.08	2007.2916	2014.9584	7.67
SPLT	16.43	43.51	Split	0.26	2004.3750	2012.2916	7.92
PORT	12.28	44.49	Ravenna	0.53	1996.5416	2014.8750	18.33
CEUT	-5.31	35.90	Ceuta	0.58	2001.8690	2006.9290	5.06
EIIV	15.08	37.51	Catania	2.01	2007.9584	2014.8750	6.92
ANCG	13.50	43.60	Ancona	2.47	2010.3750	2014.9584	4.58
MALA	-4.42	37.71	Malaga	2.63	2003.0416	2014.9584	11.92
GENO	8.92	44.42	Genova	2.73	1998.5530	2010.9890	12.44
NAPO	14.28	40.87	Napoli	3.23	2008.5416	2014.9584	6.42
DUBR	18.11	42.65	Dubrovnik	3.97	2000.7186	2010.9890	10.27
VALE	-0.34	39.48	Valencia	4.87	2001.0416	2014.9584	13.92
GIUR	18.43	40.12	Otranto	6.24	2007.9584	2014.9584	7.00
SPAN	20.71	38.83	Levkas	6.81	2007.3750	2014.9584	7.58
AUT1	23.00	40.57	Thessaloniki	9.34	2005.2916	2014.9584	9.67
FISC	14.79	40.77	Salerno	10.90	2011.8750	2014.9584	3.08
FRRA	14.29	42.42	Ortona	12.20	2010.9584	2014.9584	4.00
CAGZ	8.97	39.14	Cagliari	14.74	2002.4247	2010.9890	8.56
PORE	13.60	45.23	Rovinj	16.09	2011.8750	2014.9584	3.08
PLAN	1.99	41.42	Barcellona	17.21	2006.6250	2014.9584	8.33

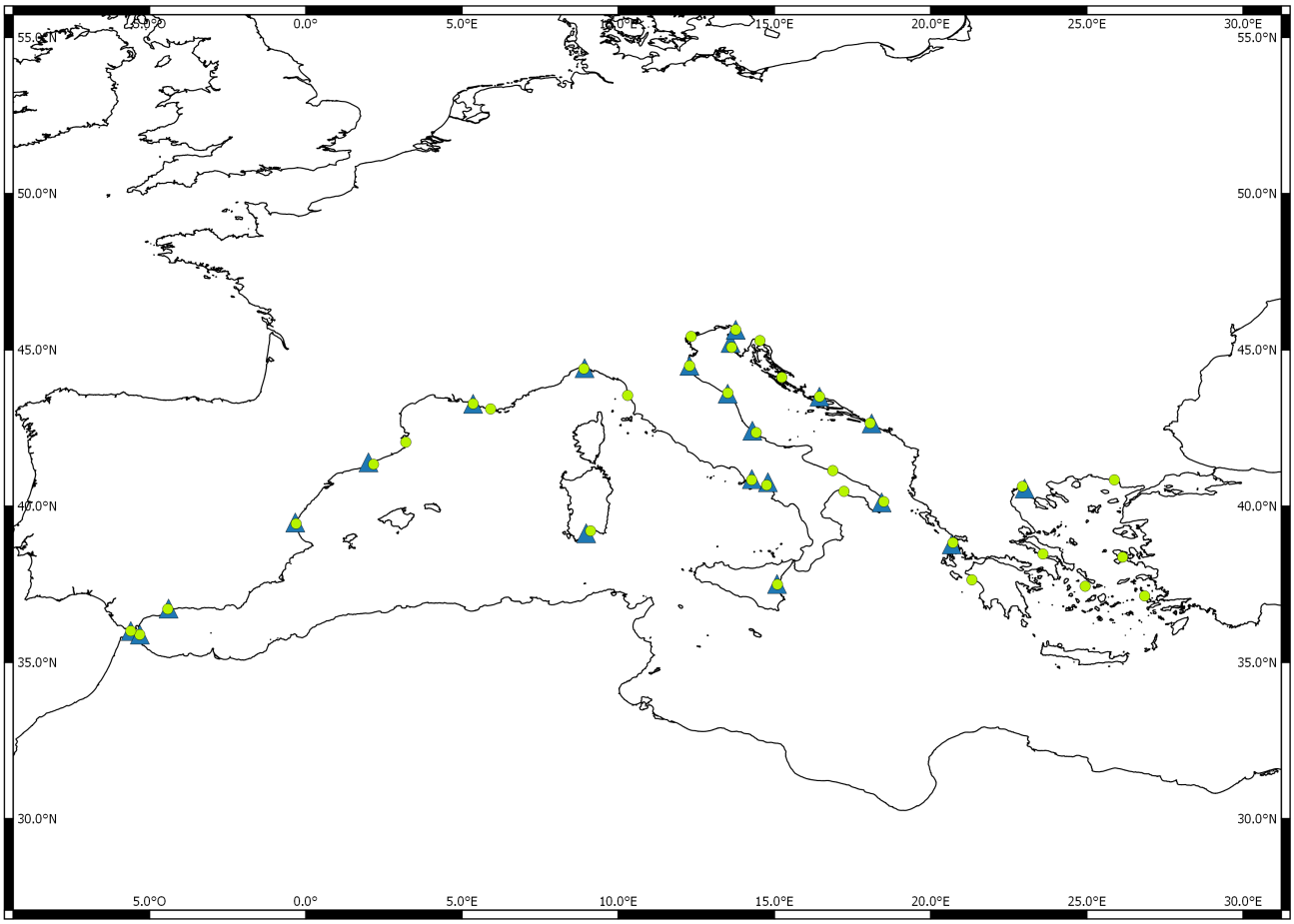

Figure 2.4: *Tide gauges (yellow dots) and nearest GPS station (blue triangle) used in this study.*

2.4 Satellite radar altimetry data

Two different satellite altimetry datasets were used: the AVISO (Archiving, Validation and Interpretation of Satellite Oceanographic data) [http://www.aviso.oceanobs.com/en/altimetry/index.html] and the Climate Change Initiative (CCI) [http://www.esa-sealevel-cci.org/]. Both were compared to the tide gauge data, in order to assess which was the most suitable for coastal studies.

2.4.1 Satellite data from AVISO

The AVISO data used are the SSALTO/DUACS Mediterranean Sea multi-mission gridded sea-level anomalies (SLA). DUACS (Data Unification Altimeter Combination System) is the SSALTO (Segment Sol multi-missions d'ALTimétrie, d'orbitographie et de localisation précise) multi-mission altimeter data processing

system. The DUACS system processes records from all satellite altimetry missions. The so called "all-sat-merged" data are obtained by combining observations from all available satellites over a selected time period. The period investigated in this analysis is from 1993 to 2014, thus, the dataset used is based on ten satellites: TOPEX/Poseidon (T/P), Jason-1 (J1), Jason-2 (J2), ERS-1 (E1), ERS-2 (E2), GFO, Envisat (EN), Cryosat-2 (C2), Saral/Altika (AL), HY-2A (H2). Figure 2.5 shows the list of available satellites in all-sat-merged products.

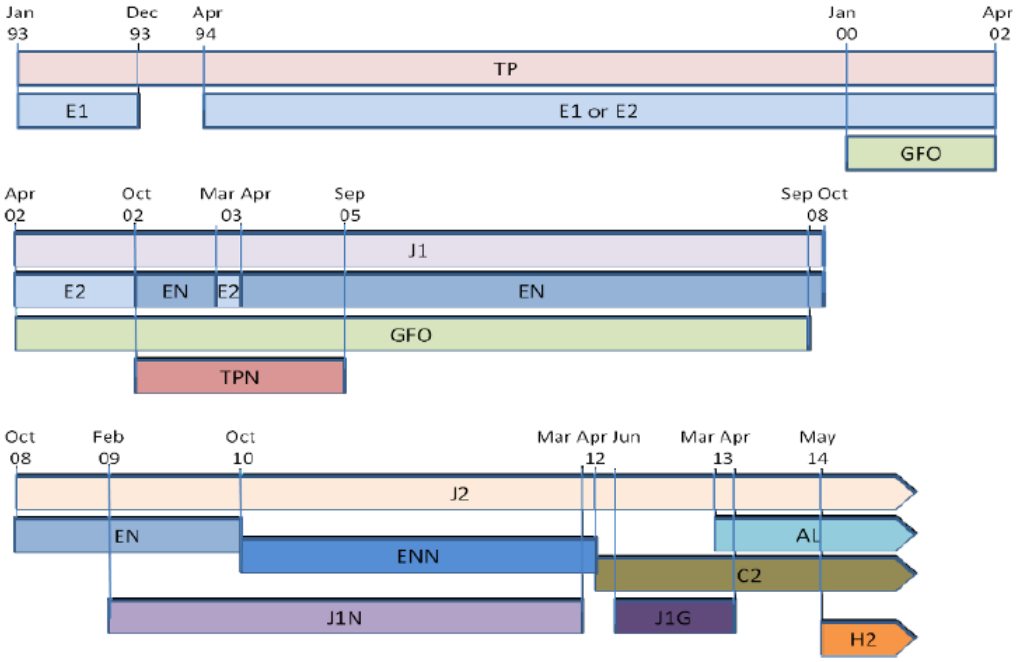

Figure 2.5: *Temporal availability of satellites in all-sat-merged products (from AVISO).*

The AVISO SLA, from different missions, consists of data interpolated into daily regular grids by means of the so called "objective analysis" [Le Traon et al., 1998; Ducet et al., 2000]. The data are provided corrected for instrumental errors, satellite position errors, signal delays and geophysical effects. A complete list of all the models can be found in AVISO User Handbook SSALTO/DUACS (M(SLA) and M(ADT) Near-Real Time and Delayed time, CLS, edition 4.4, 2015). The inverse barometer (IB) effect is accounted in the dynamic atmospheric correction (DAC) [Carrere and Lyard, 2003]. The DAC is a correction combining the high frequencies of a barotropic ocean model (MOG2D-G), forced by wind and pressure, with the low frequencies of the IB correction [Carrere and Lyard, 2003]. The provided SLA grid has spatial resolution of $1/8° \times 1/8°$, the closest point to each tide gauge station has been used to compare the two techniques (tide gauge and

radar altimetry), over the 22 years analysis period 1993-2014.

2.4.2 Climate Change Initiative project

The Climate Change Initiative (CCI) is a program of the European Space Agency (ESA), started in 2010, with the task of reprocessing all satellite altimetry data from all missions. The main objective is to produce a consistent sea-level record covering the past two decades [Ablain et al., 2015]. A set of new altimeter corrections were evaluated and compared by CCI with those used for the AVISO products. A major improvement in sea-level estimations derived from the use of pressure data from the ERA-interim reanalysis, instead of data from operational fields database. The new pressure data, produced by the European Centre for Medium-Range Weather Forecasts, were used (ECMWF) in the CCI project [Dee et al., 2011] to calculate the DAC and the dry tropospheric correction and have led to significant improvements both in reducing the GMSL error and in the estimates at regional spatial scale [Carrere et al., 2015]. The new model of the wet tropospheric delay [Fernandes et al., 2010, 2014] presents significant improvements particularly as regards the coastal and polar regions. In these particular areas, in fact, the data collected by the on-board microwave radiometers are difficult to use because of land or ice contamination. To overcome this problem, the observations of the on-board instrument and of GNSS measurements are combined in a new correction called GNSS-derived path delay (GPD). In addition, new orbit solutions were developed and selected for the ERS-1 and ERS-2 missions, improving the orbit correction for these two satellites [Rudenko et al., 2012]. The CCI products used in this thesis work are the SLA monthly grid time series with spatial resolution of 0.25°. The CCI dataset is available in the time frame 1993-2013, therefore the comparisons among the CCI altimetry data, the AVISO altimetry and the tide gauge records could only be carried out over this period. The satellites included in the CCI merged products are the same as in the AVISO dataset, except for the HY-2A mission, which starts in April 2014. Figure 2.6 shows, as an example, both the AVISO and the CCI SLA grids in the Adriatic Sea used in this work.

The following Table 2.4 provides, both for the AVISO and the CCI datasets, a complete list of the distances between the tide gauge location and the closest point of the gridded SLA.

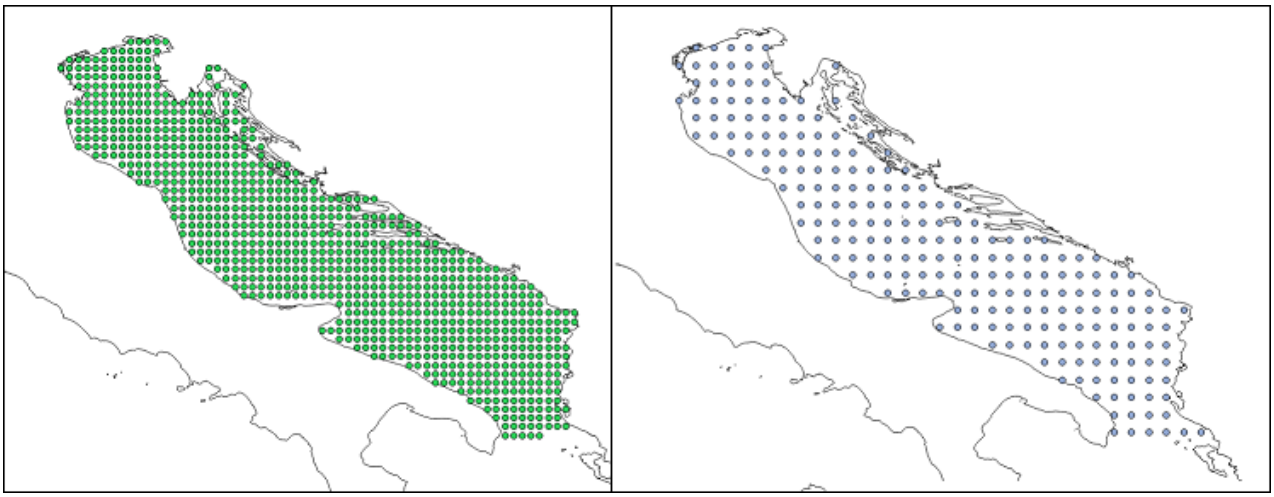

Figure 2.6: *Sample of gridded SLA in the Adriatic Sea. Left panel: AVISO gridded product, spatial resolution of 1/8 °× 1/8 ° (∼ 13 km). Right panel: CCI gridded product, spatial resolution of 1/4 °× 1/4 ° (∼ 28 km)*

Table 2.4: *Distances between the tide gauge locations and the satellite SLA gridded data over the Mediterranean Sea. The first column identifies the tide gauge station, the second and third columns show the distance between the tide gauge and the nearest point of the AVISO grid and the CCI grid, respectively.*

Tide gauge (TG)	Distance TG-AVISO data (km)	Distance TG-CCI data (km)
Alexandroupolis	6.17	4.59
Ancona	2.47	3.44
Bakar	7.58	6.14
Barcelona	3.80	12.40
Bari	6.98	15.60
Cagliari	14.74	26.15
Catania	2.01	13.78
Ceuta	5.08	13.36
Dubrovnik	10.71	18.35
L'Estartit	9.35	6.92
Genova	10.24	18.77
Katakolon	4.85	13.21
Khalkis North	10.33	8.63
Khios	7.78	16.52
Leros	8.18	15.95
Levkas	11.70	9.96
Livorno	9.14	6.51
Malaga	3.24	24.70
Marseille	5.01	9.00
Napoli	3.23	10.29
Ortona	9.33	17.49
Otranto	7.15	16.37
Ravenna	6.44	17.24
Rovinj	5.72	13.32
Salerno	10.90	19.65
Siros	10.26	8.21
Split	7.65	4.76
Taranto	14.31	25.19
Tarifa	8.66	9.28
Thessaloniki	5.58	42.90
Toulon	5.97	14.34
Trieste	7.10	25.95
Valencia	4.53	8.32
Venezia	8.19	14.97
Zadar	15.57	13.77

Chapter 3

Data Analysis

The aim of this study is to compare mean sea level (MSL) trends derived from the analysis of tide gauge time series with trends obtained from satellite altimetry data. The tide gauge sea level data required a certain amount of corrections,for this purpose, GPS time series have been acquired to estimate the possible VLM affecting the tide gauge records. Some of the coordinate time series are characterized by jumps and/or sudden discontinuities, which must be removed in order to reliably estimate the vertical velocity trends. The specific corrections applied on each dataset are illustrated in detail in this chapter.

Before proceeding with the description of the procedures exploited to correct the time series, it is worthwhile to give an overview of the STARS software [Bruni et al., 2014; Rodionov, 2004, 2006], used in the analysis to identify the possible discontinuities present in the GPS and tide gauge data.

3.1 The STARS methodology for the detection of discontinuities in time series

As introduced previously in section 2.2.2, 7 sea level time series, acquired from the RMN network, present clear discontinuities in the records, due to instrument changes. Additionally, the daily GPS coordinate time series, downloaded from the NGL database, can be affected by sudden jumps, occurring for different reasons, for example: earthquakes, changes in the station equipment, antenna mounting problems, etc. These discontinuities must be properly accounted for and removed to prevent inconsistencies in the estimation of the long-term trends. To accurately detect discontinuities in time series, it was adopted the methodological procedure developed by Bruni et al. (2014), based on the STARS algorithm, originally devel-

oped by Rodionov (2004, 2006) for climatological research. A short explanation of the discontinuities identification strategy is reported here, a complete description of the STARS algorithm can be found in Bruni et al. (2014).

The STARS procedure relies on three different parameters:

- The cut-off length L, representing the minimum time interval between two consecutive discontinuities;
- p, the significance level of the Student's t-test used in the algorithm;
- H, the Huber parameter [Huber, 1964], used to minimize the influence of the noisiest data.

For the cut-off length L, four different values are adopted: 10, 15, 20 and 25 days. Before applying the STARS algorithm, a linear trend is estimated and subtracted from the series, a mean seasonal cycle is computed from the residuals and removed from the data. The STARS strategy for discontinuities identification is divided in two steps. First, a point x_j of the time series is considered a jump candidate if either:

$$x_j < m_1 - t\sqrt{\frac{2\sigma_L^2}{L}} \quad \text{(Case 1)} \tag{3.1}$$

or

$$x_j > m_1 + t\sqrt{\frac{2\sigma_L^2}{L}} \quad \text{(Case 2)} \tag{3.2}$$

where:

- t is the value of the performed t-test with $2L - 2$ degrees of freedom at the given significance level p.
- σ_L is the mean standard deviation, computed over all possible L time intervals in the series.
- m_1 is a local mean estimated over the window $[x_{j-L},\ x_{j-1}]$, giving weights to the data based on the Huber parameter, H.

The second step consists in the analysis of each jump candidates, discriminating over significant discontinuities and local fluctuations:

$$x_{jk} < m_1 - t\sqrt{\frac{2\sigma_L^2}{L}} \quad \text{(Case 1)} \tag{3.3}$$

$$x_{jk} > m_1 + t\sqrt{\frac{2\sigma_L^2}{L}} \quad \text{(Case 1)} \tag{3.4}$$

for $k = 1, ..., L$, and where

$$x_{jk} = \frac{1}{k} \sum_{l=0}^{k-1} x_{j+l} \tag{3.5}$$

If the inequality is valid for all the progressive means, x_{jk}, within the L days after day j, the jump candidate is accepted. On the basis of the outcomes of the different cut-off lengths L, namely $L = 10,\ 15,\ 20$ and 25 days, among all the discontinuities detected, only those common to all the four cut-off lengths are retained. Once the jumps have been identified, the time series are corrected accordingly and a consistent long-term trend can be computed.

3.2 Correction of tide gauge data and derivation of mean sea level trends

According to the IOC (Intergovernmental Oceanographic Commission) Manual on Sea Level Measurement and Interpretation (UNESCO, 1985), the instantaneous measurement of sea level by tide gauges can be expressed as the sum of three components:

$$\eta(x_i,\ y_i,\ t) = \eta_{Tide}(x_i,\ y_i,\ t) + \eta_{Meteo}(x_i,\ y_i,\ t) + \eta_{SL}(x_i,\ y_i,\ t) \tag{3.6}$$

where

- x_i, y_i are the station coordinates;
- η_{Tide} indicates the tidal component of the sea level, consisting in periodic movements of the sea, due to the combined effects of the gravitational forces exerted by the Moon, the Sun and Earth's rotation;
- η_{Meteo} is the meteorological component, due to variations of the atmospheric pressure and of the wind speed, causing irregular movements of the sea surface;
- η_{SL} is the local sea level component.

Each component is caused by separate physical processes, thus, each part can be considered independent from the others. In order to obtain long-term trends from the sea level time series, specific corrections must be applied to remove the tidal and the meteorological components. The sea-level records downloaded from the PSMSL database are monthly mean values in which the tidal component has

already been removed. The data from RMN archive are hourly values; they require a specific filtering method to obtain daily means and to remove the tides from the sea level time series.

3.2.1 Doodson X0 filter

Daily means from hourly data were obtained applying a low-pass filter, namely, the Doodson X0 filter. Firstly proposed by Doodson (1921) and extended by Pugh (1987), the purpose of this filter is to remove the main tidal frequencies from hourly sea level elevations, obtaining a mean value for each day. The Doodson X0 filter is a point-to-point moving average filter [Shenoi, 2006]. A moving average filter can be thought of as a window of a certain size, moving along the series one element at a time. The middle element of the window is replaced with the average of all elements in the window. The window of the X0 filter is 39 hours large, the central element is the sea level at noon of the analyzed day. Given the time-variant signal $X(t)$, the filtered value $X_F(t)$ is computed from the following equation [Pugh, 1987]:

$$X_F(t) = \frac{1}{30}\left\{F_0 \cdot X(t) + \sum_{m=1}^{19} F(m) \cdot [X(t+m) + X(t-m)]\right\} \tag{3.7}$$

where F_0 is the weight of the central element, $X(t)$, with t = 12h00. The filter, $F(m)$, is symmetric, so that $F(m) = F(-m)$, and can be expressed as:

$$F(m) = (2,\ 1,\ 1,\ 2,\ 0,\ 1,\ 1,\ 0,\ 2,\ 0,\ 1,\ 1,\ 0,\ 1,\ 0,\ 0,\ 1,\ 0,\ 1) \tag{3.8}$$

Other variants of the Doodson X0 exist, as described in Godin (1972) and Demerliac (1974). However, their main mechanisms differ very slightly from the filter described in this paragraph and their results are very similar to those obtain with the X0 filter [Holgate et al., 2013]. This filter was applied to the 13 time series downloaded from the RMN archive, in order to obtain time series of daily values, with the tidal component of the sea level removed.

3.2.2 Datum shift and monthly mean computation

The 13 filtered sea-level records were inspected for possible discontinuities, using the STARS algorithm. Among them, 7 present a sudden jump due to the installation of new tide gauge instruments, during summer 1998. The sizes of these

discontinuities were evaluated and the time series corrected accordingly. Figure 3.1 shows, as an example, the daily time series of Catania, before and after the mentioned correction was applied.

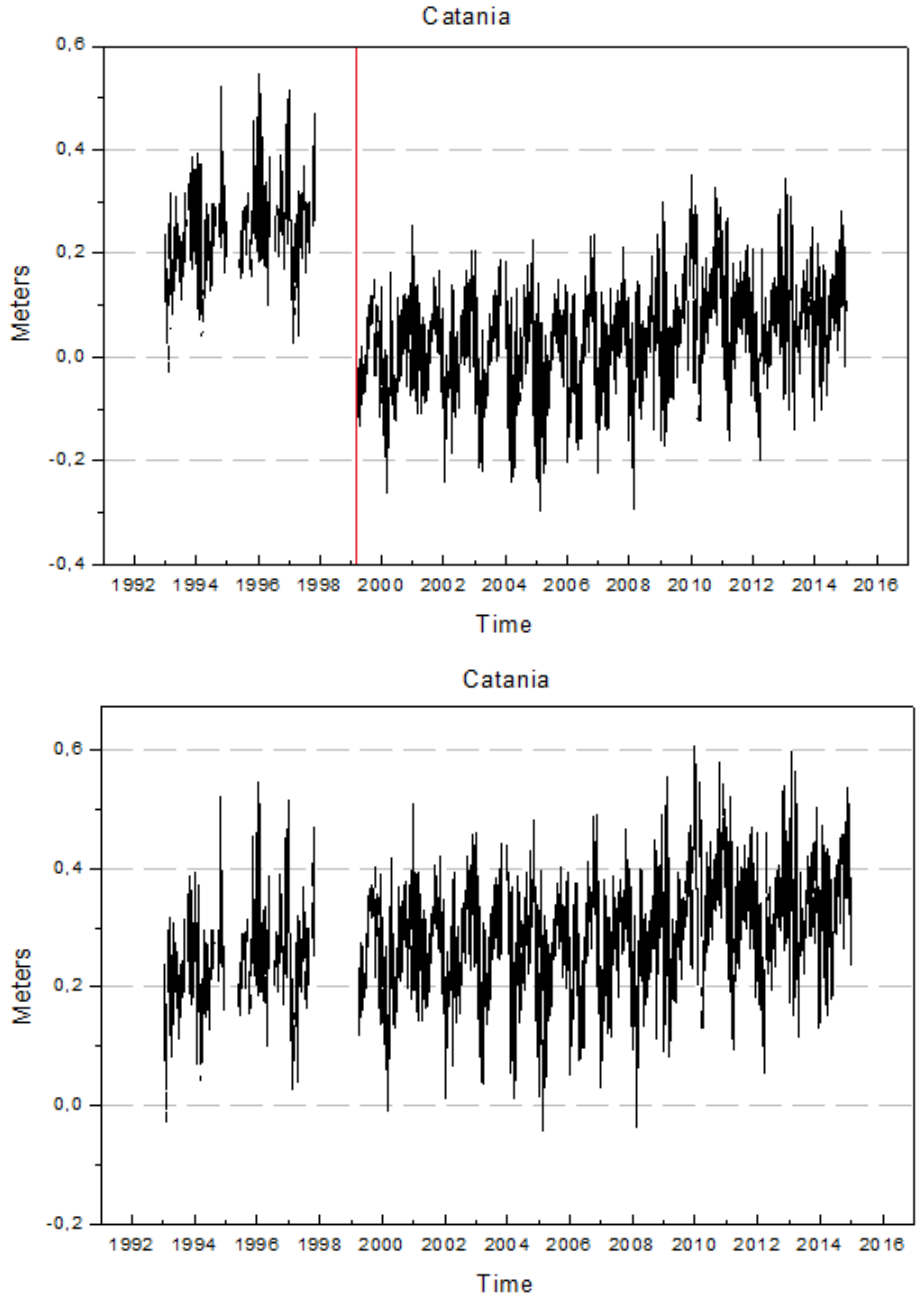

Figure 3.1: *Daily sea level values of the Catania tide gauge. The detected discontinuity is indicated by the red line (top panel). The magnitude of the jump has been estimated with the STARS algorithm in order to accurately correct the records (bottom panel).*

A complete list of the estimated discontinuities is presented in Table 3.1.

Table 3.1: *List of the discontinuities identified in the sea level time series obtained from the RMN network. The first column identifies the tide gauge station, the second shows the day in which the discontinuity has been detected, the third column presents the size of the discontinuity in centimeters.*

Time series	Date	Discontinuities magnitude (cm)
Bari	28/07/1998	+79.98
Catania	02/04/1999	+25.42
Livorno	08/07/1998	-38.84
Napoli	25/07/1998	-34.96
Otranto	07/07/1998	+83.86
Salerno	30/7/1999	+24.84
Taranto	26/07/1998	-90.24

The 7 stations corrected in this way will be indicated with an asterisk in the following tables. Once the discontinuities in the time series have been removed, the daily values were averaged to obtain monthly means. Following the PSMSL recommendations, when more than 15 days were missing in a month, the mean value has not been computed. The sea level data downloaded from the RMN network were organized in the same format as that of the time series from PSMSL, thus, further analysis of sea level data will be the same for all the records.

3.2.3 Linear regression and mean seasonal cycle

At this stage, all the sea level data are monthly mean time series. The mean sea level trend for the 22 years period, 1993-2014, can be computed by fitting a simple line to the series, as shown in Zervas (2001, 2009):

$$y_i = bt_i + r_i \tag{3.9}$$

where y_i are the monthly mean sea level values, t_i represents the time in decimal years format and r_i are the residuals. b is the slope of the least squares best-fit line, and can be expressed as:

$$b = \frac{\sum_i (t_i - T)(y_i - Y)}{\sum_i (t_i - T)^2} \tag{3.10}$$

where T and Y are the means of t_i and y_i, respectively. The standard error of the trend is:

$$s_b = \sqrt{\frac{\sum_i (y_i - Y)^2 - b \sum_i (t_i - T)(y_i - Y)}{(n-2) \sum_i (t_i - T)^2}} \tag{3.11}$$

where n is the number of monthly mean sea-level values.

The mean seasonal cycle can be considered as the regular, repeatable variation of the sea level over the course of a year. The mean seasonal cycles of coastal water levels are caused by a superposition of mean seasonal cycles due to air pressure, wind, water temperature, salinity, ocean currents, and river discharge [Zervas, 2009]. Once the linear trend has been calculated, the seasonal component can be estimated from the residuals of the time series. For N years of data, the mean seasonal cycle is computed by averaging the residuals of each calendar month, according to the following equation [Tsimplis and Woodworth, 1994]:

$$\overline{M_j} = \frac{1}{N} \sum_{k=1}^{N} M_{jk} \tag{3.12}$$

where M_{jk} indicates the sea level residual of the *j-th* month of the *k-th* year. The averages of the 12 calendar months calculated in this way form the mean seasonal cycle. This seasonal component was then subtracted from the time series of each tide gauge station.

The mean seasonal cycles at six selected representative stations are shown in Figures 3.2 to 3.7, with two years displayed for clarity reasons. The mean seasonal cycles computed for all the tide gauge stations have annual amplitudes ranging between 40 and 100 mm, with the highest found in Valencia, and the lowest at the Alexandroupolis tide gauge station. The main contribution to the sea level cycle in the Mediterranean Basin is the steric component [Gomis et al., 2008]. The cycle peaks between October and November everywhere, except in the Aegean Sea, where it peaks in August. The water levels are the lowest in late winter, around February and March, for the whole Basin.

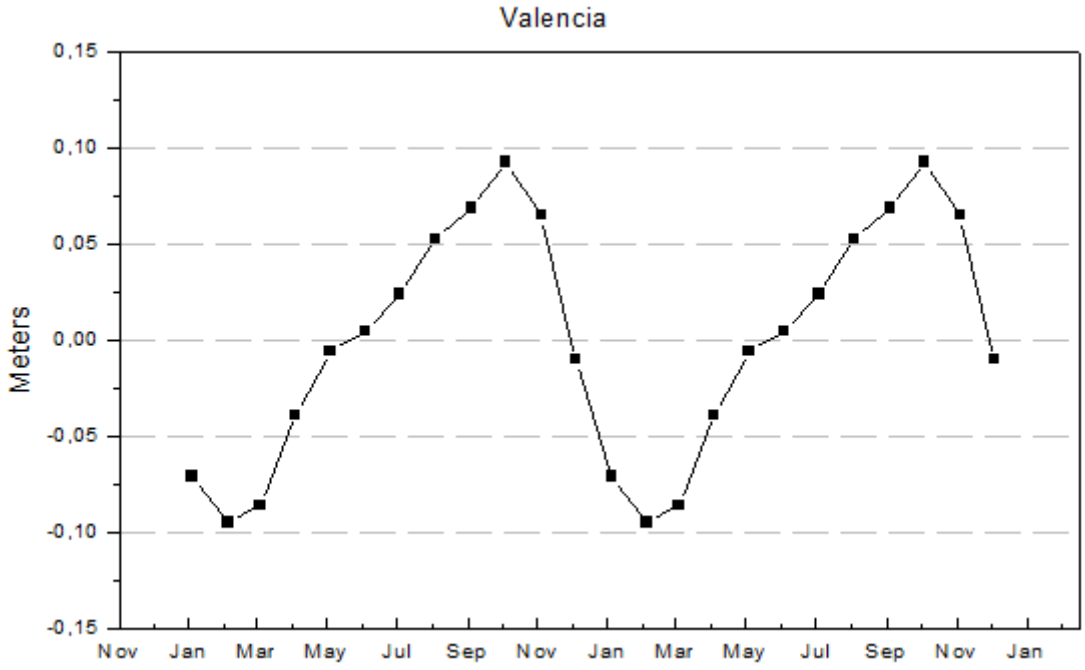

Figure 3.2: *Mean seasonal cycle of the Valencia tide gauge displayed for a 2-year period.*

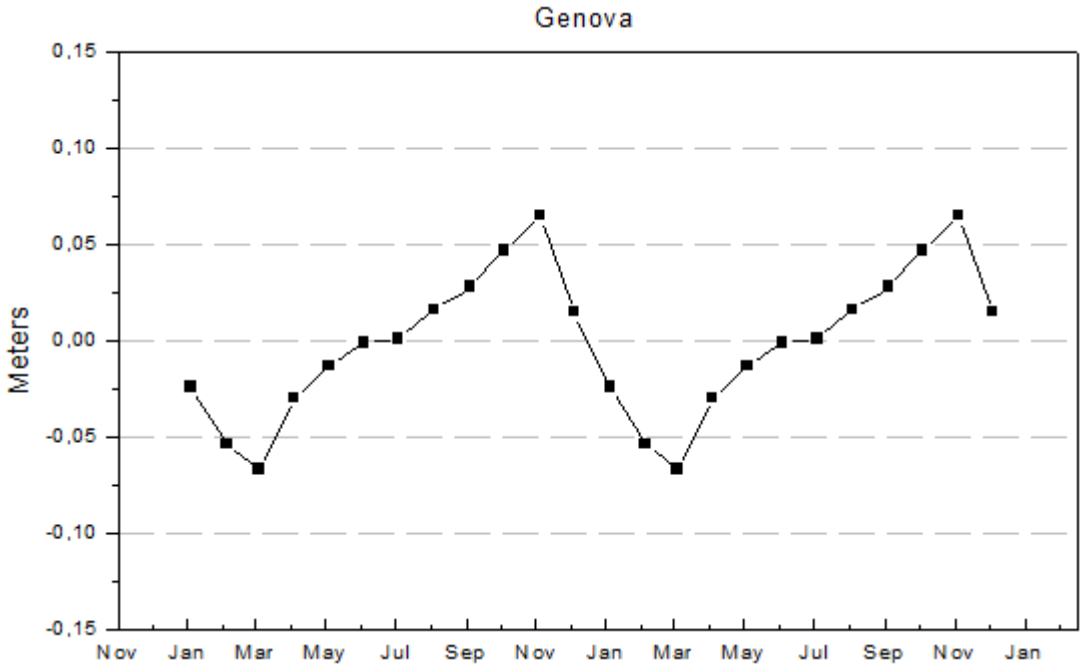

Figure 3.3: *Mean seasonal cycle of the Genova tide gauge displayed for a 2-year period.*

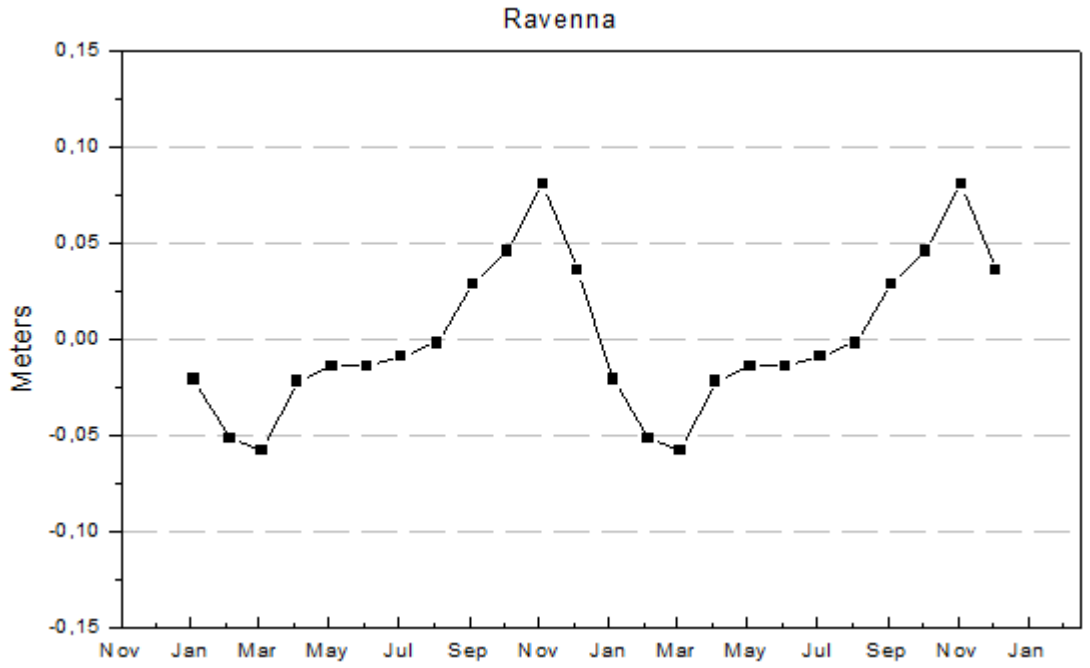

Figure 3.4: *Mean seasonal cycle of the Marina di Ravenna tide gauge displayed for a 2-year period.*

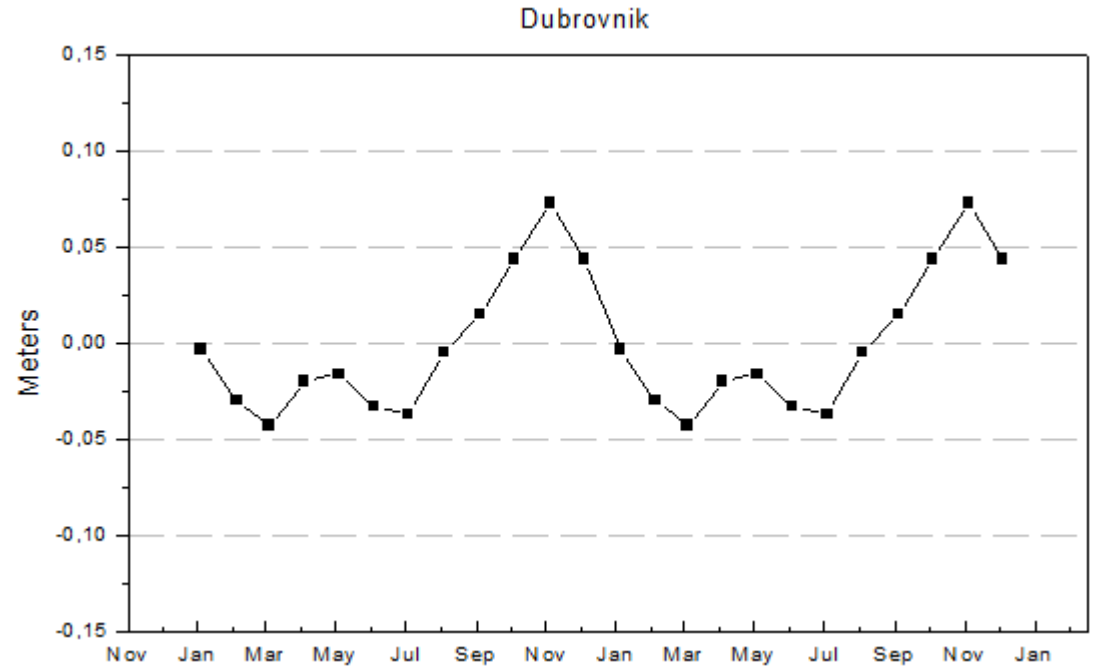

Figure 3.5: *Mean seasonal cycle of the Dubrovnik tide gauge displayed for a 2-year period.*

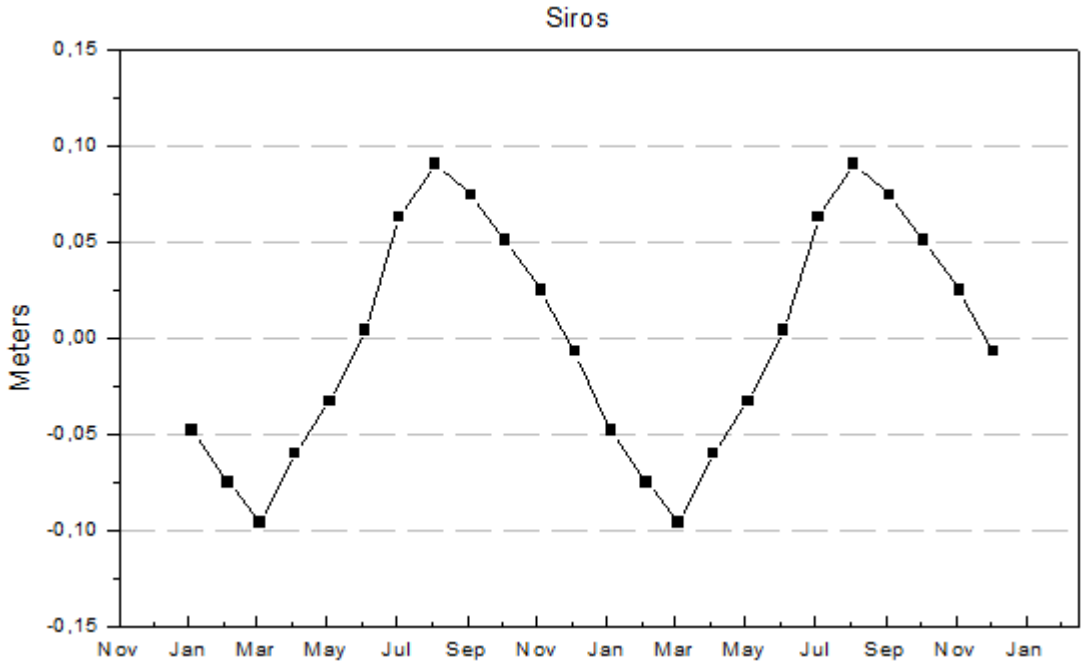

Figure 3.6: *Mean seasonal cycle of the Siros tide gauge displayed for a 2-year period.*

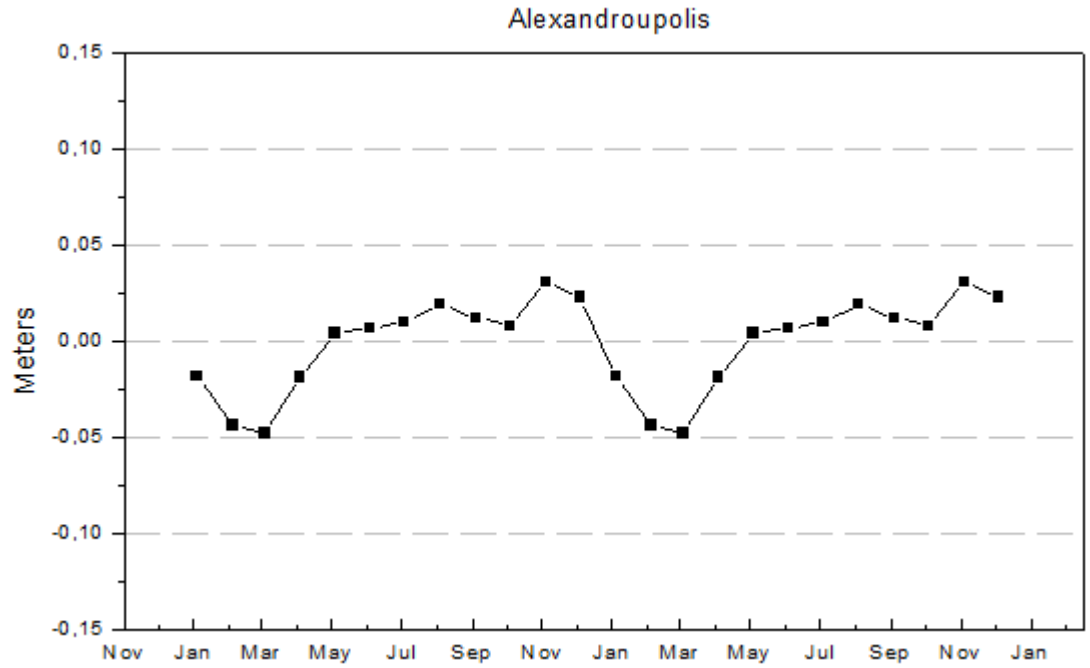

Figure 3.7: *Mean seasonal cycle of the Alexandroupolis tide gauge displayed for a 2-year period.*

3.2.4 Inverse Barometer correction

According to Eq. (3.6), the sea level time series need to be corrected for the tidal and meteorological effects, in order to obtain the mean sea level. As described previously in section 3.2.1, the tidal component, η_{Tide}, has been removed using a specific filter. On the contrary, the meteorological component, η_{Meteo}, has not been removed yet from the time series. The meteorological component of the sea level can be expressed as the sum of two elements:

$$\eta_{Meteo} = \eta_{IB} + \eta_{HF} \tag{3.13}$$

where η_{IB} is the inverse barometer effect, due to the low frequency response of the sea-surface to atmospheric pressure variations [Wunsch and Stammer, 1997], and η_{HF} is the high frequency response to pressure forcing and wind effects [Carrere and Lyard, 2003]. The high frequency response is relevant only on periods below 10 days [Fukumori et al., 1998], therefore, since monthly averaged data were used in this analysis, the effect of η_{HF} is minimized and no correction is needed.

The inverse barometer effect requires a correction, based on atmospheric pressure data at the sea level surface. The pressure records used in this work are those of the NCEP/NCAR (National Centers for Environmental Prediction/National Center for Atmospheric Research) Reanalysis 1, described in Kalnay et al., 1996. A full list of all the exploited models and the available records of this dataset can be retrieved at the following website: [https://climatedataguide.ucar.edu/climate-data/ncep-ncar-r1-overview]. The data are archived on grids with spatial resolution of 2.5°.

The downloaded records were monthly mean atmospheric pressure values at the sea level surface. The time series were selected at the geographical locations of the 35 tide gauge stations used in this work, over the analysis period 1993-2014. The pressure and the de-seasoned tide gauge data were de-trended, and a linear regression was computed between these residual series:

$$p_i = ks_i + \zeta_i \tag{3.14}$$

where p_i are the de-trended monthly atmospheric pressure values in millibar, s_i are the de-trended monthly sea level values in centimeters, k is the slope of the least squares best-fit line and ζ_i the residuals. Then, the IB correction was applied by using the coefficient k:

$$S_i^{IB} = S_i - kp_i \tag{3.15}$$

where S_i are the tide gauge data and S_i^{IB} are the tide gauge records corrected for the IB effect. At this stage of the analysis, the tide gauge data are de-seasoned monthly mean sea level values, filtered for the tidal component and corrected for the effect of atmospheric pressure variations. These are the values that have been compared, in term of linear trends, with the data derived from satellite altimetry, although, the possible VLM affecting the trends has not been estimated yet. The following tables (Tables 3.2, 3.3, 3.4) present the sea level trends obtained from the monthly mean time series, the de-seasoned records, and the de-seasoned time series corrected for the IB effect.

Table 3.2: *Mean sea level trends over the period 1993-2014, obtained from tide gauge data in the Eastern Mediterranean Sea. Column 1 indicates the tide gauge station, columns 2 to 4 report the trends derived from monthly mean sea level data, de-seasoned monthly mean sea level data, and de-seasoned monthly mean sea level data corrected for the IB effect, respectively. The trends were obtained from linear regressions and associated are the relevant standard errors.*

	Trend and Standard error (mm/yr) 1993-2014		
Tide Gauge	Original data	De-seasoned data	De-seasoned data, IB applied
Alexandroupolis	4.33 ± 0.72	4.18 ± 0.68	4.16 ± 0.57
Katakolon	6.12 ± 0.66	5.98 ± 0.50	6.04 ± 0.44
Khalkis North	6.35 ± 0.71	6.02 ± 0.57	6.14 ± 0.49
Khios	2.87 ± 0.79	2.78 ± 0.72	2.77 ± 0.65
Leros	1.80 ± 0.69	1.82 ± 0.57	1.73 ± 0.55
Levkas	9.82 ± 0.71	9.36 ± 0.57	9.54 ± 0.47
Siros	3.85 ± 0.88	3.65 ± 0.59	3.57 ± 0.53
Thessaloniki	5.55 ± 0.78	5.38 ± 0.64	5.34 ± 0.54

Table 3.3: *Mean sea level trends over the period 1993-2014, obtained from tide gauge data in the Western Mediterranean Sea. Column 1 indicates the tide gauge station, columns 2 to 4 report the trends derived from monthly mean sea level data, de-seasoned monthly mean sea level data, and de-seasoned monthly mean sea level data corrected for the IB effect, respectively. The trends were obtained from linear regressions and associated are the relevant standard errors.*

	Trend and Standard error (mm/yr) 1993-2014		
Tide Gauge	Original data	De-seasoned data	De-seasoned data, IB applied
Barcelona	6.31 ± 0.80	5.98 ± 0.58	5.93 ± 0.37
Cagliari	4.40 ± 0.76	3.98 ± 0.51	4.14 ± 0.38
Catania*	5.27 ± 0.70	4.97 ± 0.55	4.92 ± 0.39
Ceuta	2.14 ± 0.57	1.97 ± 0.44	1.97 ± 0.36
Genova	3.00 ± 0.78	2.85 ± 0.66	3.08 ± 0.49
L'Estartit	3.86 ± 0.69	3.59 ± 0.53	3.59 ± 0.34
Livorno*	2.88 ± 0.80	2.63 ± 0.68	3.03 ± 0.45
Malaga	3.46 ± 0.67	3.05 ± 0.49	3.05 ± 0.42
Marseille	4.80 ± 0.77	4.61 ± 0.64	4.70 ± 0.42
Napoli*	7.75 ± 0.69	7.50 ± 0.58	7.90 ± 0.40
Salerno*	4.20 ± 0.84	4.13 ± 0.70	3.75 ± 0.52
Taranto*	5.48 ± 0.84	4.99 ± 0.70	5.04 ± 0.55
Tarifa	5.35 ± 0.57	5.19 ± 0.45	5.20 ± 0.39
Toulon	3.70 ± 0.70	3.46 ± 0.57	3.62 ± 0.37
Valencia	5.45 ± 0.92	4.95 ± 0.60	4.85 ± 0.45

Table 3.4: *Mean sea level trends over the period 1993-2014, obtained from tide gauge data in the Adriatic Sea. Column 1 indicates the tide gauge station, columns 2 to 4 report the trends derived from monthly mean sea level data, de-seasoned monthly mean sea level data, and de-seasoned monthly mean sea level data corrected for the IB effect, respectively. The trends were obtained from linear regressions and associated are the relevant standard errors.*

	Trend and Standard error (mm/yr) 1993-2014		
Tide gauge	Original data	De-seasoned data	De-seasoned data, IB applied
Ancona	3.27 ± 0.97	2.81 ± 0.82	3.08 ± 0.55
Bakar	3.34 ± 0.89	3.19 ± 0.79	3.19 ± 0.52
Bari*	4.68 ± 0.89	4.60 ± 0.77	4.77 ± 0.46
Dubrovnik	5.23 ± 0.77	4.97 ± 0.67	4.94 ± 0.46
Ortona	6.20 ± 1.18	6.23 ± 1.03	6.72 ± 0.74
Otranto*	4.26 ± 0.79	3.81 ± 0.67	3.81 ± 0.48
Ravenna	7.36 ± 0.81	7.13 ± 0.71	7.13 ± 0.53
Rovinj	2.23 ± 0.87	1.96 ± 0.75	1.96 ± 0.48
Split	4.51 ± 0.81	4.31 ± 0.72	4.31 ± 0.50
Trieste	5.30 ± 0.82	5.05 ± 0.70	5.05 ± 0.46
Venezia	6.78 ± 0.83	6.52 ± 0.72	6.52 ± 0.45
Zadar	2.50 ± 0.94	2.35 ± 0.82	2.48 ± 0.57

3.2.5 Standard Error accounting for serial autocorrelation

The linear trends and their standard errors were estimated by using a linear regression. While a trend value obtained with this method is accurate, the standard error of that trend, s_b, is substantially underestimated. In fact, this estimated error is valid only if the residual values, r_i, are serially uncorrelated [Box and Jenkins, 1976]. This condition is often not valid in time series analysis [Box and Jenkins, 1976; Box et al, 1978], and, in particular, it usually not valid for sea-level time series [Zervas, 2001]. Even after removing the mean seasonal cycle, the residual time series is serially autocorrelated. Each monthly value is partially correlated with the value of the previous month and the value of the following month. Therefore, the monthly sea-level data y_i can be expressed in the form of an autoregressive first order process [Zervas, 2009]:

$$y_i = bt_i + \rho_i(y_{i-1} - bt_{i-1}) + \varepsilon_i \tag{3.16}$$

where b and t_i have the same meaning as in Eq. 3.9, $i-1$ indicates the previous data value, and ε_i represents the unpredictable part of the residuals. The predictable part of the time series from the previous month residual is represented by ρ_1, called the lag-1 autoregressive coefficient [Maul and Martin, 1993]. The value of the lag-1 coefficient ρ_1 oscillates between -1 and +1, when equals to 0 the next value is completely unpredictable. This procedure does not alter the value of the trends, but leads to a larger standard error s_b. With a lag-1 coefficient ρ_1, the effective sample size, n, is reduced to n_1, following the equation [Wilks 2006]:

$$n_1 = n\frac{1-\rho_1}{1+\rho_1} \tag{3.17}$$

thus, the standard error s_b increases to a value s_{b1}

$$s_{b1} = s_b F_l = s_b\sqrt{\frac{1+\rho_1}{1-\rho_1}} \tag{3.18}$$

where F_l is called the variance inflation factor. The effect of the factor F_l on the standard errors is shown in Table 3.5.

Table 3.5: *Effect of temporal autocorrelation of the de-trended time series on standard errors [Zervas, 2009]. The first column indicates possible values of the autoregressive coefficient ρ_1, the second column presents the variance inflation factor relative to the ρ_1 value, the last column show the ratio between the standard errors calculated with autoregressive process of first order and with linear regression.*

Autoregressive Coefficient ρ_1	Variance Inflation Factor F_l	Ratio of Standard errors s_{b1}/s_b
0	1.0	1.0
0.2	1.5	1.2
0.4	2.3	1.5
0.6	4.0	2.0
0.8	9.0	3.0

Accounting for the serial correlation of the residual time series, the standard errors associated with the trends of the de-seasoned records corrected for the IB effect, have been recalculated. The average of all the trend standard errors are presented in Table 3.6, for the two different methods of calculation.

Table 3.6: *Average of the standard errors calculated with linear regression and with autoregressive process of first order. Column 1 presents the average of all the trend standard errors for the specific method of calculation listed in column 2.*

Average standard errors	Method of calculation
0.48	Linear regression
0.63	Autoregressive Residuals of Order 1

The standard errors calculated with the autoregressie process were then multiplied by 1.96 according to Box et al. (1978), in order to obtain the 95% confidence interval (CI) of each trend. The results are shown in Tables 3.7, 3.8, 3.9.

Table 3.7: *Eastern Mediterranean Sea: trends estimated over the period 1993-2014. The data are the de-seasoned tide gauge data, with IB correction applied. Column 1 identifies the tide gauge station, column 2 lists the trends with the standard errors obtained with linear regression, column 3 the variance inflation factor, column 4 shows the trends with standard errors, s_{b1}, derived from autoregressive process, and column 5 presents the trends with the 95% confidence interval (1.96 s_{b1}).*

Tide Gauge	De-seasoned data, IB applied (mm/yr)	Variance inflation factor F_l	Trend with s_{b1} (mm/yr)	Trend with s_{b1} 95% CI (mm/yr)
Alexandroupolis	4.16 ± 0.57	1.61	4.16 ± 0.92	4.16 ± 1.80
Katakolon	6.04 ± 0.44	1.25	6.04 ± 0.55	6.04 ± 1.08
Khalkis North	6.14 ± 0.49	1.35	6.14 ± 0.66	6.14 ± 1.29
Khios	2.77 ± 0.65	1.61	2.77 ± 1.05	2.77 ± 2.05
Leros	1.73 ± 0.55	1.48	1.73 ± 0.82	1.73 ± 1.60
Levkas	9.54 ± 0.47	1.20	9.54 ± 0.57	9.54 ± 1.11
Siros	3.57 ± 0.53	1.41	3.57 ± 0.75	3.57 ± 1.47
Thessaloniki	5.34 ± 0.54	1.38	5.34 ± 0.75	5.34 ± 1.47

Table 3.8: *Eastern Mediterranean Sea: trends estimated over the period 1993-2014. The data are the de-seasoned tide gauge data, with IB correction applied. Column 1 identifies the tide gauge station, column 2 lists the trends with the standard errors obtained with linear regression, column 3 the variance inflation factor, column 4 shows the trends with standard errors, s_{b1}, derived from autoregressive process, and column 5 presents the trends with the 95% confidence interval (1.96 s_{b1}).*

Tide Gauge	De-seasoned data, IB applied (mm/yr)	Variance inflation factor F_i	Trend with s_{b1} (mm/yr)	Trend with s_{b1} 95% CI (mm/yr)
Barcelona	5.93 ± 0.37	1.13	5.93 ± 0.42	5.93 ± 0.82
Cagliari	4.14 ± 0.38	1.13	4.14 ± 0.43	4.14 ± 0.84
Catania*	4.92 ± 0.39	1.13	4.92 ± 0.44	4.92 ± 0.86
Ceuta	1.97 ± 0.36	1.15	1.97 ± 0.41	1.97 ± 0.81
Genova	3.08 ± 0.49	1.23	3.08 ± 0.60	3.08 ± 1.18
L'Estartit	3.59 ± 0.34	1.14	3.59 ± 0.39	3.59 ± 0.76
Livorno*	3.03 ± 0.45	1.17	3.03 ± 0.53	3.03 ± 1.04
Malaga	3.05 ± 0.42	1.23	3.05 ± 0.51	3.05 ± 1.01
Marseille	4.70 ± 0.42	1.15	4.70 ± 0.48	4.70 ± 0.94
Napoli*	7.90 ± 0.40	1.13	7.90 ± 0.45	7.90 ± 0.89
Salerno*	3.75 ± 0.52	1.33	3.75 ± 0.69	3.75 ± 1.36
Taranto*	5.04 ± 0.55	1.55	5.04 ± 0.85	5.04 ± 1.67
Tarifa	5.20 ± 0.39	1.17	5.20 ± 0.47	5.20 ± 0.89
Toulon	3.62 ± 0.37	1.14	3.62 ± 0.42	3.62 ± 0.82
Valencia	4.85 ± 0.45	1.24	4.85 ± 0.56	4.85 ± 1.09

Table 3.9: *Eastern Mediterranean Sea: trends estimated over the period 1993-2014. The data are the de-seasoned tide gauge data, with IB correction applied. Column 1 identifies the tide gauge station, column 2 lists the trends with the standard errors obtained with linear regression, column 3 the variance inflation factor, column 4 shows the trends with standard errors, s_{b1}, derived from autoregressive process, and column 5 presents the trends with the 95% confidence interval (1.96 s_{b1}).*

Tide gauge	De-seasoned data, IB applied (mm/yr)	Variance inflation factor F_l	Trend with s_{b1} (mm/yr)	Trend with s_{b1} 95% CI (mm/yr)
Ancona	3.08 ± 0.55	1.51	3.08 ± 0.83	3.08 ± 1.62
Bakar	3.19 ± 0.52	1.44	3.19 ± 0.75	3.19 ± 1.47
Bari*	4.77 ± 0.46	1.16	4.77 ± 0.53	4.77 ± 1.04
Dubrovnik	4.94 ± 0.46	1.25	4.94 ± 0.58	4.94 ± 1.13
Ortona	6.72 ± 0.74	1.36	6.72 ± 1.01	6.72 ± 1.97
Otranto*	3.81 ± 0.48	1.18	3.81 ± 0.56	3.81 ± 1.11
Ravenna	7.13 ± 0.53	1.61	7.13 ± 0.85	7.13 ± 1.67
Rovinj	1.96 ± 0.48	1.32	1.96 ± 0.64	1.96 ± 1.25
Split	4.31 ± 0.50	1.33	4.31 ± 0.67	4.31 ± 1.31
Trieste	5.05 ± 0.46	1.33	5.05 ± 0.61	5.05 ± 1.20
Venezia	6.52 ± 0.45	1.32	6.52 ± 0.59	6.52 ± 1.16
Zadar	2.48 ± 0.57	1.37	2.48 ± 0.78	2.48 ± 1.53

3.3 Discontinuities in GPS time series and vertical velocities estimation

GPS coordinate time series can be affected by abrupt discontinuities, hindering the accurate estimation of trends. The series shall be corrected calculating the magnitude of these sudden jumps. The records have been analyzed using the STARS methodology [Bruni et al., 2014], as described in section 3.1. A preprocessing phase was introduced, in order to remove the outliers from the dataset. The series were then de-trended and de-seasoned, before applying STARS. The vertical, East and North component of each station position can be treated separately because jumps might not affect all three positions in the same way [Bruni et al., 2014], thus, for the scope of this study, only the vertical components were analyzed. A threshold for the minimum size of an identifiable jumps was also adopted from Bruni et al. (2014) , to account for the noise level of the time series. This

threshold depends on the value of σ_L, the mean standard deviation computed over all possible L time intervals in the series, through an exponentially decaying function, derived empirically. The threshold is computed using the following equation:

$$y = Ae^{\left(-\frac{\sigma_L}{b}\right)} + y_0 \tag{3.19}$$

where A, b, and y_0 are empirical parameters and y is the threshold, given in percentages of σ_L. Thus, only discontinuities with magnitude greater than that of the defined threshold were corrected. Additionally, the size of the data set used in this analysis (21 time series) allows to check the output of the STARS software manually. If consecutive jumps, in opposite directions, were detected within a period of three month, the difference between their respective magnitudes have been computed and compared to the jump acceptance threshold [Bruni et al., 2014]. Figure 3.8 shows the coordinate time series of the MARS (Marseille) GPS, before and after the analysis with STARS.

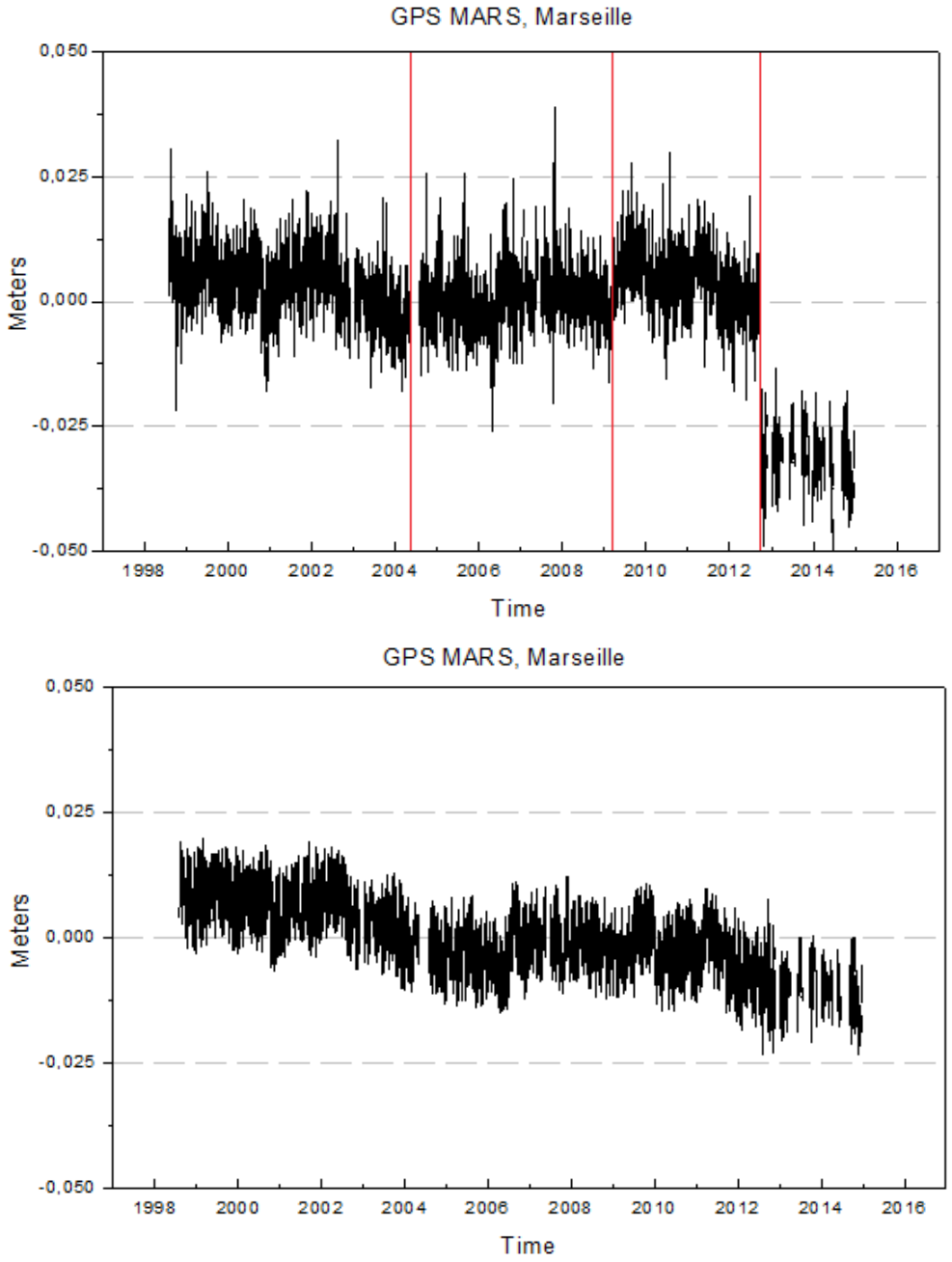

Figure 3.8: *GPS daily vertical coordinate time series of the MARS (Marseille) station. Top panel: the time series downloaded from the NGL. Red lines indicates the discontinuities detected by the STARS software. Bottom panel: the time series after the removal of the discontinuities.*

Among the 21 GPS coordinate time series, only the 15 downloaded from the NGL database were analyzed with the STARS algorithm. In fact, the station positions discontinuities are already corrected in the data available from the SONEL archive, using a specific methodology described in many studies [Wöppelmann et

al. 2007; Bouin and Wöppelmann, 2010; Santamarìa-Gòmez et al., 2012]. Also, the time series of the TRIM (Trieste) and PORT (Ravenna) stations, obtained from the DIFA (UNIBO), have been corrected previously with the same STARS procedure described in this section. Discontinuities were found in almost half of the analyzed records, namely for the stations of Catania, Ortona, Malaga, Marseille, Napoli, Tarifa and Valencia. The details of the detected jumps are presented in Table 3.10.

Table 3.10: *Discontinuities detected in the GPS daily vertical coordinate time series. Each column refers to one of the stations listed above. For each jump, the date of occurrence, the estimated magnitude (in millimeters) and the originating causes are reported.*

Detected jumps	**EIIV (Catania)**	**FRRA (Ortona)**	**MALA (Malaga)**	**MARS (Marseille)**	**NAPO (Napoli)**	**TARI (Tarifa)**	**VALE (Valencia)**
Date 1° jump	09/03/2011	04/03/2011	13/10/2005	29/07/2004	05/11/2009	12/02/2011	10/08/2005
Magnitude 1° jump (mm)	+6.11	-10.96	-14.21	-5.06	+18.01	+10.15	+12.14
Cause 1° jump	Unknown	Unknown	Unknown	Receiver change	Unknown	Unknown	Unknown
Date 2° jump	---	04/09/2013	12/08/2008	18/03/2009	18/03/2010	---	---
Magnitude 2° jump (mm)	---	+26.44	+8.29	-5.32	-1.30	---	---
Cause 2° jump	---	Unknown	Receiver Change	Antenna change	Unknown	---	---
Date 3° jump	---	---	25/12/2009	27/09/2012	07/01/2011	---	---
Magnitude 3° jump (mm)	---	---	-5.24	+28.06	-9.16	---	---
Cause 3° jump	---	---	Unknown	Receiver Change	Unknown	---	---
Date 4° jump	---	---	23/02/2013	---	09/03/2011	---	---
Magnitude 4° jump (mm)	---	---	-9.10	---	-5.28	---	---
Cause 4° jump	---	---	Unknown	---	Unknown	---	---

To identify the causes of the detected discontinuities, the IGS format log files were checked for the listed GPS sites. These files contain the metadata of the stations and should report any installation changes. However, some files are only partially complete and not updated. Among the 16 discontinuities found, only four were attributed to equipment changes. The remaining 75% were flagged as of unknown origin. Long-term trends were finally computed from the corrected

time series. The data were averaged in monthly mean values, rejecting those months having less than 15 days of data, and the same linear regression process, as described in section 3.2.3, was performed. The trends thus obtained for every station are reported in Table 3.11.

Table 3.11: *Trends of VLM estimated with linear regression. Column 1 lists the station acronym, column 2 the location of the nearest tide gauge, column 3 the total data span and column 4 the estimated trend with the associated standard errors.*

GPS Station ID	Nearest tide gauge	Time series duration (years)	Trend with standard error (mm/yr)
MARS	Marseille	16.33	-1.11 ± 0.05
TARI	Tarifa	4.58	-2.77 ± 0.17
TRIM	Trieste	7.67	0.94 ± 0.10
SPLT	Split	7.92	0.05 ± 0.18
PORT	Ravenna	18.33	-5.67 ± 0.10
CEUT	Ceuta	5.06	0.53 ± 0.39
EIIV	Catania	6.92	-1.94 ± 0.15
ANCG	Ancona	4.58	1.12 ± 0.33
MALA	Malaga	11.92	0.13 ± 0.17
GENO	Genova	12.44	0.03 ± 0.26
NAPO	Napoli	6.42	-3.90 ± 0.27
DUBR	Dubrovnik	10.27	-1.76 ± 0.16
VALE	Valencia	13.92	-1.00 ± 0.10
GIUR	Otranto	7.00	-0.44 ± 0.17
SPAN	Levkas	7.58	-1.23 ± 0.11
AUT1	Thessaloniki	9.67	-1.71 ± 0.11
FISC	Salerno	3.08	-0.02 ± 0.15
FRRA	Ortona	4.00	-1.81 ± 0.51
CAGZ	Cagliari	8.56	-0.57 ± 0.07
PORE	Rovinj	3.08	-0.28 ± 0.39
PLAN	Barcellona	8.33	-1.61 ± 0.11

3.4 Satellite altimetry data analysis

The satellite data used in this analysis are the SSALTO/DUACS Mediterranean Sea multi-mission gridded daily SLAs, available from AVISO, and the SLA monthly grid time series provided by ESA CCI project. Differently from the tide gauge data, satellite altimetry records are distributed after the tidal and meteorological components have been removed from the time series. It should be noted that, while the tide gauge data were corrected for the IB effect, the DAC applied on the satellite records accounts for both the IB effect and the high frequency response of the sea-level to pressure and wind variations.

The daily time series from AVISO were averaged to obtain monthly mean values, the same format as that of the CCI data. Then, the mean seasonal cycle was calculated and removed from each time series of both datasets, following the procedure previously described in section 3.2.3 (Eq. 3.12). The mean sea level trends were estimated through linear regression (Eq. 3.9, 3.10) and the associated standard errors were calculated accounting for the serial autocorrelation (Eq. 3.18). Tables 3.12, 3.13 and 3.14 present the obtained results. The trends for the CCI data are referred to the period 1993 – 2013.

Table 3.12: *Mean sea-level trends derived from monthly de-seasoned satellite altimetry data over the Eastern Mediterranean Sea. Column 1 identifies the location of the nearest tide gauge, column 2 presents the trends computed from the AVISO records over the period 1993-2014, with the 95% confidence interval, column 3 shows the trends of the CCI data over the period 1993-2013, with the 95% confidence interval.*

Nearest Tide Gauge	Trends from AVISO de-seasoned data with 95% CI (1993-2014) (mm/yr)	Trends from CCI de-seasoned data with 95% CI (1993-2013) (mm/yr)
Alexandroupolis	3.95 ± 1.12	4.51 ± 1.36
Katakolon	3.29 ± 0.69	3.75 ± 0.85
Khalkis North	3.42 ± 0.96	2.51 ± 1.01
Khios	3.90 ± 1.10	2.68 ± 1.06
Leros	3.98 ± 0.98	4.36 ± 1.08
Levkas	2.57 ± 0.73	3.41 ± 0.99
Siros	4.47 ± 1.00	4.59 ± 1.11
Thessaloniki	3.02 ± 1.37	1.99 ± 1.32

Table 3.13: *Mean sea-level trends derived from monthly de-seasoned satellite altimetry data over the Western Mediterranean Sea. Column 1 identifies the location of the nearest tide gauge, column 2 presents the trends computed from the AVISO records over the period 1993-2014, with the 95% confidence interval, column 3 shows the trends of the CCI data over the period 1993-2013, with the 95% confidence interval.*

Nearest Tide Gauge	Trends from AVISO de-seasoned data with 95% CI (1993-2014) (mm/yr)	Trends from CCI de-seasoned data with 95% CI (1993-2013) (mm/yr)
Barcelona	2.29 ± 0.53	2.01 ± 0.59
Cagliari	2.42 ± 0.57	2.74 ± 0.63
Catania*	0.97 ± 0.86	2.94 ± 0.90
Ceuta	2.29 ± 0.65	5.08 ± 0.78
Genova	2.67 ± 0.57	3.66 ± 0.57
L'Estartit	2.41 ± 0.61	2.64 ± 0.60
Livorno*	2.91 ± 0.61	2.24 ± 0.66
Malaga	3.16 ± 0.69	4.43 ± 0.72
Marseille	2.87 ± 0.69	2.84 ± 0.70
Napoli*	2.95 ± 0.65	3.32 ± 0.74
Salerno*	2.90 ± 0.63	2.28 ± 0.68
Taranto*	2.74 ± 0.80	3.65 ± 0.78
Tarifa	2.29 ± 0.59	5.20 ± 0.73
Toulon	2.64 ± 0.63	3.03 ± 0.69
Valencia	1.87 ± 0.49	2.72 ± 0.56

Table 3.14: *Mean sea-level trends derived from monthly de-seasoned satellite altimetry data over the Adriatic Sea. Column 1 identifies the location of the nearest tide gauge, column 2 presents the trends computed from the AVISO records over the period 1993-2014, with the 95% confidence interval, column 3 shows the trends of the CCI data over the period 1993-2013, with the 95% confidence interval.*

Nearest Tide Gauge	Trends from AVISO de-seasoned data with 95% CI (1993-2014) (mm/yr)	Trends from CCI de-seasoned data with 95% CI (1993-2013) (mm/yr)
Ancona	4.12 ± 0.96	3.44 ± 0.97
Bakar	3.80 ± 0.96	2.79 ± 0.66
Bari*	3.83 ± 0.73	3.05 ± 0.79
Dubrovnik	3.41 ± 0.80	3.37 ± 0.79
Ortona	4.14 ± 0.86	3.96 ± 0.98
Otranto*	3.63 ± 0.74	3.41 ± 0.81
Ravenna	4.28 ± 0.90	3.37 ± 1.48
Rovinj	4.33 ± 0.96	2.22 ± 1.30
Split	3.93 ± 0.92	3.26 ± 0.87
Trieste	4.01 ± 1.07	2.76 ± 1.40
Venezia	4.18 ± 0.92	3.40 ± 0.99
Zadar	4.04 ± 0.96	3.04 ± 1.04

Chapter 4

Comparison of mean sea level trends

This chapter focuses on the comparison between the trends obtained from the analysis of tide gauge and satellite radar altimetry sea level data. In section 4.1, the period 1993-2014 is analyzed; the satellite trends deduced from the AVISO records are compared with the mean sea level trends obtained from the 35 tide gauge stations selected in the Mediterranean area. Section 4.2 presents the comparison over the period 1993-2013, introducing the CCI satellite data in order to assess which of the two different satellite data records was the most suitable for coastal studies.

4.1 Period 1993-2014: linear trends from tide gauge and AVISO satellite data

The data compared in this section are the de-seasoned monthly mean gridded SLA, downloaded from AVISO, and the de-seasoned monthly mean sea level time series of the 35 tide gauge stations selected for this study. The comparison has been performed in term of linear trends, using the nearest satellite altimeter grid point to each station.

For the sites where GPS data were available, in case a significant vertical velocity was estimated, the tide gauge time series have been corrected for the VLM. According to Eq. 2.1, the relative sea level trend, estimated by tide gauge data, was summed to the VLM found at this site, in order to obtain an absolute sea level trend, comparable with the one calculated from satellite altimetry data. The standard error associated to the trend corrected in this way was computed by

means of the propagation of uncertainties [Taylor, 1982]:

$$s = \sqrt{(s_{b1})^2 + (s_{VLM})^2} \tag{4.1}$$

where s_{b1} is the standard error of the relative sea level trend, accounting for residuals autocorrelation, and s_{VLM} the error associated to the VLM trend.

Additionally, at each station, the correlation coefficient between the satellite altimetry and the tide gauge data was computed [Taylor, 1982]:

$$r = \frac{\sum_{i=1}^{n}(x_i - X)(y_i - Y)}{\sqrt{\sum_{i=1}^{n}(x_i - X)^2}\sqrt{\sum_{i=1}^{n}(y_i - Y)^2}} \tag{4.2}$$

where x_i are the tide gauge data, y_i the satellite data, X and Y the mean of x_i and y_i, respectively, and n the number of mean sea-level values. The correlation coefficients have been calculated using the tide gauge time series corrected for the VLM for those sites where such correction has been estimated.

The results are presented in the followint Tables 4.1, 4.2, and 4.3.

Table 4.1: *Eastern Mediterranean Sea: mean sea level trends, estimated over the period 1993-2014, and VLMs. Column 1 identifies the tide gauge station, column 2 lists the sea level trends computed from the tide gauge data, column 3 presents the VLM correction computed from the available GPS observations to be applied to the tide gauge data, column 4 displays the tide gauge mean sea level trends corrected for the VLM, when available, column 5 lists the sea level trends estimated from the nearest satellite altimeter grid point and column 6 the correlation coefficient between the two de-seasoned monthly time series where, when available, the tide gauge data have been corrected for the VLM.*

Tide Gauge	Relative sea-level trend (mm/yr)	VLM trend (mm/yr)	Absolute sea-level trend (mm/yr)	Sea-level trend from altimetry (AVISO) (mm/yr)	Correlation Coefficient r
Alexandroupolis	4.16 ± 1.80	---	---	3.95 ± 1.12	0.74
Katakolon	6.04 ± 1.08	---	---	3.29 ± 0.69	0.71
Khalkis North	6.14 ± 1.29	---	---	3.42 ± 0.96	0.74
Khios	2.77 ± 2.05	---	---	3.90 ± 1.10	0.73
Leros	1.73 ± 1.60	---	---	3.98 ± 0.98	0.72
Levkas	9.54 ± 1.11	-1.23 ± 0.11	8.31 ± 1.14	2.57 ± 0.73	0.63
Siros	3.57 ± 1.47	---	---	4.47 ± 1.00	0.78
Thessaloniki	5.34 ± 1.47	-1.71 ± 0.11	3.63 ± 1.49	3.02 ± 1.37	0.73

Table 4.2: *Western Mediterranean Sea: mean sea level trends, estimated over the period 1993-2014, and VLMs. Column 1 identifies the tide gauge station, column 2 lists the sea level trends computed from the tide gauge data, column 3 presents the VLM correction computed from the available GPS observations to be applied to the tide gauge data, column 4 displays the tide gauge mean sea level trends corrected for the VLM, when available, column 5 lists the sea level trends estimated from the nearest satellite altimeter grid point and column 6 the correlation coefficient between the two de-seasoned monthly time series where, when available, the tide gauge data have been corrected for the VLM.*

Tide Gauge	Relative sea-level trend (mm/yr)	VLM trend (mm/yr)	Absolute sea-level trend (mm/yr)	Sea-level trend from altimetry (AVISO) (mm/yr)	Correlation Coefficient r
Barcelona	5.93 ± 0.82	-1.61 ± 0.11	4.32 ± 0.85	2.29 ± 0.53	0.64
Cagliari	4.14 ± 0.84	-0.57 ± 0.07	3.57 ± 0.85	2.42 ± 0.57	0.61
Catania*	4.92 ± 0.86	-1.94 ± 0.15	2.98 ± 0.91	0.97 ± 0.86	0.58
Ceuta	1.97 ± 0.81	0.53 ± 0.39	2.50 ± 1.11	2.29 ± 0.65	0.60
Genova	3.08 ± 1.18	0.03 ± 0.26	---	2.67 ± 0.57	0.66
L'Estartit	3.59 ± 0.76	---	---	2.41 ± 0.61	0.76
Livorno*	3.03 ± 1.04	---	---	2.91 ± 0.61	0.75
Malaga	3.05 ± 1.01	0.13 ± 0.17	---	3.16 ± 0.69	0.58
Marseille	4.70 ± 0.94	-1.11 ± 0.05	3.59 ± 0.95	2.87 ± 0.69	0.72
Napoli*	7.90 ± 0.89	-3.90 ± 0.27	4.00 ± 1.02	2.95 ± 0.65	0.77
Salerno*	3.75 ± 1.36	-0.02 ± 0.15	---	2.90 ± 0.63	0.63
Taranto*	5.04 ± 1.67	---	---	2.74 ± 0.80	0.78
Tarifa	5.20 ± 0.89	-2.77 ± 0.17	2.43 ± 0.98	2.29 ± 0.59	0.69
Toulon	3.62 ± 0.82	---	---	2.64 ± 0.63	0.74
Valencia	4.85 ± 1.09	-1.00 ± 0.10	3.85 ± 1.11	1.87 ± 0.49	0.48

Table 4.3: *Adriatic Sea: mean sea level trends, estimated over the period 1993-2014, and VLMs. Column 1 identifies the tide gauge station, column 2 lists the sea level trends computed from the tide gauge data, column 3 presents the VLM correction computed from the available GPS observations to be applied to the tide gauge data, column 4 displays the tide gauge mean sea level trends corrected for the VLM, when available, column 5 lists the sea level trends estimated from the nearest satellite altimeter grid point and column 6 the correlation coefficient between the two de-seasoned monthly time series where, when available, the tide gauge data have been corrected for the VLM.*

Tide Gauge	Relative sea-level trend (mm/yr)	VLM trend (mm/yr)	Absolute sea-level trend (mm/yr)	Sea-level trend from altimetry (AVISO) (mm/yr)	Correlation coefficient r
Ancona	3.08 ± 1.62	1.12 ± 0.33	4.20 ± 1.75	4.12 ± 0.96	0.71
Bakar	3.19 ± 1.47	---	---	3.80 ± 0.96	0.69
Bari*	4.77 ± 1.04	---	---	3.83 ± 0.73	0.74
Dubrovnik	4.94 ± 1.13	-1.76 ± 0.16	3.18 ± 1.14	3.41 ± 0.80	0.75
Ortona	6.72 ± 1.97	-1.81 ± 0.51	4.91 ± 2.23	4.14 ± 0.86	0.75
Otranto*	3.81 ± 1.11	-0.44 ± 0.17	3.37 ± 1.15	3.63 ± 0.74	0.73
Ravenna	7.13 ± 1.67	-5.67 ± 0.10	1.46 ± 1.69	4.28 ± 0.90	0.68
Rovinj	1.96 ± 1.25	-0.28 ± 0.39	---	4.33 ± 0.96	0.63
Split	4.31 ± 1.31	0.05 ± 0.18	---	3.93 ± 0.92	0.75
Trieste	5.05 ± 1.20	0.91 ± 0.10	5.96 ± 1.21	4.01 ± 1.07	0.80
Venice	6.52 ± 1.16	---	---	4.18 ± 0.92	0.71
Zara	2.48 ± 1.53	---	---	4.04 ± 0.96	0.69

The two datasets show significant correlation almost at every site, with correlation coefficients up to 0.8. The highest correlation was found in the Northern Adriatic Sea, where the correlation coefficient of the Trieste station is equal to 0.80. In the Aegean Sea, the tide gauge and the satellite altimetry signals were well correlated at all stations, with coefficients ranging between 0.72-0.78. Lower values were found in the Alboran Sea (0.58-0.60) and, in particular, at the Valencia station (0.48), in the Balearic Sea.

The absolute sea-level trends obtained from satellite altimetry range between 0.96-4.47 mm/yr, with the lowest value found in the Ionian Sea, near Catania, and the highest in the Aegean sea, close to the Siros Island. The Adriatic Sea presents high positive rates, especially in the northern part, where the largest trends found near Ravenna and Rovinj are equal to 4.28 ± 0.90 mm/yr and 4.33 ± 0.96 mm/yr, respectively.

The relative trends, computed from tide gauge data, differ significantly from

site to site, most likely reflecting differences in the VLM affecting the stations. Sea level trends larger than 5 mm/yr were found in 12 sites, with the three stations of Levkas, Ravenna and Naples exhibiting sea-level rates larger than 7 mm/yr. Generally, the relative trends corrected for the VLM are comparable with those computed from satellite altimetry, within the 95% confidence interval. The cases analyzed are described in detail in the following paragraphs.

4.1.1 Tide gauges along the Spanish, French and Western Italian coasts

In the Gibraltar Straits, a small uplift has been detected in Ceuta, 0.53 ± 0.39 mm/yr, while significant land subsidence was estimated in Tarifa, equal to -2.77 ± 0.17 mm/yr. Similar rates were found by Garcìa et al. (2012), using differences between tide gauge and satellite data. The sea-level trends of both stations, corrected for the respective VLM, turn out to be consistent with those estimated, for each station, at the nearest satellite altimeter grid point.

Moving to the Alboran Sea, no significant VLM, 0.13 ± 0.17 mm/yr, has been estimated at the Malaga station. The relative sea-level trend measured by the tide gauge, equal to 3.05 ± 1.01 mm/yr, is in agreement with the absolute trend derived from satellite altimetry, 3.16 ± 0.69 mm/yr.

In the Balearic Sea, a smaller mean sea-level rise has been found from altimetry data, 1.87 ± 0.49 mm/yr, near Valencia. The relative trend estimated from the tide gauge data is 4.85 ± 1.09 mm/yr, about 3 mm/yr higher than the satellite altimetry estimate, while the VLM computed from the VALE GPS time series indicates s a subsidence rate of -1.00 ± 0.10 mm/yr. The VLM has been computed over a period of time of about 13 years, good enough to estimate a reliable trend; however, the GPS time frame does not overlap completely with the tide gauge data record.

Similar results were found at the Barcelona station, where the tide gauge sea-level trend, 4.32 ± 0.85 mm/yr, corrected for the ground component, is about 2 mm/yr higher than the absolute trend estimated by satellite altimetry data, 2.29 ± 0.53. In this site, the distance between the tide gauge and the GPS (PLAN) stations is about 17 km, and this could be considered as a potentially contributing error source. In fact, a recent study by Tomás et al. (2014), performed using InSAR measurements, has assessed that the rate of subsidence in Barcelona shows differences even in the order of 1 mm/yr from one area to the other of the city, and is somewhat higher near the coast. Thus, it is likely that the VLM estimated

at the GPS station does not reflect the real ground motion affecting the tide gauge records.

No GPS records were available for the L'Estartit station. The absolute and relative sea-level are comparable, although, the difference between the two trends suggests a small subsidence rate of about 1 mm/yr, which is in agreement with the value found by Garcìa et al. (2012).

Along the Southern French coast, the tide gauges at Marseille and Toulon have been analyzed. The GPS at the Marseille site shows a negative VLM rate of -1.11 $\pm$ 0.05 mm/yr, while no GPS station is available at Toulon. The sea-level trend in Marseille, corrected for the subsidence, is very close to that of the neighboring Toulon station (3.59 $\pm$ 0.95 mm/yr, 3.62 $\pm$ 0.82 mm/yr, respectively), and both trends are comparable to the satellite-derived trends, within the 95% confidence interval.

Along the Western Italian coast, the four sites of Genoa, Livorno (in the Ligurian Sea), Naples and Salerno (in the Tyrrhenian Sea) were analyzed. Higher sea-level trends, both absolute and relative, were found in the south at the Naples and Salerno stations. A significant land subsidence of -3.90 $\pm$ 0.27 mm/yr has been measured in Naples, while no significant VLM has been estimated at the other three stations. The rate of sea-level rise at the Naples tide gauge, corrected for the VLM, is comparable to the trend computed from satellite data. The tide gauge-derived trends of the two sites in the Ligurian Sea and that of the Salerno station show a good agreement with the satellite-derived estimate, without corrections for the VLM.

In Cagliari, on the Sardinia Southern coast, a small subsidence has been detected, leading to a corrected sea-level trend of 3.57 $\pm$ 0.85 mm/yr, consistent with the absolute trend of 2.42 $\pm$ 0.57 mm/yr, estimated at the nearest satellite altimeter grid point.

No GPS station has been found near the Taranto station. The sea-level rise obtained from the tide gauge data is higher than the absolute sea-level trend derived from the satellite altimetry, suggesting land subsidence at this site. This is in agreement with previous investigations concerning this area, were negative trends of VLM have been found [Fenoglio-Marc et al., 2004]. Despite the lacking of information on the VLM, the two trends are consistent, within the 95% confidence interval.

For the Catania station, located on the Sicilian Eastern coast, the coastal sea-level trend estimated from satellite altimetry is almost equal to zero, 0.97 $\pm$ 0.86 mm/yr. This low sea-level rise near the coast is in agreement with the results of

Braitenberg et al. (2010), who found, for the period 1992-2009, a negative sea-level rate in the Ionian Sea, decreasing towards the Eastern Sicilian coast where it turns into small positive values (Fig. 4.1).

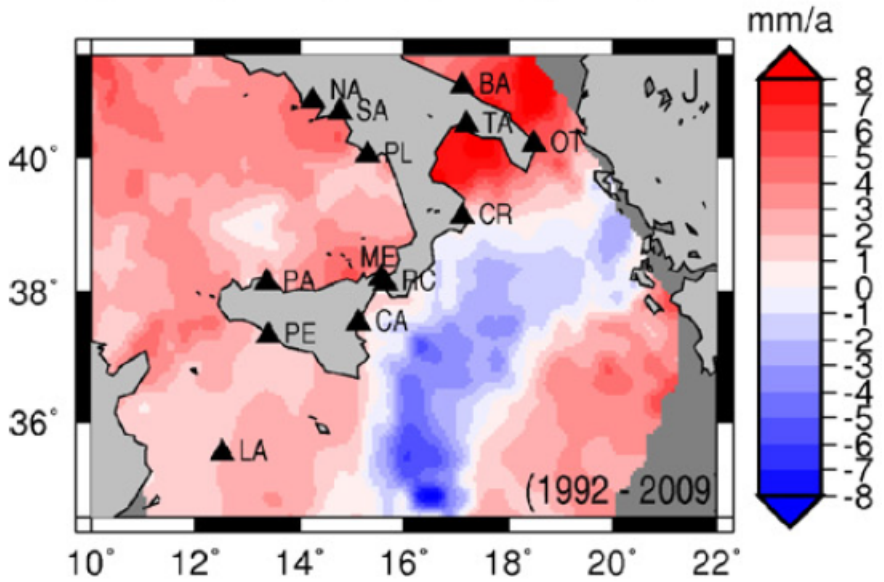

Figure 4.1: *Map of SSH change in the Ionian Sea from satellite altimetry data, over the time interval 1992-2008 [From Braitenberg et al., 2010].*

Although the tide gauge trend has been corrected for subsidence, estimated from the GPS time series, the absolute trend thus computed is higher, 2.98 ± 0.91 mm/yr, than the value obtained from satellite altimetry.

The relative sea-level trends computed from tide gauge data, the sea-level trends corrected for the VLM, and the satellite altimetry-derived trends described in this section, are graphically compared in Figure 4.2.

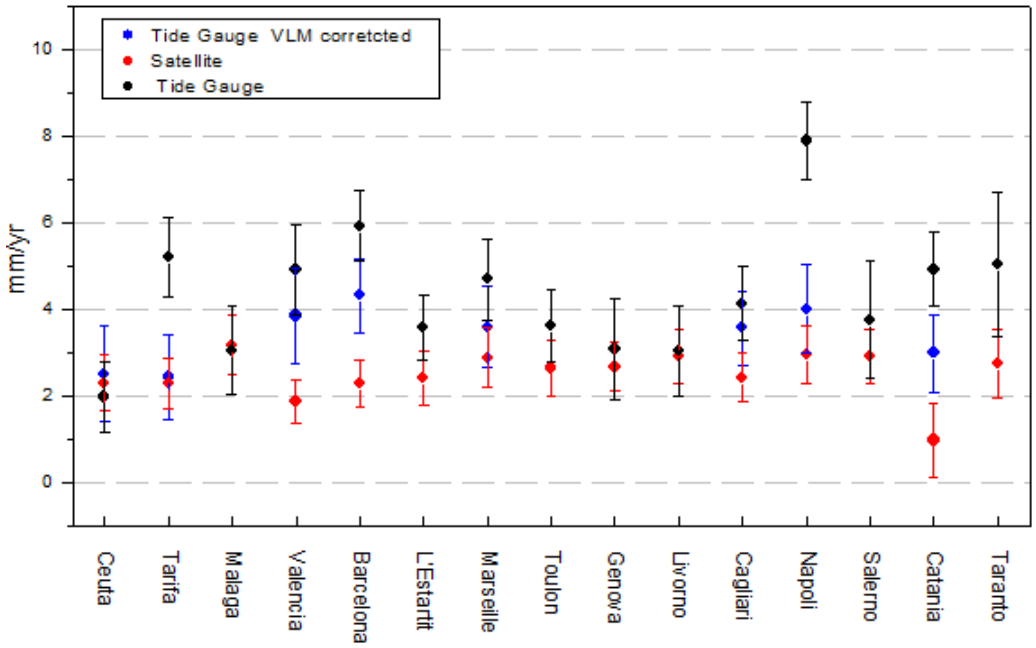

Figure 4.2: *Sea-level trends computed from tide gauge and satellite data along the Spanish, French and Italian Western coasts. The black points identify the trends estimated from the tide gauge data, the red points those from the satellite altimeter data, and the blue points the tide gauge trends corrected for the VLM. Error bars represent the 95% confidence interval.*

4.1.2 Greek tide gauges

Along the Greek coast, 8 tide gauge stations were investigated. Unfortunately, GPS data were available only for two of these stations, namely the Levkas and Thessaloniki sites.

The highest relative sea-level trend of this study has been estimated at the Levkas station, 9.54 ± 1.11 mm/yr, on the Western coast of Greece. This value is almost 7 mm/yr higher than the absolute trend estimated at the nearest satellite grid point, 2.57 ± 0.73 mm/yr, suggesting a strong subsidence rate at this site. The VLM trend computed from the time series of the SPAN GPS, over a seven year time span (2007-2014) is equal to -1.23 ± 0.11 mm/yr, reducing the tide gauge trend to a value of 8.31 ± 1.14 mm/yr.

The two stations of Katakolon and Khalkis North present similar relative sea-level trends, 6.04 ± 1.08 mm/yr, 6.14 ± 1.29 mm/yr, respectively, and absolute trends, 3.29 ± 0.69 mm/yr, 3.42 ± 0.96 mm/yr, respectively. These values suggest a rate of VLM approximately equal to -2.75 mm/yr for the two sites, in agreement with other studies. In fact, land subsidence has been found in these regions during the SELF project [Zerbini et al., 1996; Becker et al., 2002], also, Garcìa et al.

(2012) estimated a rate of VLM around -3 mm/yr for the Khalkis North station, over the period 1993-2007.

For the islands of Siros, Leros and Khios, in the Aegean Sea, the trends computed from satellite data are larger than those calculated from the tide gauge records, suggesting a small uplift rate for the three sites. In any case, the trends obtained from the two techniques are comparable, within the 95% confidence interval. The Siros station presents the highest absolute sea-level trend found over the time period considered in this study, equal to 4.47 ± 1.00 mm/yr, while the two sites of Leros and Khios show absolute sea-level trends around 4 mm/yr. Small uplift rates in this area have been found in other works [Fenoglio-Marc et al., 2004; Garcìa et al., 2007]. Although not included in this analysis, since it did not cover the three years of data required to estimate a reliable vertical velocity [Blewitt and Lavallée, 2002], a VLM trend has been computed from the vertical component time series of the Khios CH00 GPS station. These GPS data were acquired from the NGL database, and a vertical trend of 1.48 ± 1.30 mm/yr has been estimated for the two-year period 2012-2014, in agreement with the hypothesis of uplift in this area.

Finally, the tide gauges of Thessaloniki and Alexandroupolis have been analyzed in the northern part of the Aegean Sea. The trend estimated from the tide gauge data in Alexandroupolis is consistent with the trend derived from satellite altimetry; both value are close to 4 mm/yr. In Thessaloniki, the available GPS allowed to compute the VLM trend of the site, finding a rate of subsidence equal to -1.71 ± 0.11 mm/yr. The trend measured by the tide gauge, corrected for the vertical land motion, is comparable to the absolute sea-level trend.

The rates of mean sea-level rise, obtained from the analysis of the satellite records, tide gauge data and tide gauge corrected for GPS vertical velocities, along the Greek coasts are graphically compared in Figure 4.3.

4.1.3 Tide gauges in the Adriatic Sea

Twelve tide gauge stations have been analyzed in the Adriatic Sea, with GPS data available for 8 of them.

Along the east coast of the Adriatic Sea, the three tide gauge stations at Dubrovnik, Split and Zadar have been analyzed in the Dalmatian region. A significant trend of VLM has been found only in Dubrovnik, where a subsidence rate of -1.76 ± 0.16 was estimated. The Split GPS gave a VLM rate of 0.05 ± 0.18 mm/yr, while no GPS time series is available in Zadar. The trend in Dubrovnik,

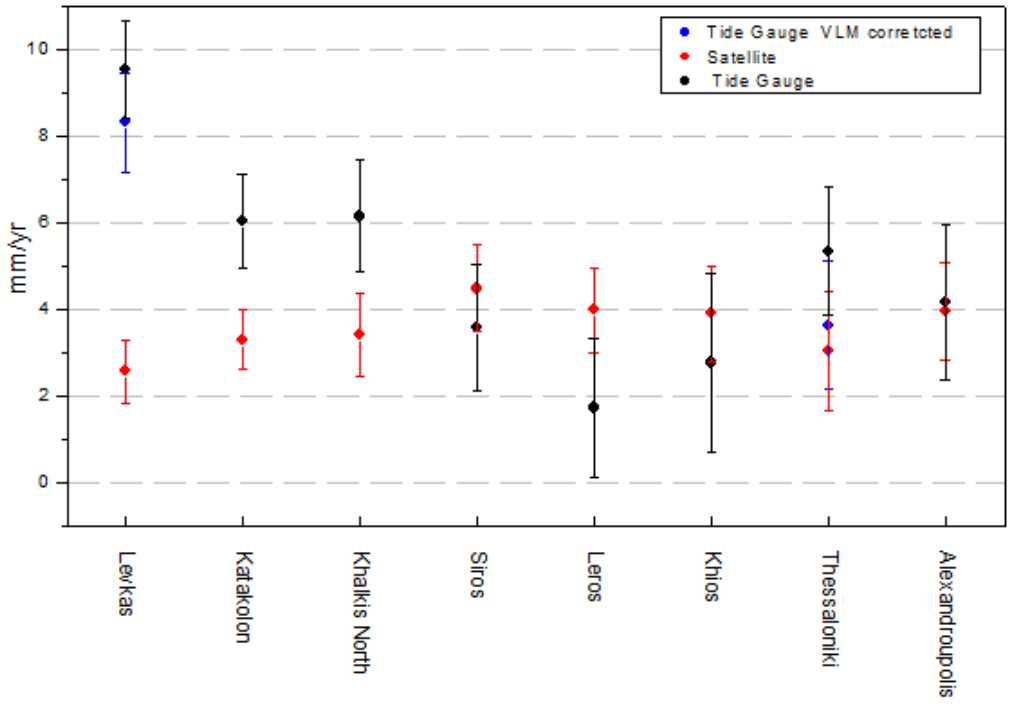

Figure 4.3: *Sea-level trends computed from the tide gauge and the satellite data along the Greek coasts. The black points identify the trends estimated from the tide gauge data, the red points the sea level trend from the satellite altimeter data, and the blue points the tide gauge trends corrected for the VLM. Error bars represent the 95% confidence interval.*

corrected for the VLM, and the two relative trends at the Split and Zadar stations are comparable with those estimated from satellite altimetry. The absolute sea-level trends increase from south to north, with a rate of sea-level rise equal to 3.41 $\pm$ 0.80 mm/yr in Dubrovnik, 3.93 $\pm$ 0.92 mm/yr in Split and 4.04 $\pm$ 0.96 mm/yr in Zadar.

In the Southern Adriatic, sea-level trends around 3.70 mm/yr were found from the satellite data for the two neighboring stations of Otranto and Bari. A small rate of land subsidence has been detected from the data of the GPS station in Otranto, -0.44 $\pm$ 0.17 mm/yr, obtaining a sea-level trend of 3.37 $\pm$ 1.15 mm/yr by applying this VLM correction to the rate measured by the tide gauge. No suitable GPS was found near Bari, but the relative trend is comparable with the absolute one, within the 95% confidence interval.

In the Central Adriatic, on the Italian coast, two sites have been analyzed. In Ortona, a large relative sea-level trend of 6.72 $\pm$ 1.97 mm/yr has been estimated, associated with a significant rate of land subsidence, -1.81 $\pm$ 0.51 mm/yr, measured from the local GPS. On the contrary, in Ancona, the relative sea-level trend, 3.08

± 1.62 mm/yr, is affected by land uplift equal to 1.12 ± 0.33 mm/yr. The mean sea-level trends estimated, for each station, at the nearest satellite grid point are similar, 4.14 ± 0.86 mm/yr in Ortona and 4.12 ± 0.96 mm/yr in Ancona. The two trends measured by the tide gauges have been corrected for the estimated VLM, obtaining values comparable with the absolute sea-level rise computed from satellite altimetry.

In the Northern Adriatic, a total of 5 stations have been selected for this analysis. Along the Croatian coast, the two stations of Bakar and Rovinj were analyzed. In Bakar, the relative sea-level trend measured by the tide gauge, 3.19 ± 1.47 mm/yr, is comparable with the absolute trend computed from the AVISO data, 3.80 ± 0.96 mm/yr. No GPS data were available, but the small difference between the two trends shows that the site might be subjected to a small uplift rate, which is in agreement with the results found by Fenoglio-Marc et al. (2012). On the coast of the Istrian Peninsula, the relative sea-level trend, 1.96 ± 1.25 mm/yr, of the Rovinj tide gauge is significantly smaller than the absolute mean sea-level rise derived from the satellite records, 4.33 ± 0.96 mm/yr. This suggests that land uplift might affect the tide gauge site; however, no significant VLM has been estimated from the nearest GPS (PORE) station, 0.28 ± 0.39 mm/yr., This GPS station is located more than 16 km northward with respect to the tide gauge site, and the data span is only three years long (2011-2014), the minimum required to compute a reliable vertical velocity.

The northernmost location of this study is the Trieste tide gauge station. The relative sea-level trend measured from the tide gauge data, 5.05 ± 1.20 mm/yr, is almost 1 mm/yr higher than absolute sea level rise, 4.01 ± 1.07 mm/yr. A relatively small positive VLM, equal to 0.91 ± 0.10 mm/yr, was found from the analysis of the GPS data over the period 2007-2014,. Becker et al. (2002) detected land subsidence in Trieste, whereas Garcìa et al. (2012) found no significant land motion over the period 1993-2007. However, both the sea-level trend obtained from the tide gauge data, and the one corrected for the VLM, 5.96 ± 1.21 mm/yr, are consistent, within the 95% confidence interval, with the mean sea-level rise estimated from satellite altimetry.

Finally, high relative sea-level trends were found in Marina di Ravenna and Venice, 7.13 ± 1.67 mm/yr and 6.52 ± 1.16 mm/yr, respectively. These two stations are located in the Po Plain, a zone which is subjected to both natural and anthropogenic subsidence [Zerbini et al., 2007]. In Venice, the VLM has been investigated in many studies, over different periods, showing high spatial and temporal variations [Zerbini et al., 1996; Becker et al., 2002; Tosi et al., 2002;

Strozzi et al., 2009]. Zerbini et. Al. (2015) have realized a non-linear subsidence correction by analyzing the sea-level data starting from the end of the 1800 and by using all available benchmarks heights from levelling measurements, InSAR and GPS vertical information. The corrected Venice tide gauge data were made available for this work (Zerbini, personal communication) and lead to an estimate of the absolute sea-level trend equal to 4.02 ± 1.18 mm/yr, in very good agreement with the rate estimated from satellite altimetry for the closest point to the Venetian coast. In Marina di Ravenna, the natural subsidence has been greatly enhanced by anthropogenic activities, primarily gas and groundwater extraction, during the second half of the twentieth century [Zerbini et al., 2007]. The GPS was installed in Marina di Ravenna in 1996, in close proximity of the tide gauge [Zerbini et al., 1996; Becker et al., 2002]. A strong subsidence rate, equal to -5.67 ± 0.10 mm/yr, is derived when the GPS vertical time series is approximated by a linear fit, over the period 1996-2014. By correcting the relative sea-level trend for this VLM, an absolute sea-level rate of 1.46 ± 1.69 mm/yr is obtained. This trend is definitely lower than the value, 4.28 ± 0.90 mm/yr, estimated with satellite altimetry data for the closest point to the Marina di Ravenna coastal area. Also for this tide gauge, Zerbini et al. (2015), have realized a non-linear subsidence correction using the tide gauge data from the end of the 1800, benchmarks heights from levelling measurements, InSAR and GPS height time series. For the period 1993-2014, the absolute sea level series thus obtained by Zerbini et al. (2015, personal communication) was used to estimate the VLM that turns out to be 4.16 ± 1.67, quite comparable to the result provided by the satellite altimetry data. For the two stations of Venice and Marina di Ravenna, new correlation coefficients were calculated between the tide gauge time series corrected for the non-linear VLM and the AVISO satellite data. Using these records, the correlation coefficients estimated increase, exhibiting a value equal to 0.78 for both sites. The sea-level trends obtained from the analysis in the Adriatic Sea are graphically compared in Figure 4.4.

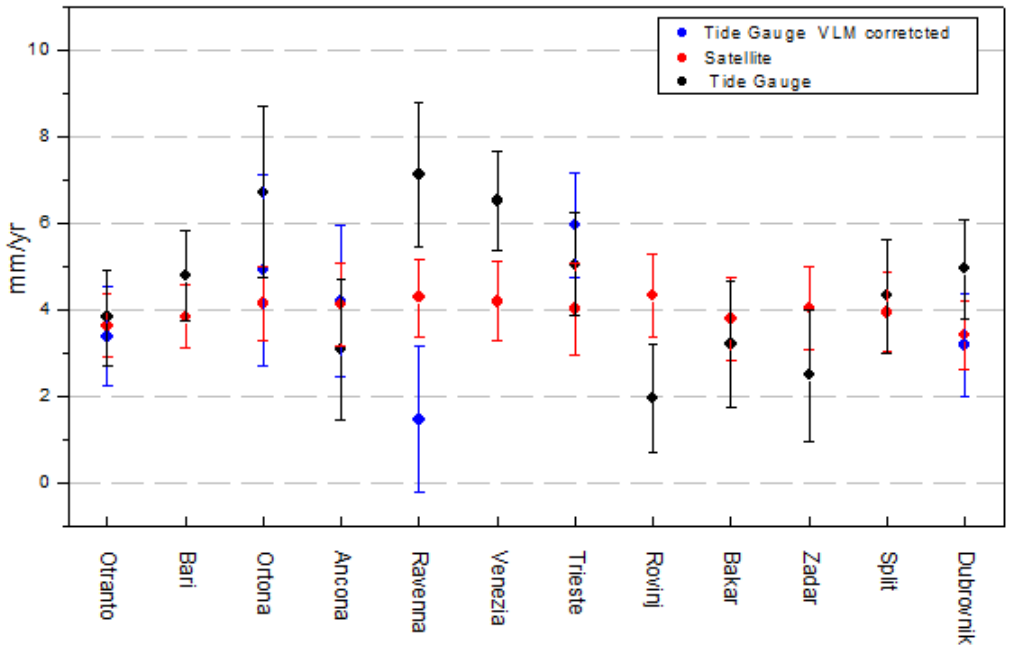

Figure 4.4: *Sea-level trends computed from tide gauge and satellite data in the Adriatic Sea. The black points identify the trends estimated from the tide gauge data, the red points the sea-level trend from the satellite altimeter data, and the blue points the tide gauge trends corrected for the VLM. Error bars represent the 95% confidence interval.*

4.2 Period 1993-2013: tide gauges, AVISO and CCI satellite data

In this section, the CCI data are introduced as a further comparison between tide gauge and satellite records. Due to the shorter data span of the CCI time series, the sea-level trends described in the previous section were recalculated over the period 1993-2013.

Before proceeding with the comparison of the datasets, it is worthwhile to recall the main differences between the CCI and AVISO data sets:

- SLA grids of spatial resolution equal to $1/8° \times 1/8°$ and $1/4° \times 1/4°$ for the CCI data, respectively;
- the introduction in GNSS data analysis of the wet tropospheric delay correction, in the CCI data [Fernandes et al., 2014];
- the use of pressure data from ERA-interim reanalysis for the computation of the dry tropospheric correction and the dynamic atmospheric correction

(DAC) for the CCI records [Carrere et al., 2015].

In this section, the tide gauge sea-level trends of the 21 sites equipped with GPS are the absolute trends, meaning that the VLM correction has been applied. The Trieste tide gauge data were not corrected for the GPS-derived vertical land motion because the GPS time series only partially overlaps the 1993-2014 sea-level data span. For Marina di Ravenna and Venice, the values derived from the land subsidence correction presented in Zerbini et al. (2015), were adopted. Additionally, the correlation coefficients between the tide gauge time series and the CCI records have been calculated (see Eq. 4.2). The sea-level trends computed from the tide gauge data and the two satellite altimetry datasets are presented separately in two tables: Table 4.4 shows the stations where the tide gauge data were corrected for the VLM, the remaining locations are listed in Table 4.5.

The tide gauge and the CCI time series are always positively correlated, with correlation coefficients ranging between 0.5 and 0.75. A slightly higher correlation was obtained in section 4.1 with the data from AVISO, especially in the Northern Adriatic. Here, the best correlation has been obtained in the Aegean Sea, at the three Islands of Siros, Leros and Khios ($r = 0.75$, 0.74 and 0.74, respectively).

Considering the 22 sea-level trends corrected for the VLM, the three datasets turns out to be consistent, within the 95% confidence interval, almost everywhere. Differences larger than 2 mm/yr between the rate estimated from the AVISO and CCI records were found in three sites (Ceuta, Tarifa and Catania), the differences at the other sites range between 0.5 and 1 mm/yr.

By using the CCI data, two anomalous large sea-level rates were found for the Ceuta, 5.08 $\pm$ 0.78 mm/yr, and Tarifa, 5.20 $\pm$ 0.73 mm/yr, stations, in the Gibraltar Straits, while the trends computed from the AVISO and the tide gauge time series are in very good agreement, approximately equal to half the rates derived from the CCI records.

In Rovinj, the best agreement is found between the tide gauge and CCI trends. In paragraph 4.1.3, the difference between the trends computed from the tide gauge and the AVISO satellite records was attributed to an underestimation of the VLM. Over the period analyzed in the present section, a 2 mm/yr discrepancy is still present between the tide gauge, 1.96 $\pm$ 1.25 mm/yr, and the AVISO-derived trend, 3.85 $\pm$ 1.33 mm/yr. On the contrary, the mean sea-level rise derived from the CCI records, 2.30 $\pm$ 1.30 mm/yr is consistent with the rate computed from the tide gauge data.

No significant sea-level rise has been found in Catania, 0.42 $\pm$ 0.89 mm/yr,

Table 4.4: *Sea-level trends over the period 1993-2013, computed from tide gauge, CCI and AVISO data sets. Column 1 identifies the tide gauge station, column 2 lists the trend computed from the tide gauge data and corrected for the VLM, column 3 the sea level rate estimated from the CCI satellite data, column 4 the correlation coefficient between the tide gauge and the CCI time series and column 5 the sea-level trend computed from the AVISO satellite records.*

Tide Gauge	Tide gauge corrected for VLM (mm/yr)	CCI data (mm/yr)	Correlation coefficient r	AVISO data (mm/yr)
Ancona	3.32 ± 1.71	3.46 ± 0.97	0.62	3.70 ± 1.00
Dubrovnik	3.18 ± 1.14	3.38 ± 0.79	0.74	3.02 ± 0.84
Ortona	3.60 ± 2.23	3.97 ± 0.98	0.69	3.58 ± 0.89
Otranto*	2.84 ± 1.16	3.43 ± 0.81	0.68	3.06 ± 0.78
Ravenna	4.38 ± 1.76	3.37 ± 1.48	0.65	3.88 ± 0.94
Rovinj	1.96 ± 1.25	2.30 ± 1.30	0.57	3.85 ± 1.33
Split	4.31 ± 1.31	3.28 ± 0.87	0.65	3.47 ± 0.93
Trieste	4.61 ± 1.22	2.79 ± 1.40	0.60	3.49 ± 1.13
Venezia	3.38 ± 1.18	3.42 ± 0.99	0.66	3.73 ± 0.96
Barcelona	4.32 ± 0.84	2.01 ± 0.59	0.64	1.95 ± 0.58
Cagliari	3.91 ± 0.92	2.74 ± 0.63	0.60	2.30 ± 0.61
Catania*	2.64 ± 0.94	2.94 ± 0.90	0.54	0.42 ± 0.89
Ceuta	2.50 ± 1.11	5.08 ± 0.78	0.55	2.55 ± 0.68
Genova	2.59 ± 1.23	3.66 ± 0.57	0.58	2.36 ± 0.59
Malaga	3.18 ± 1.01	4.43 ± 0.72	0.50	3.42 ± 0.70
Marseille	2.98 ± 1.00	2.84 ± 0.70	0.65	2.54 ± 0.72
Napoli*	3.47 ± 1.06	3.32 ± 0.74	0.69	2.66 ± 0.68
Salerno*	3.27 ± 1.44	2.28 ± 0.68	0.61	2.62 ± 0.67
Tarifa	2.43 ± 0.98	5.20±0.73	0.58	2.45 ± 0.62
Valencia	3.85 ± 1.09	2.72±0.56	0.51	1.80 ± 0.52
Levkas	8.57 ± 1.22	3.41 ± 0.99	0.59	2.04 ± 0.76
Thessaloniki	3.61 ± 1.59	1.99 ± 1.32	0.66	3.02 ± 1.37

Table 4.5: *Sea-level trends over the period 1993-2013, computed from tide gauge, CCI and AVISO data sets. Column 1 identifies the tide gauge station, column 2 lists the relative sea-level trend measured by the tide gauge, column 3 the sea-level rate estimated from the CCI satellite data, column 4 the correlation coefficient between the tide gauge and the CCI time series, and column 5 the sea-level trend computed from the AVISO satellite records.*

Tide Gauge	Relative sea-level (mm/yr)	CCI data (mm/yr)	Correlation coefficient r	AVISO data (mm/yr)
Bakar	3.10 ± 1.53	3.35 ± 0.66	0.64	3.48 ± 1.03
Bari*	4.08 ± 1.09	3.11 ± 0.79	0.66	3.41 ± 0.79
Zara	2.48 ± 1.53	3.04 ± 1.04	0.63	3.66 ± 1.02
L'Estartit	3.24 ± 0.80	2.64 ± 0.60	0.66	1.96 ± 0.62
Livorno*	3.04 ± 1.13	2.24 ±0.66	0.69	2.66 ± 0.66
Taranto*	4.40 ± 1.74	3.65 ±0.78	0.69	2.08 ± 0.82
Toulon	3.15 ± 0.86	3.03 ± 0.69	0.61	2.19 ± 0.64
Alexandroupolis	4.43 ± 1.94	4.51 ± 1.36	0.69	3.91 ± 1.22
Katakolon	5.87 ± 1.15	3.75 ± 0.85	0.62	2.97 ± 0.73
Khalkis North	6.20 ± 1.37	2.51 ± 1.01	0.59	3.42 ± 0.96
Khios	2.77 ± 2.05	2.68 ± 1.06	0.74	3.64 ± 1.20
Leros	1.34 ± 1.73	4.36 ± 1.08	0.74	3.65 ± 1.04
Siros	3.33 ± 0.77	4.59 ± 1.11	0.75	4.05 ± 1.07

from the AVISO records, over the period 1993-2013. However, a positive trend of 2.64 ± 0.94 mm/yr was computed from the tide gauge data, corrected for the land subsidence affecting the site. In section 4.1.1, a similar situation has been discussed for the period 1993-2014. The sea-level rise derived from the CCI records is equal to 2.94 ± 0.90 mm/yr, which is in agreement with the trend computed using the tide gauge data.

For the tide gauges where no information is available concerning the VLM, the two satellite datasets turns out to be consistent at all sites, the only difference larger than 1 mm/yr was found in Taranto, where a smaller rate of sea-level rise, 2.08 ± 0.82 mm/yr, is obtained from the AVISO data. The trend computed from the CCI records, 3.65 ± 0.78 mm/yr, is comparable with the relative sea-level trend measured by the tide gauge, 4.40 ± 1.74 mm/yr.

The trends computed from the tide gauge and the CCI records are very similar in Toulon, 3.15 ± 0.86 mm/yr, 3.03 ± 0.69 mm/yr, respectively, Alexandroupolis,

4.43 ± 1.94 mm/yr, 4.51 ± 1.36 mm/yr, respectively, and Khios, 2.77 ± 2.05 mm/yr, 2.68 ± 1.06 mm/yr, respectively. These values are also comparable with rate obtained from the AVISO data, within the 95% confidence interval.

Overall, the CCI data have provided better results in Rovinj and Catania, while the trends computed in the Gibraltar Straits appeared to be anomalously large. At the other stations, both AVISO and CCI derived trends are comparable, and, in some cases, the sea-level rate from the CCI data is almost equal to the trends determined by the tide gauge data. The linear trends obtained from the three datasets, over the period 1993-2013 are graphically compared in Figures 4.5 and 4.6.

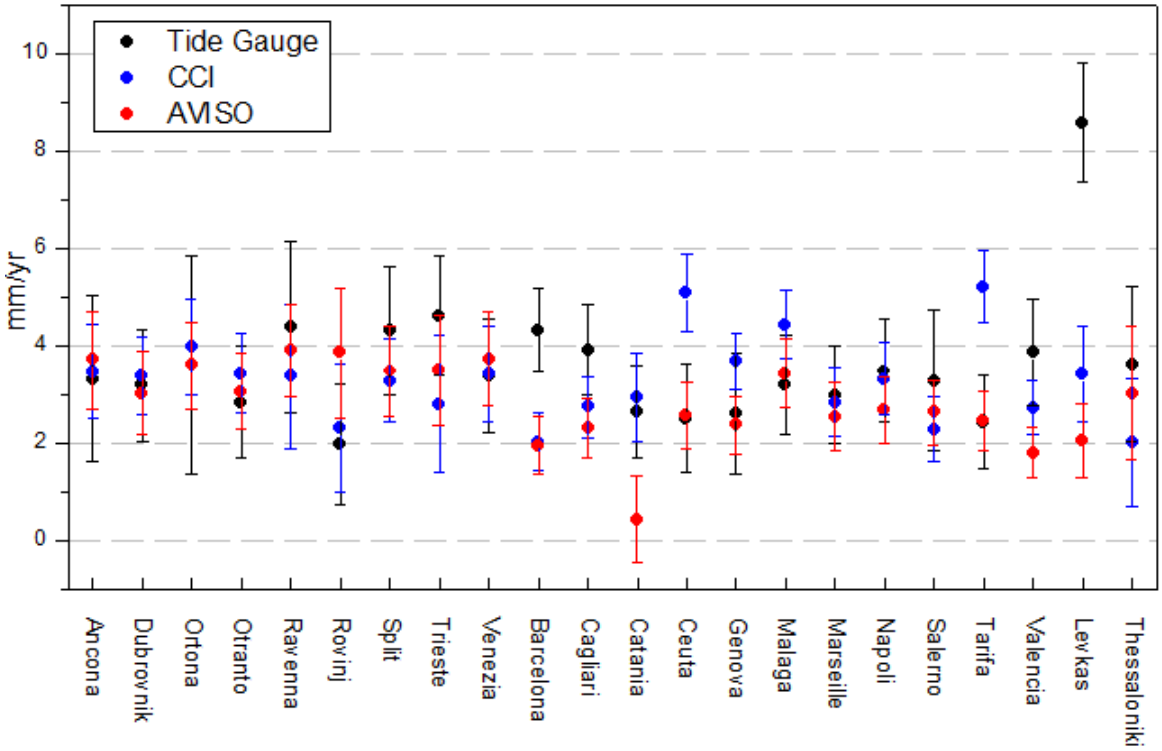

Figure 4.5: *Sea-level trends computed from tide gauge, CCI and AVISO data sets over the period 1993-2013. The black points identify the trends estimated from the tide gauge data corrected for the VLM, the red points the trends from the AVISO satellite time series, and the blue points the trends estimated from the CCI records. Error bars represent the 95% confidence interval.*

A map of the differences between the trends computed from the AVISO and CCI data, over the whole Mediterranean Sea, has been provided by Prof. Fenoglio-Marc (personal communication), for the period 1993-2013 (Fig 4.7). Figure 4.8 presents the differences of the trends over the Adriatic Sea.

This spatial distribution of the differences is in agreement with the results

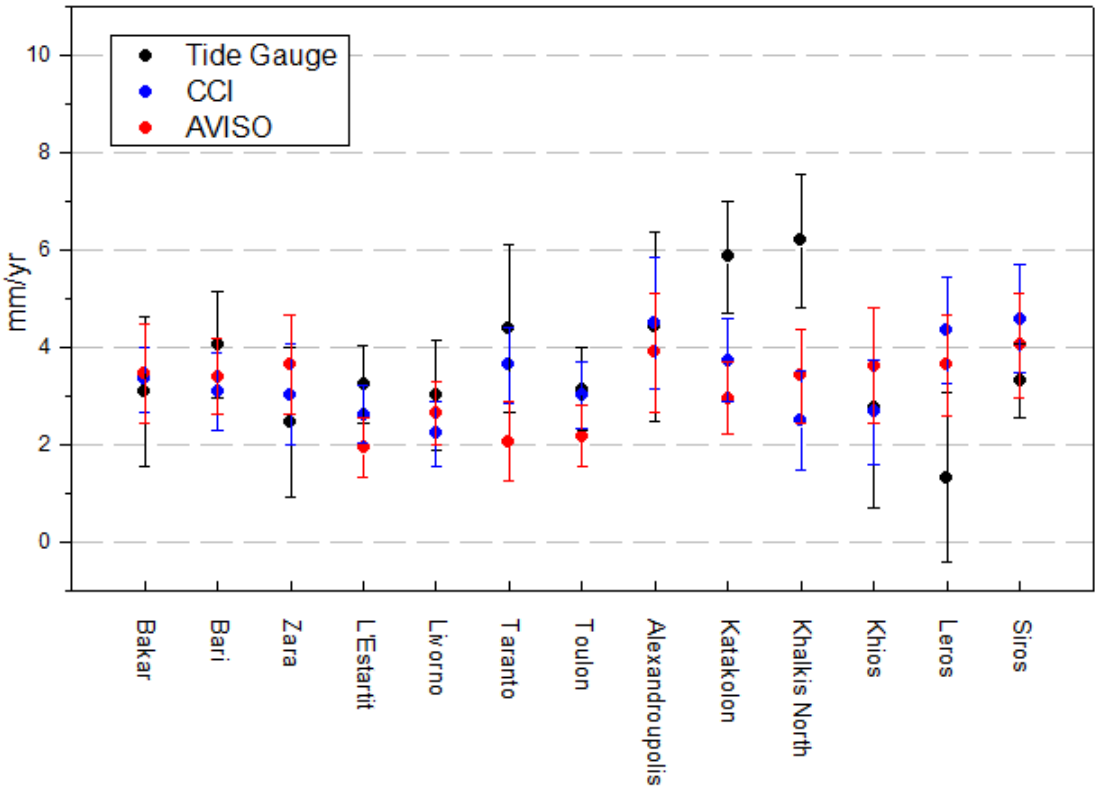

Figure 4.6: *Sea-level trends computed from tide gauge, CCI and AVISO data, over the period 1993-2013. The black points identify the relative sea-level trends estimated from the tide gauge data, the red points the trends from the AVISO satellite data, and the blue points the trends estimated from the CCI records. Error bars represent the 95% confidence interval.*

presented in this section. In fact, the discrepancies between the trends computed from the two satellite datasets are within 0.50 mm/yr, except in a few locations as, for example, in the Northern Adriatic and the Eastern Sicilian coast.

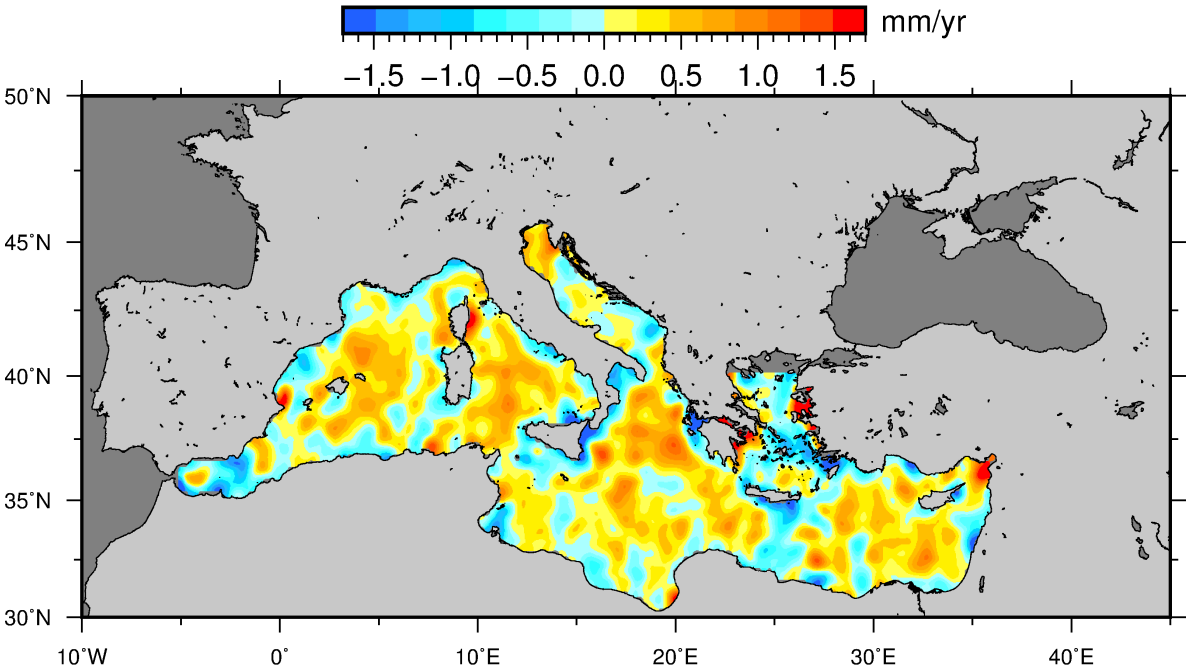

Figure 4.7: *Differences of the trends computed from AVISO and CCI satellite data in the Mediterranean Sea, over the period 1993-2013 (Courtesy of Prof. L. Fenoglio-Marc).*

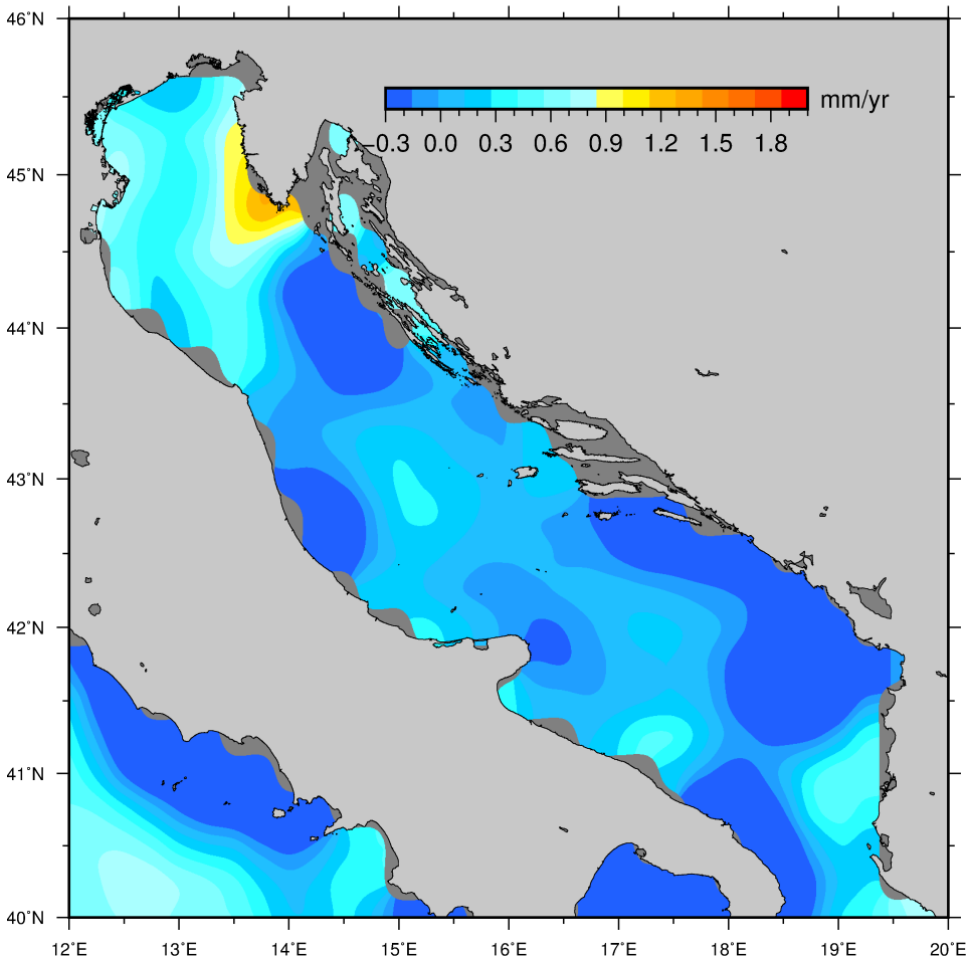

Figure 4.8: *Differences of the trends computed from AVISO and CCI satellite data in the Adriatic Sea, over the period 1993-2013 (Courtesy of Prof. L. Fenoglio-Marc).*

Chapter 5

Conclusions and Outlook

In this thesis, linear absolute sea level trends have been estimated in the Mediterranean Basin from the data of the two main sea level observation techniques: tide gauges and satellite radar altimetry. A comparison between the rates obtained at specific sites has been performed, in order to assess the consistency of the results.

Tide gauge data have been extracted from two networks: 22 stations with monthly time series were selected from the PSMSL data set, and 13 Italian stations with hourly data were chosen from the RMN data set, for a total of 35 sites in the Mediterranean Sea area. For 7 Italian sites, the estimation of a datum shift in summer 1998 has been necessary. These discontinuities were corrected using the STARS methodology [Bruni et al., 2014]. The RMN data have been averaged in monthly means. The IB correction was performed on the 35 tide gauge time series by means of linear regression coefficients estimated between monthly atmospheric pressure values from NCEP/NCAR Reanalysis 1 [Kalnay et al., 1996] and sea level data.

The satellite altimetry data used were those distributed by AVISO, in the form of daily time series, and by ESA, in the framework of the CCI project, in the form of monthly values. The daily data from AVISO were averaged in monthly values. The satellite data from the two different sources are distributed already corrected for the IB effect. The absolute sea level trends have been computed in correspondence of the nearest satellite altimeter grid point to each station.

The seasonal component has been evaluated for each time series, to obtain deseasoned monthly data set. Linear sea level trends were then computed, and the associated standard errors have been calculated accounting for the autocorrelation of the residuals.

The first period analyzed spans 22 years: from 1993 to 2014, during which the trends derived from the tide gauge data and the AVISO satellite altimetry time series have been compared. The relative sea level trends differ significantly from point to point likely because of local VLM affecting the tide gauge observations. Trend values not corrected for subsidence range from 1.7 to 9.5 mm/yr. The lowest value, equal to 1.73 ± 1.60 mm/yr, was found in the Leros island station, in the Aegean Sea, while values up to three time larger were detected at 8 stations. The highest relative trend, equal to 9.54 ± 1.11 mm/yr, has been found in the Lefkada island station, in the Eastern Ionian Sea. Values up to 7 mm/yr were detected in 4 sites, namely Ortona, Marina di Ravenna and Venice, located along the Italian coastline of the Adriatic Sea, and Naples, on the Italian Western coast of the Tyrrhenian Sea. These relative trends need to be corrected for the possible VLM affecting the tide gauge site. GPS stations were selected within 20 km from the tide gauge station and with time series at least three years long. The close proximity of the GPS to the tide gauge site should ensure as much as possible that the VLM affecting the tide gauge station is correctly identified. For the 35 sites investigated, 21 GPS stations satisfy these selection criteria. Discontinuities present in GPS time series were corrected using the STARS methodology and linear VLMs have been computed. The ground component was removed by summing the relevant VLM with the relative linear trend obtained from the analysis of observations of each tide gauge. Among these 21 GPS stations, land subsidence has been found in 13 sites, with the highest values detected in Naples, -3.90 ± 0.27 mm/yr, and Marina di Ravenna, -5.67 ± 0.10 mm/yr. Uplift rates have been identified in three locations, up to 1 mm/yr in Ancona and Trieste, and around 0.5 mm/yr in Ceuta. No significant VLM have been found for the remaining 5 stations.

The 21 tide gauge sea level trends corrected for the VLM have been compared to those estimated from the AVISO satellite altimetry data. These trends are consistent, within the 95% confidence interval almost at every station. Differences in some sites might be due to the spatial distance between the tide gauge and the nearest GPS station, or to the shorter time span of the GPS time series with respect to the tide gauge records. In the case of the Marina di Ravenna and Venice stations, analyses of the long term (centennial) time series, performed by different authors, have shown that the local subsidence can hardly be represented by a simple linear trend. Zerbini et al. (2015) have modeled the subsidence behavior with a non-linear curve by using leveling benchmarks, GPS and SAR observations, at both stations. By using these non-linear VLM corrections, the tide gauge sea-level trends turn out to be in excellent agreement with the coastal value derived

from satellite altimetry.

Considering the 14 stations where no information on the GPS-derived VLM is available, 11 relative sea level trends are in agreement with the values obtained from the AVISO data, suggesting that, at these sites, vertical land motions might be small. Differences in the order of 2 mm/yr were found between the absolute and relative trends at two stations, namely Khalkis North and Katakolon, in Greece. This suggests the presence of land subsidence, in agreement with previous investigations concerning these sites [Zerbini et al., 1996; Becker et al., 2002].

An additional comparison has been performed between the monthly VLM-corrected tide gauge time series and the AVISO monthly time series of the grid point nearest to the coast. These pairs of data sets have been correlated; the results show significant positive correlation in almost all cases, ranging from 0.6 to 0.8. The only exception is the Valencia site, where the correlation coefficient turns out to be 0.48.

The CCI satellite records have been compared with the AVISO and tide gauge data, over the period 1993-2013, due to the presently shorter time span of the CCI products. Generally, the monthly CCI and tide gauge time series present a slightly smaller correlation with respect to the coefficients computed between the tide gauge and the AVISO records. The trends computed from the three different data sets are consistent, except in two locations, Tarifa and Ceuta in the Gibraltar Straits area, where the differences of the trends estimated from the two satellite data sets are in the order of 2 mm/yr.

In conclusion, all the linear sea-level trends computed in this work, for the 35 selected tide gauge stations in the Mediterranean Sea, over both analyzed periods, 1993-2014 and 1993-2013, are positive. The 21 stations corrected for the VLM, using GPS data, provide a mean sea-level trend in the order of 3.7 mm/yr, in agreement with recent estimates of the global mean sea-level rise.

The main limitation of the tide gauge technique is that GPS stations in close proximity of the tide gauge are not always available, despite the recommendations of major international programs. Also, in many stations, the time interval for which GPS data are available does not overlap with that of the tide gauge data, in general, the GPS time series are shorter than the sea-level time series. Therefore, one possibility is to propagate the VLM correction to the past, assuming a linear and uniform behavior over the whole period analyzed. Comparing the tide gauge sea level trends corrected for the VLM with coastal absolute sea level trends estimated by satellite radar altimetry, consistent results are found almost at all sites. This demonstrates the importance of the GPS data to achieve a reliable

separation in the tide gauge data between the real sea-level variations/changes and the land vertical motions. For those sites lacking of GPS receiver, information on the local VLM can be extrapolated from the differences between the satellite altimetry-derived absolute trend and the relative trend estimated from the tide gauge data. In these particular cases, the results found are mostly in agreement with VLM estimates derived by previous investigations. Overall, both the AVISO and CCI sea level gridded products have provided trends consistent with those estimated from the VLM corrected-tide gauge records.

For what concerns future studies of GPS-corrected tide gauge records, results might improve as the GPS time series will become longer. Also, it shall be pointed out that the number of tide gauge equipped with co-located permanent GPS stations is still limited. The installation of new GPS stations, suitable for tide gauge applications, is mandatory and recommended by international organizations and programs.

Acknowledgement

The altimeter products used in this study were produced by Ssalto/Duacs, distributed by AVISO with support from CNES (http://www.aviso.altimetry.fr/duacs/), and by ESA in the framework of the CCI project (http://www.esa-sealevel-cci.org/). I acknowledge ISPRA (http://www.mareografico.it/) and PSMSL (http://www.psmsl.org/data/obtaining/) for the tide gauge data, NGL (http://geodesy.unr.edu/) and SONEL (http://www.sonel.org/-GPS-.html) for the GPS data. All these data are freely available through their respective web portal. I sincerely thank Prof. S. Zerbini for the GPS data of Trieste and Marina di Ravenna and for the vertical land motion rate of Venice and Marina di Ravenna. I acknowledge Prof. L. Fenoglio-Marc for providing the maps of the trend differences over the Mediterranean and Adriatic Sea.

Bibliography

Ablain, M., A. Cazenave, G. Valladeau, and S. Guinehut (2009), A new assessment of the error budget of global mean sea level rate estimated by satellite altimetry over 1993-2008, *Ocean Sci.,* 5(2), 193–201. doi:10.5194/os-5-193-2009.

Ablain, M., A. Cazenave, G. Larnicol, M. Balmaseda, P. Cipollini, Y. Faugère, M. J. Fernandes, O. Henry, J. A. Johannessen, P. Knudsen, O. Andersen, J. Legeais, B. Meyssignac, N. Picot, M. Roca, S. Rudenko, M. G. Scharffenberg, D. Stammer, G. Timms, and J. Benveniste (2015), Improved sea level record over the satellite altimetry era (1993–2010) from the Climate Change Initiative project, *Ocean Sci.,* 11, 67-82. doi:10.5194/os-11-67-2015.

Alley, R.B., P.U. Clark, P. Huybrechts and I. Joughin (2005), Ice-sheets and sea-level changes, *Science 310,* 456–60.

Antonov, J. I., S. Levitus, and T. P. Boyer (2005), Thermosteric sea level rise, 1955–2003, *Geophys. Res. Lett., 32,* L12602. doi:10.1029/2005GL023112.

Arendt, A., et al. (2012), Randolph Glacier Inventory [v2.0]: A Dataset of Global Glacier Outlines. Global Land Ice Measurements from Space, Boulder Colorado, USA. Digital Media 32 pp.

Ballu, V., M.-N. Bouin, P. Siméoni, W.C. Crawford, S. Calmant, J.-M. Boré, T. Kanas, B. Pelletier (2011), Comparing the role of absolute sea-level rise and vertical tectonic motions in coastal flooding, Torres Islands (Vanuatu), in *Proceedings of the National Academy of Sciences of the United States of America,* Sleep, N.H. (Ed.), Stanford University, Stanford. doi:10.1073/pnas.1102842108.

Becker, M., et al. (2002), Assessment of height variations by GPS at Mediterranean and Black Sea coast tide gauges from the SELF Projects, *Global Planet. Change,* 34, 5–35.

Beckley, B. D., N. P. Zelensky, S. A. Holmes, F. G. Lemoine, R. D. Ray, G. T. Mitchum, S. D. Desai and S. T. Brown (2010), Assessment of the Jason-2 Extension to the TOPEX/ Poseidon, Jason-1 sea-surface height time series for global mean sea level monitoring, *Mar. Geodesy,* 33, 447–471.

Bevis, M., W. Scherer, M.A. Merrifield (2002), Technical issues and recommendations related to the installation of continuous GPS stations at tide gauges, *Mar. Geod.,* 25, 87–99.

Bird, E. C. F. (1987), The modern prevalence of beach erosion, *Mar. Pollut. Bull., 18(4),* 151–157.

Bird, E. C. F. (1996), Coastal erosion and rising sea level, in *Sea Level Rise and Coastal Subsidence,* edited by J. D. Millimann and B. U. Haq, pp. 87–103, Kluwer Acad., Dordrecht, the Netherlands.

Blewitt, G., and D. Lavallée (2002), Effect of annual signals on geodetic velocity, *J. Geophys. Res.*, 107, B72145. doi:10.1029/2001JB000570.

Boening, C., J. K. Willis, F. W. Landerer, R. S. Nerem (2012), The 2011 La Nina: So strong, the oceans fell, *Geophys. Res. Lett.,* 39, L19602. doi:10.1029/2012GL053055.

Bouin, M-N., and G. Wöppelmann (2010) Land motion estimates from GPS at tide gauges: a geophysical evaluation, *Geophysical Journal International,* 180, 193-209. doi:10.1111/j.1365-246X.2009.04411.x.

Box, G.E.P., and G.M. Jenkins (1976), Time Series Analysis: Forecasting and Control (revised edition), Holden Day, San Francisco.

Box, G.E.P., W.G. Hunter and J.S. Hunter (1978), Statistics for Experimenters: An Introduction to Design, Data Analysis and Model Building, John Wiley and Sons Inc., New York, USA., ISBN-13:9780471093152, Pages:653.

Braitenberg, C., P. Mariani, L. Tunini, B. Grillo, I. Nagy (2010), Vertical crustal movements from differential tide gauge observations and

satellite altimetry in southern Italy, *J. Geodynam.,* 51, 233-244. doi: 10.1016/j.jog.2010.09.003.

Brown, G. S. (1977), The averageimpulse response of a rough surface and its applications, *IEEE Trans. Antennas Propag.,* 25, 67–74.

Bruni, S., S. Zerbini, F. Raicich, M. Errico, E. Santi (2014), Detecting discontinuities in GNSS coordinate time series with STARS: case study, the Bologna and Medicina GPS sites, *J. Geod.,* 88:1203-1214. doi:10.1007/s00190-014-0754-4.

Callahan, P. S. (1984), Ionospheric variations affecting alimeter measurements: A brief synopsis, *Mar. Geod.,* 8, 249-263.

Carrere, L. and F. Lyard (2003), Modeling the barotropic response of the global ocean to atmospheric wind and pressure forcing – comparison with observations, *Geophys. Res. Lett.,* 30(6), 1275.

Carrere, L., Y. Faugère, and M. Ablain (2015) Improvement of pressure derived corrections for altimetry using the ERA-Interim dataset, *Ocean Sci. Discuss.* under review.

Cartwright, D. E., and R. J. Tayler (1971), New computations of the tide-generating potential, *Geophys. J. R. Astr. Soc.,* 23, 45-74.

Cazenave, A., and W. Llovel (2010), Contemporary sea level rise, *Annual Review of Marine Science,* pp. 145–173, Annual Reviews, Palo Alto, Calif. doi:10.1146/annurev-marine-120308-081105.

Cazenave, A., O. Henry, S. Munier, B. Meyssignac, T. Delcroix, W. Llovel, H. Palanisamy, M. Becker (2012), ENSO influence on the global mean sea level over 1993-2010, *Mar. Geod.,* 35(S1), 82–97. doi:10.1080/01490419.2012.718209.

Cartwright, D. E., and A. C. Edden (1973), Corrected tables of tidal harmonics, *Geophys. J. R. Astr. Soc.,* 33, 253-264.

Cazenave, A. and G. Le Cozannet (2014), Sea level rise and its coastal impacts, *Earth's Future*, 2: 15–34. doi:10.1002/2013EF000188.

Chambers, D. (2011), ENSO-correlated fluctuations in ocean bottom pressure and wind-stress curl in the North Pacific, *Ocean Science Discussions* 8, no. 4:1631-1655.

Chambers, D. P., M. A. Merrifield, R. S. Nerem (2012), Is there a 60-year oscillation in global mean sea level?, *Geophys. Res. Lett.,* 39, L18607. doi:10.1029/2012GL052885.

Chao, B. F., Y. H. Wu, Y. S. Li (2008), Impact of artificial reservoir water impoundment on global sea level, *Science*, 320, 212–214. doi:10.1126/science.115458.

Chelton, D. B., and P. J. McCabe (1985), A review of satellite altimeter measurement of sea surface wind speed: With a proposed new algorithm, *J. Geophys. Res.,* 90, 4707–4720.

Chelton, D. B., E. J. Walsh, and J. L. MacArthur (1989), Pulse compression and sea level tracking in satellite altimetry, *J. Atmos. Oceanic Technol.,* 6, 407–438.

Chelton, D. B., J. C. Ries, B. J. Haines, L. L. Fu, and P. S. Callahan (2001), Satellite altimetry, in *Satellite Altimetry and Earth Sciences: A Handbook of Techniques and Applications,* edited by L.-L. Fu and A. Cazenave, pp. 1–131, Vol. 69, Int. Geophys. Series. Academic Press, San Diego, Calif.

Church, J. A., et al. (2010) Ocean temperature and salinity contributions to global and regional sea-level change, in *Understanding Sea-Level Rise and Variability,*[J. A. Church, P. L. Woodworth, T. Aarup and W. S. Wilson (eds.)], Wiley-Blackwell, Hoboken, NJ, USA, pp. 143-176.

Church, J. A., and N. J. White (2011), Sea-level rise from the late 19th to the early 21st century, *Surv. Geophys., 32(4-5),* 585–602. doi:10.1007/s10712-011-9119-1.

Church, J. A., N. J. White, L. F. Konikow, C. M. Domingues, J. G. Cogley, E. Rignot, J. M. Gregory, M. R. van den Broeke, A. J. Monaghan, I. Velicogna (2011), Revisiting the Earth's sea-level and energy budgets from 1961 to 2008, *Geophys. Res. Lett.,* 38, L18601. doi:10.1029/2011GL048794.

Church, J.A., P.U. Clark, A. Cazenave, J.M. Gregory, S. Jevrejeva, A. Levermann, M.A. Merrifield, G.A. Milne, R.S. Nerem, P.D. Nunn, A.J. Payne,

W.T. Pfeffer, D. Stammer, A.S. Unnikrishnan (2013), Sea Level Change, in *Climate Change 2013: The Physical Science Basis. Contribution of Working Group I to the Fifth Assessment Report of the Intergovernmental Panel on Climate Change*, [Stocker, T.F., D. Qin, G.-K. Plattner, M. Tignor, S.K. Allen, J. Boschung, A. Nauels, Y. Xia, V. Bex and P.M. Midgley (eds.)]. Cambridge University Press, Cambridge, United Kingdom and New York, NY, USA.

Cogley, J. G. (2009), A more complete version of the World Glacier Inventory, *Ann. Glaciol.*, 50, 32–38.

Couhert, A., L. Cerri, J.-F. Legeais, M. Ablain, N. P. Zelensky, B. J. Haines, F. G. Lemoine, W. I. Bertiger, S. D. Desai, and M. Otten (2015), Towards the 1 mm/yr stability of the radial orbit error at regional scales, *Adv. Space Res.,* 55, 2–23. doi:10.1016/j.asr.2014.06.041.

Dee, D., S. Uppala, A. Simmons, P. Berrisford, P. Poli, S. Kobayashi, U. Andrae, M. Balmaseda, G. Balsamo, P. Bauer et al. (2011), The ERA-Interim reanalysis: configuration and performance of the data assimilation system, *Q. J. R. Meteorol. Soc.*, 137: 553–597. doi:10.1002/qj.828

Demerliac, M. A. (1974), Calcul du niveau moyen journalier, *Annales Hydrographiques du SHOM, 5°eme serie,* 2, 49–57.

Desai, S. D. (2002), Observing the pole tide with satellite altimetry, *J. Geophys. Res.,* 107(C11), 3186. doi:10.1029/2001JC001224.

Dieng, H. B., A. Cazenave, K. von Schuckmann, M. Ablain, and B. Meyssignac (2015), Sea level budget over 2005–2013: missing contributions and data errors, *Ocean Sci.,* 11, 789–802. doi:10.5194/os-11-789-2015.

Doodson, A.T. (1921), The Harmonic Development of the Tide-Generating Potential, *Proceedings of the Royal Society of London,* series A, vol. 100, n. 704, pp. 305-329.

Dorandeu, J., and P.-Y. Le Traon (1999), Effects of global mean atmospheric pressure variations on mean sea level changes from TOPEX/Poseidon, *J. Atmos. Oceanic Tech.,* 16, 1279-1283.

Douglas, B.C. (1991), Global sea level rise, *J. Geophys. Res. Oceans,* 96. doi:10.1029/91jc00064.

Douglas, B.C. (1997), Global sea rise: a redetermination, *Surv. Geophys.,* 18. doi:10.1023/a:1006544227856.

Douglas, B.C. (2001), Sea level change in the era of the recording tide gauge, in *Sea Level Rise: History and Consequences. Int. Geophys. Ser.,* Douglas, B.C., M. Kearney, S. Leatherman (Eds.), vol. 75. Academic, San Diego, pp. 37–64. chap. 3.

Ducet, N., P.Y. Le Traon, G. Reverdin (2000), Global high-resolution mapping of ocean circulation from TOPEX/Poseidon and ERS-1 and -2, *J. Geophys. Res.,* 105(C8):19477–19498. doi:10.1029/2000JC900063

Durack, P. J., and S. E. Wijffels (2010), Fifty-Year Trends in Global Ocean Salinities and Their Relationship to Broad-Scale Warming, *J. Climate,* 23, 4342–4362. doi:10.1175/2010JCLI3377.1.

Erez, J. (1978), Vital effect on stable-isotope composition seen in foraminifera and coral skeletons, *Nature,* 273, 199-202. doi:10.1038/273199a0.

Fenoglio-Marc, L., C. Dietz, and E. Groten (2004), Vertical Land Motion in the Mediterranean Sea from Altimetry and Tide Gauge Stations, *Mar. Geod.,* 27:3-4, 683-701. doi:10.1080/01490410490883441.

Fenoglio-Marc, L., C. Braitenberg, and L. Tunini (2012), Sea level variability and trends in the adriatic sea in 19932008 from tide gauges and satellite altimetry, *Phys. Chem. Earth*, Parts A/B/C 40–41(0):47–58. doi:10.1016/j.pce.2011.05.014.

Fernandes, M. J., C. Lázaro, A. L. Nunes, N. Pires, L. Bastos, and V. B. Mendes (2010), GNSS-derived Path Delay: an approach to compute the wet tropospheric correction for coastal altimetry, *IEEE Geosci. Remote Sens. Lett.,* 7, 596–600. doi:10.1109/LGRS.2010.2042425.

Fernandes, M.J., C. Lázaro, M. Ablain, N. Pires (2015), Improved wet path delays for all ESA and reference altimetric missions, *Remote Sensing of Environment*, 169, 50–74. doi:10.1016/j.rse.2015.07.023.

Fukumori, I., R. Raghunath and L. Fu (1998), Nature of global large-scale sea level variability in relation to atmospheric forcing: A modeling study, *J. Geophys. Res.,* 103, 0148-0227. doi: 10.1029/97JC02907.

Garcìa, D., I. Vigo, B. F. Chao, and M.C. Martìnez (2007), Vertical Crustal Motion along the Mediterranean and Black Sea Coast Derived from Ocean Altimetry and Tide Gauge Data, *Pure Appl. Geophys.,* 164, 851-863.

García, F., M. Vigo, D. García-García, J. Sánchez-Reales (2012), Combination of multisatellite altimetry and tide gauge data for determining vertical crustal movements along northern mediterranean coast, *Pure Appl. Geophys.*, 169(8), 1411–1423.

Gardner, A. S., et al. (2013), A reconciled estimate of glacier contributions to sea level rise: 2003 to 2009, *Science,* 340, 852–857.

Godin, G. (1972), The Analysis of Tides, University of Toronto Press, Toronto.

Gomis, D., S. Ruiz, M. Sotillo, E. Álvarez-Fanjul, J. Terradas (2008), Low frequency Mediterranean sea level variability: the contribution of atmospheric pressure and wind, *Glob. Planet. Change,* 63(2–3), 215-229. doi:10.1016/j.gloplacha.2008.06.005.

Gomis, D., M. N. Tsimplis, M. Marcos, L. Fenoglio-Marc, B. Pérez, F. Raicich, I. Vilibić, G. Wöppelmann, and S. Monserrat (2012), Mediterranean sea level variability and trends, in *Mediterranean climate: from past to future,* edited by P. Lionello, pp. 251–293. Elsevier.

Gregory, J.M., J.A. Church, G.J. Boer, K.W. Dixon, G.M. Flato, D.R. Jackett et al. (2001), Comparison of results from several AOGCMs for global and regional sea-level change 1900–2100, *Climate Dynamics* 18, 225–40.

Gregory, J.M., J.A. Lowe, S.F.B. Tett (2006), Simulated global-mean sea level changes over the last half-millennium, *Journal of Climate* 19, 4576–91.

Gregory, J.M., et al. (2013), Twentieth-century global mean sea level rise: Is the whole greater than the sum of the parts?, *J. Clim.,* 26, 4476–4499. doi:10.1175/JCLIM-D-12-00319.1.

Hanna, E., et al. (2013), Ice-sheet mass balance and climate change, *Nature,* 498, 51–59. doi:10.1038/nature12238.

Hay, C.C., E. Morrow, R.E. Kopp, J.X. Mitrovica(2013), Estimating the sources of global sea level rise with data assimilation techniques *Proc. Natl. Acad. Sci. USA*,110, 3692–3699.

Hay, C.C., E. Morrow, R.E. Kopp, and J.X. Mitrovica (2015), Probabilistic reanalysis of twentieth-century sea-level rise, *Nature* 517, 481–484.

Hernandez, F. and P. Schaeffer (2001), The CLS01 Mean Sea Surface: A validation with the GSFC00.1 surface.

Hirabayashi, Y., Y. Zhang, S. Watanabe, S. Koirala, S. Kanae (2013), Projection of glacier mass changes under a high-emission climate scenario using the global glacier model HYOGA2, *Hydrol. Res. Lett.,* 7, 6–11.

Holgate, S.J. (2007), On the decadal rates of sea level change during the twentieth century, *Geophys. Res. Lett.,* 34, L01602. doi:10.1029/2006GL028492.

Holgate S.J., A. Matthews, P.L. Woodworth, L.J. Rickards, M.E. Tamisiea, E. Bradshaw, P.R. Foden, K.M. Gordon, S. Jevrejeva, J. Pugh (2013), New data systems and products at the permanent service for mean sea level, *J. Coastal Res.*. 29(3):493–504.

Huber, P.J. (1964), Robust estimation of a location parameter, *Ann. Math. Stat.*, 35, 73–101.

Huybers, P. (2011), Combined obliquity and precession pacing of Late Pleistocene deglaciations, *Nature, 480,* 229–232.

IERS Conventions (2010), Gérard Petit and Brian Luzum (eds.). (IERS Technical Note ; 36) Frankfurt am Main: Verlag des Bundesamts für Kartographie und Geodäsie, 2010. 179 pp., ISBN 3-89888-989-6.

Imel, D. (1994), Evaluation of the TOPEX/POSEIDON dual-frequency ionosphere correction, *J. Geophys. Res.,* 99, 24, 895–24, 906.

IPCC (2013). *Climate Change 2013: The Physical Science Basis. Contribution of Working Group I to the Fifth Assessment Report of the Intergovernmental Panel on Climate Change.* Cambridge University Press, Cambridge, United Kingdom and New York, NY, USA.

Ishii, M., and M. Kimoto (2009) Reevaluation of historical ocean heat content variations with time-varying XBT and MBT depth bias, *Journal of Oceanography*, 65, 287–99.

Jevrejeva, S., A. Grinsted, J. C. Moore, S. Holgate (2006), Nonlinear trends and multiyear cycles in sea level records, *J. Geophys. Res.,* 111, C09012, doi:10.1029/2005/JC003229.

Jevrejeva, S., J. C. Moore, A. Grinsted, P. L. Woodworth (2008), Recent global sea level acceleration started over 200 years ago?, *Geophys. Res. Lett.,* 35, L08715. doi:10.1029/2008GL033611.

Jimenez-Munt, I., R. Sabadini, A. Gardi, and G. Bianco (2003), Active deformation in the Mediterranean from Gibraltar to Anatolia inferred from numerical modeling and geodetic and seismological data, *J. Geophys. Res.*, 108(B1), 2006. doi:10.1029/2001JB001544.

Keihm, S. J., M. A. Janssen, and C. S. Ruf, (1995), TOPEX/POSEIDON Microwave Radiometer (TMR): III. Wet tropospheric range correction algorithm and pre-launch error budget, *IEEE Trans. Geosci. Rem. Sens.,* 33, 147–161.

King, M. A. (2004), Rigorous GPS data-processing strategies for glaciological applications, *Journal of Glaciology,* 50, (171) pp. 601-607. ISSN 0022-1430.

King, M. A., M. Keshin, P. L. Whitehouse, I. D. Thomas, G. Milne, and R. E. M. Riva (2012), Regional biases in absolute sea-level estimates from tide gauge data due to residual unmodeled vertical land movement, *Geophys. Res. Lett.,* 39, L14604. doi:10.1029/2012GL052348.

Konikow, L. F. (2011), Contribution of global groundwater depletion since 1900 to sea level rise, *Geophys. Res. Lett.,* 38, L17401. doi:10.1029/2011GL048604.

Lambeck, K., H. Rouby, A. Purcell, Y. Sun, M. Sambridge (2014) Sea level and global ice volumes from the Last Glacial Maximum to the Holocene, *Proc. Natl. Acad. Sci. USA*, 111(43):15296–15303.

Leclercq, P. W., and J. Oerlemans (2012), Global and hemispheric temperature reconstruction from glacier length fluctuations, *Clim. Dyn.,* 38, 1065–1079.

Lemke, P., et al., 2007: Observations: Changes in snow, ice and frozen ground, in *Climate Change 2007: The Physical Science Basis. Contribution of Working Group I to the Fourth Assessment Report of the Intergovernmental Panel on Climate Change*, [Solomon, S., D. Qin, M. Manning, Z. Chen, M. Marquis, K. B. Averyt, M. Tignor and H. L. Miller (eds.)] Cambridge University Press, Cambridge, United Kingdom and New York, NY, USA, pp. 337–383.

Le Provost, C. (2001), Ocean tides, in *Satellite Altimetry and Earth Sciences: A Handbook of Techniques and Applications,* edited by L.-L. Fu and A. Cazenave, pp. 267–303, Vol. 69, Int. Geophys. Series. Academic Press, San Diego, Calif.

Le Traon, P.Y., F. Nadal, N. Ducet (1998) An improved mapping method of multisatellite altimeter data, *J. Atmos. Ocean. Technol.* 15(2):522–534

Le Traon, P.Y. and F. Ogor (1998) ERS-1/2 orbit improvement using T/P: The 2 cm challenge *J. Geophys. Res.,* 103, 8045-8057.

Levitus, S., et al. (2012), World ocean heat content and thermosteric sea level change (0–2000 m), 1955–2010, *Geophys. Res. Lett.,* 39, L10603. doi:10.1029/2012GL051106

Limpach P., 2010. Sea Surface Topography and Marine Geoid by Airborne Laser Altimetry and Shipborne Ultrasound Altimetry, *Geodätisch-geophysikalische Arbeiten in der Schweiz.* Volume 80. Schweizerische Geodätische Kommission. ISBN 978-3-908440-24-6.

Lisiecki, L.E. (2010), Links between eccentricity forcing and the 100,000-year glacial cycle, *Nature Geoscience, 3,* 349–352.

Llovel, W., M. Becker, A. Cazenave, S. Jevrejeva, R. Alkama, B. Decharme, H. Douville, M. Ablain, and B. Beckley (2011), Terrestrial waters and sea level variations on interannual time scale, *Global Planet. Change,* 75, 76–82, doi:10.1016/j.gloplacha.2010.10.008.

Lorbacher, K., S. J. Marsland, J. A. Church, S. M. Griffies, D. Stammer (2012), Rapid barotrophic sea-level rise from ice-sheet melting scenarios, *J. Geophys. Res.,* 117, C06003.

Marzeion, B., A. H. Jarosch, M. Hofer (2012), Past and future sea-level change from the surface mass balance of glaciers, *Cryosphere,* 6, 1295–1322.

Masson-Delmotte, V., M. Schulz, A. Abe-Ouchi, J. Beer, A. Ganopolski, J.F. Gonzalez Rouco, E. Jansen, K. Lambeck, J. Luterbacher, T. Naish, T. Osborn, B. Otto-Bliesner, T. Quinn, R. Ramesh, M. Rojas, X. Shao and A. Timmermann (2013), Information from Paleoclimate Archives, in *Climate Change 2013: The Physical Science Basis. Contribution of Working Group I to the Fifth Assessment Report of the Intergovernmental Panel on Climate Change*, [Stocker, T.F., D. Qin, G.-K. Plattner, M. Tignor, S.K. Allen, J. Boschung, A. Nauels, Y. Xia, V. Bex and P.M. Midgley (eds.)]. Cambridge University Press, Cambridge, United Kingdom and New York, NY, USA.

Masters, D., R. S. Nerem, C. Choe, E. Leuliette, B. Beckley, N. White, M. Ablain (2012), Comparison of global mean sea level time series from TOPEX/Poseidon, Jason-1, and Jason-2, *Mar. Geod.,* 35, 20–41. doi:10.1080/01490419.2012.717862.

Maul, G.A., and D.M. Martin (1993), Sea level rise at key west, Florida, 1846–1992: America's longest Instrument record? *Geophys. Res. Lett.* 20, 1955–1958.

Mayer-Gürr T., D. Rieser, E. Höck, J. M. Brockmann, W.-D. Schuh, I. Krasbutter, J. Kusche, A. Maier, S. Krauss, W. Hausleitner, O. Baur, A. Jäggi, U. Meyer, L. Prange, R. Pail, T. Fecher, T. Gruber (2012), The new combined satellite only model GOCO03s, *Abstract submitted to GGHS2012,* Venice.

Mazzotti, S., A. Lambert, N. Courtier, L. Nykolaishen, and H. Dragert (2007), Crustal uplift and sea level rise in northern Cascadia from GPS, absolute gravity, and tide gauge data, *Geophys. Res. Lett.,* 34, L15306. doi:10.1029/2007GL030283.

McGranahan, G., D. Balk, and B. Anderson (2007), The rising tide: Assessing the risks of climate change and human settlements in low elevation coastal zones, *Environ. Urban., 19(1),* 17–37. doi:10.1177/0956247807076960.

Meier, M. F., et al. (2007), Glaciers dominate eustatic sea-level rise in the 21st century, *Science,* 317, 1064–1067.

Merrifield, M. A., S. T. Merrifield, G. T. Mitchum (2009), An anomalous recent acceleration of global sea level rise, *J. Clim.,* 22, 5772–5781. doi:10.1175/2009JCLI2985.1.

Milly, P. C. D., A. Cazenave, and M. C. Gennero, (2003), Contribution of climate-driven change in continental water storage to recent sea-level rise, *Proc. Natl. Acad. Sci. U.S.A.*, 100, 13158–13161.

Milly, P. C. D., et al. (2010) Terrestrial water-storage contributions to sea-level rise and variability, in *Understanding Sea-Level Rise and Variability*, [J. A. Church, P. L. Woodworth, T. Aarup and W. S. Wilson (eds.)], Wiley-Blackwell, Hoboken, NJ, USA, pp. 226–255.

Nerem, R.S., and G.T. Mitchum (2002), Estimates of vertical crustal motion derived from differences of Topex/Toseidon and sea level measurement, *Geophys. Res. Lett.* 29, 1934.

Nerem, R. S., D. P. Chambers, C. Choe, and G. T. Mitchum (2010), Estimating mean sea level change from the TOPEX and Jason altimeter missions, *Mar. Geod., 33(1),* 435–446. doi:10.1080/01490419.2010.491031.

Ngo-Duc, T., K. Laval, J. Polcher and A. Cazenave (2005), Contribution of continental water to sea level variations during the 1997–1998 El Niño–Southern Oscillation event: Comparison between Atmospheric Model Intercomparison Project simulations and TOPEX/Poseidon satellite data, *J. Geophys. Res.*, 110, D09103.

Pavlis, N.K., S.A. Holmes, S.C. Kenyon, J.K. Factor (2008), An Earth Gravitational Model to Degree 2160: EGM2008, *presented at the 2008 General Assembly of the European Geosciences Union,* Vienna, Austria, April 13–18, 2008.

Peltier, W. R. (2001), Global glacial isostatic adjustment and modern instrumental records of relative sea level history, *Int. Geophys.,* 75:65–95.

Peltier, W. R. (2004), Global glacial isostasy and the surface of the ice-age Earth: The ICE-5G (VM2) model and GRACE, *Annu. Rev. Earth Planet. Sci.,* 32, 111–149. doi:10.1146/annurev.earth.32.082503.144359.

Picot, N., K. Case, S. Desai, P. Vincent (2003), *AVISO and PODAAC User Handbook. IGDR and GDR Jason Products.* SMM-MU-M5-OP-13184-CN (AVISO), JPL D-21352 (PODAAC).

Pinardi, N., A. Bonaduce, A. Navarra, S. Dobricic, P. Oddo (2014), The mean sea level equation and its application to the mediterranean sea, *J. Climate.* doi:10.1175/JCLI-D-13-00139.1

Ponte, R. M., and P. Gaspar (1999), Regional analysis of the inverted barometer effect over the global ocean using TOPEX/Poseidon data and model results, *J. Geophys. Res.,* 104, 15, 587-602.

PSMSL (2015) Tide Gauge Data, Retrieved 4 Jun 2015 from http://www.psmsl.org/data/obtaining/. Tech. rep., Permanent Service for Mean Sea Level (PSMSL).

Pugh, D.T. (1987), Tides, Surges and Mean Sea-Level, John Wiley and Sons, New York.

Purkey, S., and G. C. Johnson (2010), Warming of global abyssal and deep southern ocean waters between the 1990s and 2000s: Contributions to global heat and sea level rise budget, *J. Clim.,* 23, 6336–6351. doi:10.1175/2010JCLI3682.1.

Raucoules, D., G. Le Cozannet, M. Gravelle, M. de Michele, G. Wöppelmann, M. Gravelle, A. Daag, and M. Marcos (2013), Strong non-linear urban ground motion in Manila (Philippines) from 1993 to 2010 observed by InSAR, *Remote Sens. Environ.,* 139, 386-397. doi:10.1016/j.rse.2013.08.021.

Ray, R.D. (1998), Ocean self-attraction and loading in numerical tidal models, *Mar. Geod.*, 21, 181-192.

Ray, R.D. (2013), Precise comparisons of bottom-pressure and altimetric ocean tides, *J. Geophys. Res. Oceans,* 118, 4570–4584. doi:10.1002/jgrc.20336.

Rhein, M., S.R. Rintoul, S. Aoki, E. Campos, D. Chambers, R.A. Feely, S. Gulev, G.C. Johnson, S.A. Josey, A. Kostianoy, C. Mauritzen, D. Roemmich, L.D. Talley and F. Wang (2013), Observations: Ocean, in *Climate Change 2013: The Physical Science Basis. Contribution of Working Group*

I to the Fifth Assessment Report of the Intergovernmental Panel on Climate Change, [Stocker, T.F., D. Qin, G.-K. Plattner, M. Tignor, S.K. Allen, J. Boschung, A. Nauels, Y. Xia, V. Bex and P.M. Midgley (eds.)]. Cambridge University Press, Cambridge, United Kingdom and New York, NY, USA.

Rignot, E., I. Velicogna, M. R. van den Broeke, A. Monaghan, J. Lenaerts (2011), Acceleration of the contribution of the Greenland and Antarctic ice sheets to sea level rise, *Geophys. Res. Lett.,* 38, L05503. doi:10.1029/2011GL046583.

Rodionov, S.N. (2004), A sequential algorithm for testing climate regime shifts, *Geophys. Res. Lett.,* 31, L09204. doi:10.1029/2004GL019448.

Rodionov, S.N. (2006), The use of prewhitening in climate regime shift detection, *Geophys. Res. Lett.*, 31, L12707. doi:10.1029/ 2006GL025904.

Rohling, E.J., K. Grant, C.H. Hemleben, M. Siddall, B.A.A. Hoogakker, M. Bolshaw and M. Kucera (2008), High rates of sea-level rise during the last interglacial period, *Nature Geoscience 1,* 38–42.

Rudenko, S., M. Otten, P. Visser, R. Scharroo, T. Schöne, and S. Esselborn (2012), New improved orbit solutions for the ERS-1 and ERS-2 satellites, *Adv. Space Res.,* 49, 1229–1244.

Santamaría-Gómez A., M. Gravelle, X. Collilieux, M. Guichard, B. Martín Míguez, P. Tiphaneau, G. Wöppelmann (2012), Mitigating the effects of vertical land motion in tide gauge records using a state-of-the-art GPS velocity field, *Global Planet. Change,* 98-99, 6-17. doi:10.1016/j.gloplacha.2012.07.007.

Shenoi, B.A. (2006), Introduction to Digital Signal Processing and Filter Design, John Wiley and Sons, New York.

Shepherd, A., et al. (2012), A reconciled estimate of ice-sheet mass balance, *Science,* 338, 1183–1189.

Stammer, D. (2008), Response of the global ocean to Greenland and Antarctic ice melting, *J. Geophys. Res. Oceans,* 113, C06022.

Stammer, D., A. Cazenave, R. M. Ponte, M. E. Tamisiea (2013), Causes for contemporary regional sea level changes, *Annual Review of Marine Science,* vol. 5, 21-46. doi:10.1146/annurev-marine-121211-172406.

Strozzi, T., P. Teatini, L. Tosi (2009), TerraSAR-X reveals the impact of the mobile barrier works on Venice coastland stability, *Remote Sensing of Environment* 113, 2682–2688. doi:10.1016/j.rse.2009.08.001.

Tanhua, T., D. Hainbucher, K. Schroeder, V. Cardin, M. Alvarez, and G. Civitarese (2013), The Mediterranean Sea system: a review and an introduction to the special issue, *Ocean Sci.*, 9, 789–803. doi:10.5194/os-9-789-2013.

Tapley, B. D., J. C. Ries, G. W. Davis, R. J. Eanes, B. E. Schutz, C. K. Shum, M. M. Watkins, J. A. Marshall, R. S. Nerem, B. H. Putney, S. M. Klosko, S. B. Luthcke, D. Pavlis, R. G. Williamson, and N. P. Zelensky (1994), Precision orbit determination for TOPEX/POSEIDON, *J. Geophys. Res.,* 99, 24, 383–24, 404.

Tapley, B. D., B. E. Schutz, G. H. and Born (2000), in *Statistical Orbit Determination*, Academic Press, San Diego, in press.

Taylor, J. R. (1982), An introduction to error analysis: The study of uncertainties in physical measurements, Mill Valley, Calif: University Science Books.

Tomás, R., R. Romero, J. Mulas, J.J. Marturià, J.J. Mallorquí, J.M. Lopez-Sanchez, G. Herrera, F. Gutiérrez, P.J. González, J. Fernández, S. Duque, A. Concha-Dimas, G. Cocksley, C. Castañeda, D. Carrasco, P. Blanco (2014), Radar interferometry techniques for the study of ground subsidence phenomena: a review of practical issues through cases in Spain, *Environmental Earth Sciences*, 71, 163-181.

Tosi, L., L. Carbognin, P. Teatini, T. Strozzi, U. Wegmüller (2002), Evidence of the present relative land stability of Venice, Italy, from land, sea, and space observations, *Geophys. Res. Lett.,* 29 (12), 1562. doi:10.1029/2001GL013211.

Tran, N., S. Labroue, S. Philipps, E. Bronner, and N. Picot (2010), Overview and Update of the Sea State Bias Corrections for the Jason-2, Jason-1 and TOPEX Missions, *Mar. Geod.,* 33, no. 1 supp 1:348.

Tsimplis, M. N., and P. L. Woodworth (1994), The global distribution of the seasonal sea level cycle calculated from coastal tide gauge data, *J. Geophys. Res.,* 99(C8), 16031–16039. doi:10.1029/94JC01115.

UNESCO (1985), Manual on sea level measurement and interpretation, Intergovernmental Oceanographic Commission, *Manuals and Guides 14*, Institute of Oceanographic Sciences, United Kingdom.

Vaughan, D.G., J.C. Comiso, I. Allison, J. Carrasco, G. Kaser, R. Kwok, P. Mote, T. Murray, F. Paul, J. Ren, E. Rignot, O. Solomina, K. Steffen and T. Zhang (2013), Observations: Cryosphere, in *Climate Change 2013: The Physical Science Basis. Contribution of Working Group I to the Fifth Assessment Report of the Intergovernmental Panel on Climate Change*, [Stocker, T.F., D. Qin, G.-K. Plattner, M. Tignor, S.K. Allen, J. Boschung, A. Nauels, Y. Xia, V. Bex and P.M. Midgley (eds.)]. Cambridge University Press, Cambridge, United Kingdom and New York, NY, USA.

Velicogna, I. (2009), Increasing rates of ice mass loss from the Greenland and Antarctic ice sheets revealed by GRACE, *Geophys. Res. Lett.*, 36, L19503.

Vellinga, P., and S. P. Leatherman (1989), Sea level rise, consequences and policies, *Clim. Change, 15(1-2),* 175–189. doi:10.1007/bf00138851.

Wada, Y., L. P. H. van Beek, F. C. S. Weiland, B. F. Chao, Y. H. Wu, M. F. P. Bierkens (2012), Past and future contribution of global groundwater depletion to sea-level rise, *Geophys. Res. Lett.,* 39, L09402, doi:10.1029/2012GL051230.

Wada, Y., et al. (2013), Multimodel projections and uncertainties of irrigation water demand under climate change, *Geophys. Res. Lett.,* 40, 4626–4632. doi:10.1002/grl.50686.

Wahr, J. W. (1985), Deformation of the Earth induced by polar motion, *J. Geophys. Res. (Solid Earth),* 90, 9363-9368.

Wilks, D. S. (2006), Statistical methods in the atmospheric sciences, Burlington, Mass.: Academic Press.

Wong, P.P., I.J. Losada, J.-P. Gattuso, J. Hinkel, A. Khattabi, K.L. McInnes, Y. Saito, and A. Sallenger (2014), Coastal systems and low-lying areas, in *Climate Change 2014: Impacts, Adaptation, and Vulnerability. Part*

A: Global and Sectoral Aspects. Contribution of Working Group II to the Fifth Assessment Report of the Intergovernmental Panel on Climate Change, [Field, C.B., V.R. Barros, D.J. Dokken, K.J. Mach, M.D. Mastrandrea, T.E. Bilir, M. Chatterjee, K.L. Ebi, Y.O. Estrada, R.C. Genova, B. Girma, E.S. Kissel, A.N. Levy, S. MacCracken, P.R. Mastrandrea, and L.L.White (eds.)]. Cambridge University Press, Cambridge, United Kingdom and New York, NY, USA, pp. 361-409.

Woodworth, P.L. (1990), A search for accelerations in records of European mean sea level, *Int. J. Climatol.*, 10(2), 129–143.

Woodworth, P. L., and R. Player (2003), The permanent service for mean sea level: An update to the 21st century, *J. Coastal Res.,* 19(2), 287–295.

Woodworth, P.L., W.R. Gehrels, and R.S. Nerem (2011), Nineteenth and twentieth century changes in sea level, *Oceanography* 24(2):80–93. doi:10.5670/oceanog.2011.29.

Wöppelmann, G., B. Martin Miguez, M.-N. Bouin, Z. Altamimi (2007), Geocentric sea level trend estimates from GPS analyses at relevant tide gauges world-wide, *Global Planet. Change* 57, 396–406. doi:10.1016/j.gloplacha.2007.02.002.

Wöppelmann G., N. Pouvreau, A. Coulomb, B. Simon, P.L. Woodworth (2008), Tide gauge datum continuity at Brest since 1711: France's longest sea-level record, *Geophys. Res. Lett.,* 35, L22605. doi:10.1029/2008GL035783.

Wöppelmann, G., C. Letetrel, A. Santamaría-Gómez, M.-N. Bouin, X. Collilieux, Z. Altamimi, S. D. P. Williams, and B. Martin Miguez (2009), Rates of sea-level change over the past century in a geocentric reference frame, *Geophys. Res. Lett.,* 36, L12607. doi:10.1029/2009GL038720.

Wöppelmann G., G. Le Cozannet, M. de Michele, D. Raucoules, A. Cazenave, M. Garcin, S. Hanson, M. Marcos, A. Santamaría-Gómez (2013) Is land subsidence increasing the exposure to sea level rise in Alexandria, Egypt? *Geophys. Res. Lett.,* 40, 2953–2957. doi:10.1002/grl.50568.

Wunsch, C., and D. Stammer (1997), Atmospheric Loading and the Oceanic "Inverted Barometer" effect, *Rev. Geophys.,* 35, 79-107.

Zerbini, S., H.-P. Plag, T. Baker, M. Becker, et al. (1996) Sea level in the Mediterranean: a first step towards separating crustal movements and absolute sea-level variations *Global Planet. Change, 14,* 1–48.

Zerbini, S., B. Richter, F. Rocca, T. van Dam, F. Matonti (2007), A combination of space and terrestrial geodetic techniques to monitor land subsidence. Case study, the South Eastern Po Plain, Italy, *J. Geophys. Res. 112,* B05401. doi:10.1029/2006JB004338.

Zerbini, S., S. Bruni, S. del Conte, M. Errico, F. Petracca, C. Prati, F. Raicich, E. Santi (2015), Sea Level Variability in the Mediterranean, pp. G43B-1035, American Geophysical Union Fall Meeting, San Francisco, CA., 14-18 December 2015.

Zervas, C.E. (2001), Sea level variations of the United States, 1854-1999, Silver Spring, Md.: U.S. Dept. of Commerce, National Oceanic and Atmospheric Administration, National Ocean Service.

Zervas, C.E. (2009), Sea level variations of the United States, 1854-2006, Silver Sping, Md.: U.S. Dept. of Commerce, National Oceanic and Atmospheric Administration, National Ocean Service.